Dynamic Testing of Total Hip and Knee Replacements under Physiological Conditions

Dissertation

for the achievement of the academic degree
Doctor of Engineering (Dr.-Ing.)
from the
Faculty of Mechanical Engineering and
Marine Technology of the
University of Rostock

by

Sven W. Herrmann
born in Sindelfingen, Germany

First reviewer:	Rainer Bader, Prof. Dr. med. Dipl.-Ing.
Second reviewer:	Christoph Woernle, Prof. Dr.-Ing.
Third reviewer:	Darryl D. D'Lima, Prof. Ph.D. M.D.

Date of submission:	5. December 2014
Date of oral exam:	4. September 2015

urn:nbn:de:gbv:28-diss2016-0002-7

Acknowledgements

Biomechanics caught my attention during my course of studies at the University of Stuttgart and the George Washington University. Quite fascinated by the interdisciplinary interplay between engineering, biology and medicine, I took the chance in September 2009 to work as a research associate at the Biomechanics and Implant Technology Research Laboratory established at the Department of Orthopaedics of the University Medicine in Rostock. There, I was part of a research team dealing with projects in orthopedic biomechanics generously funded by the German Research Foundation (BA 3347/3-1/2 and WO 452/8-1/2), the Ministry of Education, Science and Culture of Mecklenburg-Vorpommern (grant number UR 08040), and the Hermes program of the University of Rostock. This work arose from that time.

Of course, I could have never accomplished this work without the tremendous aid, support and effort of certain individuals. I would like to use this occasion to thank and express my deepest appreciation to those accompanying me during this long journey. Rainer Bader, Professor and Head of the Biomechanics and Implant Technology Research Laboratory, for giving me the unique opportunity to contribute to this progressing field of research and providing invaluable motivation, guidance and advice. Christoph Woernle, Professor and Head of the Chair of Technical Dynamics at the University of Rostock, for sharing his outstanding experience and expertise in mechanical research and inspiring this work from the outset. Darryl D. D'Lima and his team of the Shiley Center for Orthopedic Research and Education at the Scripps Clinic for giving me an unforgettable stay in La Jolla, providing data for validation purposes and essentially promoting this work. I would also like to thank Klaus Schittkowski, Professor at the University of Bayreuth, who generously made his know-how in numerical methods available, and Stefan Lehner, researcher at the Technische Universität München, who splendidly helped me to get started in the world of biomechanical modeling. Also, I want to thank Andreas Mattke and Norbert Wolff from the Institute of Sports Science at the University of Rostock for their assistance during motion capturing. This work would not have gotten so far without the immense backup offered by János Zierath and Daniel Kluess, who also assisted in proof reading and correcting this work. I have greatly benefited from the daily interaction with my teammates Robert Souffrant, Roman Rachholz and Michael Kähler. Special thanks go to my former students Fabian Göll, Andreas Geier and Jochen Harmuth, and all my colleagues and friends crossing my path those days.

Finally, I am deeply thankful to my parents Charlotte and Walter Herrmann and my brother Marc Herrmann for being fundamental and enduring pillars. This work would certainly not have been possible without their continuous and unconditional affection, attention and encouragements throughout all these years.

Rostock, September 2015 Sven W. Herrmann

Abstract

Orthopedic treatments are well proven approaches in modern medicine to deal with joint diseases. Although deployed as last resort, implantation of total joint replacements has already been established as standard procedure with growing numbers. Despite the clinical success, however, failure constitutes a substantial problem. Besides infection, loosening and fracture, postoperative instability prevails as a major complication in daily clinical practice. Both its obscurity and the severe consequences for patients, especially in case of dislocation, make it difficult for clinicians to find appropriate countermeasures. As treatment of affected joints most commonly ends in revision surgery with further drawbacks and risks, it is of great importance to prevent instability from the outset. Prevention, however, requires comprehension of underlying mechanisms and related factors influencing the process leading to instability. In this context, there is little evidence in how exactly soft tissue structures engage during dislocation of total hip replacements (THRs). The same applies to the dynamic effect of certain implant parameters. As regards total knee replacements (TKRs), it is still unclear how both ligament and muscular structures effect the process leading to erratic, adverse or excessive motion; not to mention the lack of precise definitions of associated mechanisms.
In order to obtain insights on these issues, biomechanical investigations are invaluable which at best cope with the demands of an in vivo analysis, even for instability-associated maneuvers. As measurements in patients are afflicted with ethical objections, the purpose of this work was to present a comprehensive approach capable of testing total joint stability under dynamic, reproducible and physiological conditions. The approach is based on a hardware-in-the-loop (HiL) simulation where the anatomic and physiological environment of the implant is extracted into a mathematical model. In this respect, rigid multibody systems are used which are suitable for real-time applications, and enable incorporation of ligament and muscular structures within an inverse or forward dynamics approach. Interaction between the model and the real implant components is achieved by a physical setup composed of an industrial robot equipped with a force-torque sensor and a compliant support with displacement sensors attached to. The robot applies motion and forces onto the implant components according to the boundary conditions delivered by the model using hybrid position-force control. The decision which direction runs in position or force control mode depends on the mechanical compliance of the real contact. The sensors measure the implant response which is transferred back to the model closing the HiL control loops.

An essential aspect of this approach was the development of multibody models which define physiological test conditions within the HiL environment as regards THR and TKR testing. The validation strategy for both configurations was to compare predicted joint loading against experimental data. For THR testing, a musculoskeletal model was developed which allowed for muscle force estimations based on an inverse dynamics approach whilst the HiL simulation is in progress. The outcomes for two common maneuvers of one subject were compared to data derived from three patients with instrumented THRs revealing good agreement in trend and magnitude. Concerning TKR testing, a multibody model was implemented into the HiL environment which emulated an experimental setup with an instrumented TKR. The outline of the model enabled direct comparison to the corresponding specimen-based measurements showing overall good correlation. Based on these results, it was inferred that the HiL test system was capable of replicating comparable THR dynamics as present in patients, and TKR kinematics and loading as given under in vitro conditions.

In this sense, the HiL test system extends the repertoire of approaches commonly used in orthopedic research offering unique features. Mechanical and specimen-based test setups deliver real contact conditions, but entail difficulties concerning adequate incorporation of active muscle structures. In addition, human specimens make reproducible and comparable evaluations difficult due to time-dependent decay and individual variability. The problem of reproducibility and comparability appears to be circumvented by using model-based simulations. However, complex contact modeling is limited. Other approaches may promise physiological conditions by using prescribed load situations; though they neglect the impact of soft tissue interaction and parameter variations on musculoskeletal dynamics. These trade-offs are resolved within the HiL approach combining the advantages of real testing and model-based simulation.

Apart from proceeding optimization of the HiL test system, several challenges regarding THR stability can be addressed based on the current configuration. These include the dynamic influence of implant design and positioning, the contribution of muscular and capsular structures, or the performance of eccentric tripolar systems. In contrast, consideration of TKR instability at this stage may not comply with real load conditions present in affected patients. Substantial enhancement is seen in the implementation of a more complex ligament apparatus along with active muscle structures. In the long term, the HiL approach may not only contribute to THR and TKR stability, but may also assist in illuminating instability after total shoulder arthroplasty, or other failure mechanisms such as wear. The approach has the potential to support researchers, developers and surgeons alike in the advancement of implants and surgical techniques in case of primary, revision or tumor surgery.

Keywords HiL simulation, robot-based testing, multibody systems, musculoskeletal modeling, total hip replacement, total knee replacement, instability, dislocation, validation

Contents

Figures

Nomenclature

Abbreviations

%BW	subject's body weight in percentage
%BWm	subject's body weight times meter in percentage
BW	body weight
CAD	computer-aided design
CCD	caput-collum-diaphyseal
CT	computed tomography
EMG	electromyography
FEM	finite element method
HiL	hardware-in-the-loop
IPC	interprocess communication protocol
MBS	multibody system
MRI	magnetic resonance imaging
PCI	peripheral component interconnect
PCR	posterior cruciate retaining
PS	posterior stabilized
RoM	range of motion
TCP	transmission control protocol
THR	total hip replacement
TJR	total joint replacement
TKR	total knee replacement
UDP	user datagram protocol
VVC	varus-valgus constrained

Scalar Quantities and Variables

β	radiographic anteversion angle
ι	radiographic inclination angle
ν	femoral neck-to-shaft angle
ρ_{b}	average bone density
ρ_{s}	soft tissue density
σ_j	physiological muscle stress of j-th muscle
τ_i^{f}	applied torque in free directions
ϑ	femoral antetorsion
A_j	physiological cross section area of j-th muscle
b	number of holonomic constraints
b_{c}	number of implicit loop closure constraints
b_{z}	number of holonomic constraints of artificial joint
C_j	isometric muscle force of j-th muscle

d	femoral head diameter
f	number of degrees of freedom of open kinematic chain
f_j^{lv}	factor of muscular force-length and velocity-length properties
f_{c}	number of degrees of freedom of closed kinematic chain
f_i^{r}	force in constraint directions
h	femoral head offset
i	index for segments and coordinates
I_{c}	cost function for closed-loop redundancy problem
I_{m}	cost function for distribution problem of muscle forces
j	index for muscle forces
l	femoral neck length
l_i^{r}	torque in constraint directions
m_i	mass of i-th segment
n	number of muscle force elements
p	number of segments
q_i	i-th joint coordinate in free directions
s	femoral implant setting
t	instant of time
z_i	i-th coordinate in constraint directions

Vectors

$\bar{\boldsymbol{\alpha}}_i$	velocity-dependent rotational accelerations of i-th segment
$\bar{\boldsymbol{a}}_i$	velocity-dependent translational accelerations of i-th segment
$\bar{\boldsymbol{\eta}}$	velocity-dependent term of vector $\ddot{\boldsymbol{g}}$
$\bar{\boldsymbol{\tau}}^{\mathrm{f}}$	generalized measured and transferred torques
$\boldsymbol{a}$	vector of muscle activation levels
$\boldsymbol{f}_i^{\mathrm{e}}$	applied forces on i-th segment
$\boldsymbol{f}^{\mathrm{m}}$	absolute active muscle forces
$\boldsymbol{f}_i^{\mathrm{r}}$	reaction forces on i-th segment
$\boldsymbol{g}$	implicit loop closure constraints
$\dot{\boldsymbol{g}}$	first time derivative of vector $\boldsymbol{g}$
$\ddot{\boldsymbol{g}}$	second time derivative of vector $\boldsymbol{g}$
$\boldsymbol{l}_i^{\mathrm{e}}$	applied torques on i-th segment
$\boldsymbol{l}_i^{\mathrm{r}}$	reaction torques on i-th segment
$\boldsymbol{\lambda}^{\mathrm{c}}$	additional constraint force coordinates
$\boldsymbol{\lambda}^{\mathrm{r}}$	reaction force coordinates
$\boldsymbol{\omega}_i$	rotational velocity of i-th segment
$\dot{\boldsymbol{\omega}}_i$	rotational accelerations of i-th segment
$\boldsymbol{q}$	joint coordinates
$\dot{\boldsymbol{q}}$	first time derivative of vector $\boldsymbol{q}$
$\ddot{\boldsymbol{q}}$	second time derivative of vector $\boldsymbol{q}$
$\boldsymbol{r}_i$	position vector of i-th segment
$\boldsymbol{\tau}^{\mathrm{c}}$	generalized Coriolis and centrifugal forces as well as gyroscopic torques
$\boldsymbol{\tau}^{\mathrm{e}}$	generalized applied forces
$\boldsymbol{\tau}^{\mathrm{g}}$	generalized gravitational forces
$\boldsymbol{\tau}^{\mathrm{l}}$	generalized ligament and capsular forces

$\hat{\boldsymbol{\tau}}^{\mathrm{c}}$ Coriolis and centrifugal forces/torques as well as gyroscopic torques with respect to absolute velocities

$\hat{\boldsymbol{\tau}}^{\mathrm{e}}$ applied forces/torques with respect to absolute velocities

$\hat{\boldsymbol{\tau}}^{\mathrm{f}}$ measured and transferred torques with respect to absolute velocities

$\hat{\boldsymbol{\tau}}^{\mathrm{g}}$ gravitational forces/torques with respect to absolute velocities

$\hat{\boldsymbol{\tau}}^{\mathrm{l}}$ ligament and capsular forces/torques with respect to absolute velocities

$\hat{\boldsymbol{\tau}}^{\mathrm{m}}$ muscle forces/torques with respect to absolute velocities

$\hat{\boldsymbol{\tau}}^{\mathrm{r}}$ reaction forces/torques with respect to absolute velocities

$\boldsymbol{v}_i$ translational velocity of i-th segment

$\dot{\boldsymbol{v}}_i$ translational accelerations of i-th segment

$\boldsymbol{x}$ vector in static optimization vector

$\boldsymbol{z}$ constrained coordinates of artificial joint

$\dot{\boldsymbol{z}}$ first time derivative of vector $\boldsymbol{z}$

$\ddot{\boldsymbol{z}}$ second time derivative of vector $\boldsymbol{z}$

Matrices

$\boldsymbol{B}$ matrix of normalized force/torque directions of each muscle

$\boldsymbol{C}$ diagonal matrix of isometric muscle forces

$\boldsymbol{E}$ unit matrix

$\boldsymbol{G}$ derivative matrix of loop closure constraints

$\boldsymbol{G}^{\mathrm{T}}$ transpose of derivative matrix $\boldsymbol{G}$

$\dot{\boldsymbol{G}}$ time derivative of matrix $\boldsymbol{G}$

$\boldsymbol{I}_i$ inertia tensor of i-th segment

$\boldsymbol{J}$ global Jacobian matrix

$\boldsymbol{J}^{\mathrm{T}}$ transpose of global Jacobian matrix $\boldsymbol{J}$

$\boldsymbol{J}_{\mathrm{R}i}$ rotational Jacobi matrix of i-th segment

$\boldsymbol{J}_{\mathrm{T}i}$ translational Jacobi matrix of i-th segment

$\boldsymbol{M}$ global mass matrix

$\widehat{\boldsymbol{M}}$ mass matrix with respect to absolute velocities

$\boldsymbol{O}$ weighting matrix

$\boldsymbol{P}$ weighting matrix

$\boldsymbol{Q}$ distribution matrix of reaction forces

$\boldsymbol{S}_i$ rotation matrix of i-th segment

$\dot{\boldsymbol{J}}_{\mathrm{R}i}$ time derivative of matrix $\boldsymbol{J}_{\mathrm{R}i}$

$\dot{\boldsymbol{J}}_{\mathrm{R}i}$ time derivative of matrix $\boldsymbol{J}_{\mathrm{T}i}$

$\hat{\boldsymbol{G}}$ matrix of constrained directions in sagittal plane

$\widetilde{\boldsymbol{\omega}}_i$ skew-symmetric matrix of $\boldsymbol{\omega}_i$

1 Introduction

Orthopedic treatments are well proven approaches in modern medicine to deal with joint diseases. The main indication requiring such medical interventions is osteoarthritis [7, 374, 375]; a degenerative disease that is characterized by damage to the cartilage in synovial joints and change in the subchondral bone [94]. After physical therapy, medication and other treatments [267], joint arthroplasty often remains the last resort to restore mobility and give pain relief to the patient. During this surgical procedure the articular surfaces affected by osteoarthritis are replaced by artificial implants.

Although joint arthroplasty is deployed as last link in the chain of orthopedic treatments, implantation of total joint replacements (TJRs) has already been established as standard procedure with growing numbers. This fact is underlined by considering primary hip and knee procedures performed in Europe and the United States over the last years (Fig. 1.1). Total hip replacements (THRs) implanted in 2010 yielded around 214,000 procedures in Germany [362], almost 77,000 in England, Wales and Northern Ireland [288], and over 328,000 in the United States [62]. In the same year, bicondylar total knee replacements (TKRs) reached numbers of around 158,000 procedures undertaken in Germany [362], 85,000 in England, Wales and Northern Ireland [288], and more than 719,000 in the United States [62].

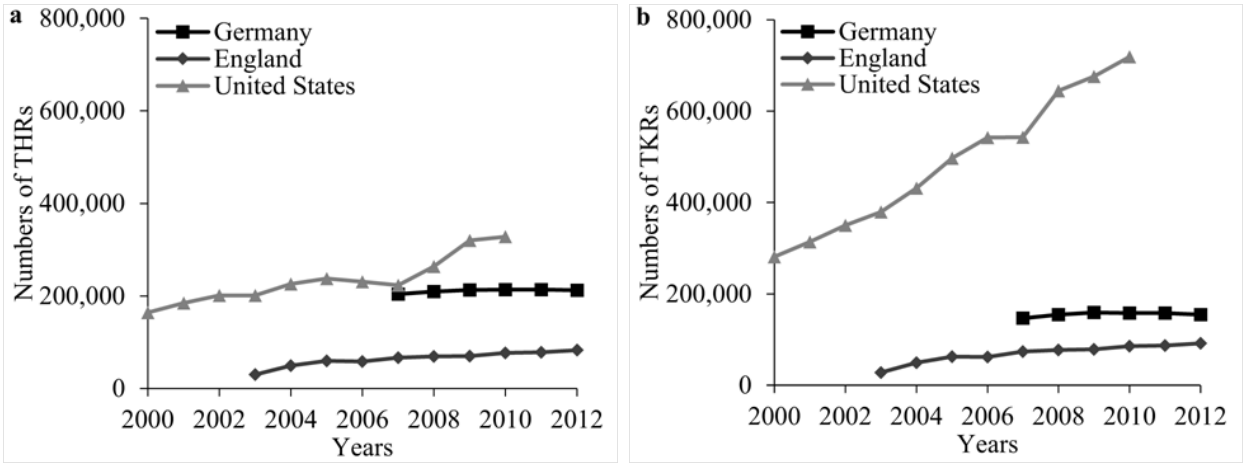

Fig. 1.1 Number of primary procedures performed in Germany [359–364], England, Wales and Northern Ireland [287, 288], and the United States [20, 58–62] **a** Primary total hip replacements. **b** Primary total knee replacements.

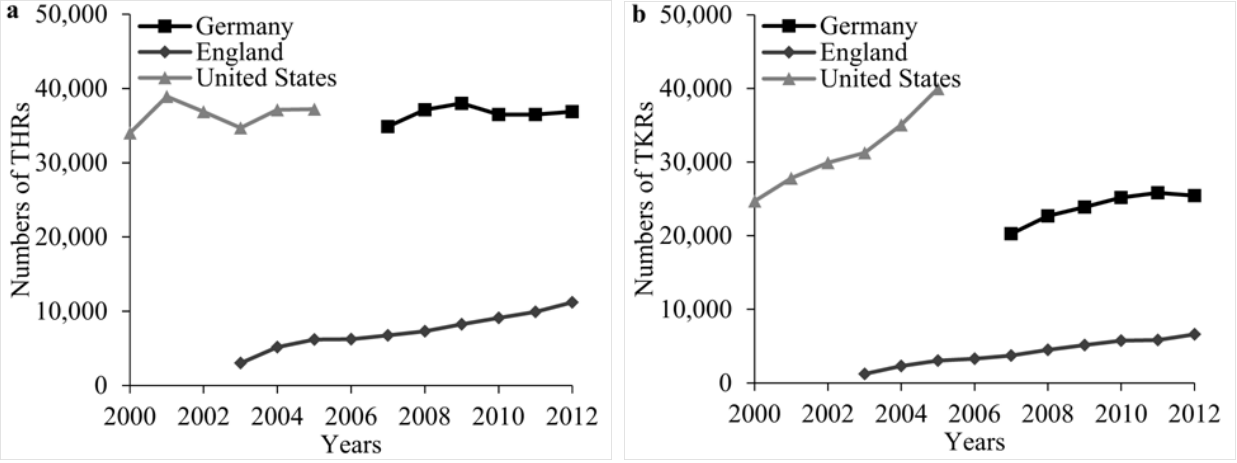

Fig. 1.2 Number of revision procedures performed in Germany [359–364], England, Wales and Northern Ireland [287, 288], and the United States [20] **a** Revised total hip replacements. **b** Revised total knee replacements.

By 2030, Kurtz et al. [227] forecast up to 572,000 THR procedures and even 3.48 million TKR procedures performed in the United States alone. These trends and prospects reflect the enormous market potential for the medical-technical industry, but at the same time the rising costs to be borne by national health care systems.

In spite of the clinical success, failure of artificial joints poses a substantial problem after total joint arthroplasty. Beyond mobility and pain relief, good clinical outcomes of TJRs comprise sufficient osteointegration, stability of the joint conjunction and a healing process free of complications. However, these demands cannot always be met in the long term which leads to revision surgery (Fig. 1.2). Studies reported that after ten years more than 5 % of all primary THRs [373] and about 4 % of all primary TKRs implanted [375] fail due to complications. Infection is a common problem for all kinds of surgery. Wear and abrasion of articulating surfaces deteriorate joint functionality but also release particles into the periprosthetic tissue. Resulting wear debris provokes an inflammatory environment which enhances osteolysis due to cellular responses [1]. Subsequent aseptic loosening of implant components or bone fracture follows from this process [161, 162]. Moreover, excessive stress in the bone bed may also entail aseptic loosening and implant breakage [13], especially when material or manufacturing defects are present.

Infection, loosening, wear and fracture constitute between 50 % and up to 70 % of all revision procedures performed after ten-years observation periods, depending on the study quoted [12, 374, 375]. However, their underlying mechanisms appear in all TJRs, rather autonomously from the joint characteristics. The remaining percentage denote complications related to biomechanical aspects of the specific joint. These will be considered in more detail for THRs and TKRs in the following.

1.1 Dislocation of Total Hip Replacements

A decennial observation performed by the Swedish Hip Arthroplasty Register in 2011 [374] reported that 26.4 % of all THR revisions were correlated to dislocation; an instability phenomena where the artificial hip joint is separated with disastrous consequences for affected patients (Fig. 1.3). In a survey evaluating over 50,000 revisions within one year [44], 22.5 % were related to dislocation and 14.1 % to other mechanical problems or complications. Other researchers allocated 19.9 % of about 11,000 cases summarized from 1999 to 2011 to prosthetic dislocation [12]. Furthermore, it was documented that patients are at higher risk to suffer from a dislocated hip especially right after surgery [373]. These findings illustrate that instability related complications such as dislocation constitute a prevailing cause for THR revision besides infection and loosening. At first glance, this appears to be quite surprising since dislocation denotes a phenomenon rarely seen in healthy hip joints. Hence, the question arises what distinguishes artificially replaced from native hip joints.

The native hip joint consists of the articulation between two bone segments: femur and pelvis [147, 341]. The femoral head is positioned within the pelvic acetabulum according to the congruency of the articulating contact surfaces which are covered by cartilage. Due to the contact, the relative mobility of both joint partners is constrained against each other in all three translational directions. Spanning from the acetabular rim to the area around the intertrochanteric line of the femur the hip joint is surrounded by capsular structures [396]. These comprise complex ligamentous systems with interconnected fiber bundles [141], which guarantee stable translational coupling on the one hand [179,190,365]. On the other hand, the ligamentous systems restrain movement in rotational directions [141, 255, 396]. The rotations are generated by adjacent muscles whereas several muscle groups incorporate not only the

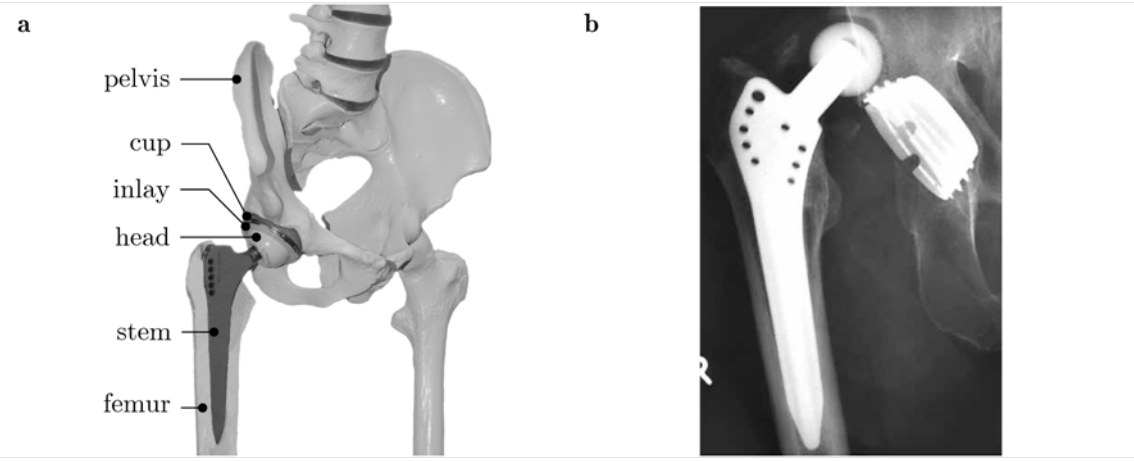

Fig. 1.3 Implanted primary THR. **a** Components of a standard THR. **b** Radiograph of a dislocated THR.

hip joint [147, 341]. Hence, movement and loading between femur and pelvis is determined by a dynamic equilibrium based on inertial and gravitational forces of the bone segments, contact forces between the cartilage surfaces, and soft tissue forces from the capsular and muscle structures.

In preoperative planning, the surgeon chooses which implant type to take, where to place the implant components and how to access the surgical site. A standard uncemented THR usually consists of four parts separated into two components: stem and head on the femoral site, and cup and inlay on the pelvic site. The design of the stem emulates the shape of the native proximal femur, with design parameters such as neck-to-shaft angle (also known as CCD angle), neck diameter and neck length. The spherical shaped head is attached to the stem taper where the mounting depth depends on the femoral offset. On the pelvic site, the cup roughly approximates the acetabulum by a hemispherical form. The inner diameter of the inserted inlay correlates with the head. Moreover, the head coverage of the acetabular component defines the center of rotation with respect to the pelvic segment. During surgery, soft tissue is incised in accordance with the surgical approach [26, 394]. Thus, muscular and capsular structures are damaged or even resected from their attachment sites. The femoral head is resected to allow setting of the stem into the femoral medullary canal. The procedure follows positioning parameters such as setting depth and stem antetorsion with respect to the femur. Likewise, the cup is placed into the prepared acetabulum and orientated by inclination and anteversion angles [282].

After implantation, there are several changes compared to the native hip joint. First, design and positioning parameters may shift the center of rotation with respect to the bone segments altering the geometric proportions within the skeletal system. As a consequence, the kinematics of the whole skeletal system may be modified whether intentional due to biomechanical reasoning or not. The vast range of motion (RoM) observed in healthy hip joints [193] may be restricted additionally when, for instance, the cup overlaps the acetabulum. Furthermore, the new geometric proportions may vary laxity or pretension of capsular structures and lever arms of the muscles. Second, each surgical intervention bears a risk of impairing nerve fibers leading to functional deficiency of muscle groups. Soft tissue may remain resected or damaged if not repaired by the surgeon. Further bone loss in case of revision or tumor surgery leads to weakness of more capsular and muscular structures. All these issues may inflict changes in motion and load distribution on the hip joint.

As these considerations seem to be quite obvious, numerous clinicians summarized potential risk factors which may contribute to instability phenomena [74, 120, 194, 212, 278, 279, 308, 335, 422]. Most of these factors were classified into categories in order to establish treatment protocols for dislocated THRs: positional with no identifiable abnormality, soft tissue imbalance and component malposition [104, 105, 323]. Cup orientation has been controversially discussed to be one of the most critical factors [36, 202, 205, 240, 261, 270, 300, 422]. The discus-

sion is enforced by the fact that there are usually deviations between preoperative planning and postoperative outcomes [95, 191]. However, varying reference frames in describing cup orientation impede comparison and evidence concerning safe cup placement [282, 421, 430]. Further analyses [120, 174, 194] suggested that cup anteversion should be regarded in combination with stem antetorsion. Other orthopedic surgeons reported differences in clinical outcomes depending on the choice of surgical approach [87, 203, 229, 326, 392]. Especially, the posterior approach appears to be afflicted with higher dislocation rates when no soft tissue repair is performed [185, 306, 353, 407]. Other studies [152, 315] indicated successful outcomes as regards hip stability by implanting an unconstrained tripolar system. While these retrospective interpretations give directions to involved risk factors, clinical studies still remain ambiguous in explaining why and how dislocations occur.

According to Amstutz et al. [3] contact between the rim of the cup/inlay and the endoprosthetic neck may elevate dislocation risk and rim wear. This component-to-component impingement determines the technical RoM of THRs for given design and positioning parameters, which should be sufficient for hip joint motion during daily living activities. Hence, researchers investigated the largest possible RoM before impingement occurs considering parameters such as implant design [23, 151, 159, 224, 225], cup orientation [23, 103, 214, 226, 261, 431], head size [52, 65], head-neck ratio [3, 103], neck-to-shaft angle [413] and stem antetorsion [214]. Motivated by clinical investigations mentioned above, cup orientation was associated with stem antetorsion in mathematical formulations to gain optimal RoM and compatible positioning [182, 414, 432]. Ko et al. [217] extended the search for optimal stem and cup placement by taking optimization techniques and daily living activities into account. Furthermore, it was found that component-to-component impingement turns into bone-to-bone impingement by increasing femoral head size [24, 345].

Although recurrent impingement can be regarded as failure mechanism alone due to substantial damage found in THR retrievals [235, 351], it does not necessarily presage dislocation. Nicholas et al. [291] detected a change in torque during contact of the prosthetic neck with the cup rim depending on the cup/inlay design. Further studies based on mechanical setups [14, 15, 119, 207, 209] or the finite element method (FEM) [215, 343–345] analyzed THR stability under idealized load and movement conditions. Their outcomes revealed that additional angular motion is required beyond the instant of first impingement before frank dislocation occurs. During this subluxation process the femoral head is levered out which is characterized by a resisting torque rising due to two contact points and dropping towards dislocation. Hence, the magnitude of the resisting torque often served as quantity and indicator for this type of dislocation mechanism.

In order to examine joint stability closer to reality, those assessments needed to be expanded by introducing physiologically more reasonable conditions. In this sense, motion analyses indicated postoperative asymmetries between the operated and contralateral side

in THR patients during gait and stair-climbing [131, 230]. On the contrary, Lamontagne et al. [231] observed similar patterns in hip joint kinetics between THR patients and healthy subjects for seating and rising maneuvers. Since instrumented THRs enable measurements in patients, the postoperative loading on the hip joint has been gathered for a variety of activities [34, 80, 81, 115, 220, 332]. Bergmann et al. [33] provided synchronized data from movement analyses for several patients in addition to the force measurements. By analyzing unexpected stumbling of instrumented patients, Bergmann et al. [35] concluded that the mechanical functionality of muscles and bones works in a well-adjusted and optimized manner which is reflected by a nearly invariant force direction during high loading found throughout all activities. Based on this biomechanical groundwork, other researchers were able to validate their musculoskeletal models against present in vivo data to predict realistic hip joint forces for routine activities using optimization techniques [5, 46, 171, 254, 273, 274, 303, 358]. Several studies using such models also reported changes in muscle loading with alterations of positioning and design parameters which impact the location of the hip joint center with respect to the pelvic or femoral bone [83, 84, 170, 238, 239]. Since then it is well known that muscular forces significantly contribute on THR joint loading.

By including static muscle forces into their specimen-based experimental setup, Bartz et al. [24] and Scifert et al. [345] observed a second dislocation mechanism besides the impingement driven one: spontaneous separation due to traction forces. Higa et al. [180] indicated spontaneous dislocation under passive conditions to occur at cup anteversion angles above 10° for flexion movements with high adduction and internal rotation. Other researchers introduced realistic motion data and compliant hip joint forces derived from musculoskeletal models to simulate dislocation scenarios [208, 283, 284]. Pedersen et al. [304] illuminated Lewinnek et al.'s safe zone for cup placement [240] in view of activity dependent load cases accounting for both dislocation mechanisms. Their study made clear to distinguish between impingement and dislocation avoidance. Using the same approach for selected maneuvers, further studies revealed declined dislocation resistance for increased lip radii of the inlay owing to decreased head coverage [113], elevated risk for obesity patients due to thigh-to-thigh contact induced spontaneous separation [112], and compromised stability benefits for head sizes beyond 40 mm with intensified wear potential at the taper [110]. Beyond that, Elkins et al. [111] defined landing zones for optimal cup placement with varying head size and stem antetorsion by addressing both dislocation and bearing wear mechanisms. They inferred from their substantial analyses that almost no improvement is gained with the use of larger heads in light of maximizing stability and minimizing wear.

Due to the discussion concerning soft tissue repair (compare above), researches [268,355] evaluated the effect of reattached muscular and capsular structures with respect to dislocation by using full-leg specimens, indicating enlarged resistance under repair. Elkins et al. [114] validated a FEM based model of a THR surrounded by capsular tissue against specimen data

from a mechanical setup to evaluate the contribution of the capsule to THR stability. Their subsequent FEM analysis for a sit-to-stand maneuver associated to dislocation exposed a dramatic loss in the resisting torque from an intact or well-repaired to a defected capsule.

The outlined studies document that several biomechanical insights have been gained concerning THR dislocation. Design as well as positioning parameters define the technical RoM up to impingement. The process until final separation of the joint partners is well understood whereas two distinct mechanisms could be identified. Under these aspects, the risk of dislocation was investigated for associated load conditions with variation of certain parameters such as cup orientation, head size and head coverage. Furthermore, it was shown that the capsule is capable of providing additional resistance against dislocation. Nevertheless, dislocation still is one of the major causes for revision surgery. The reason for this circumstance is that there is still little evidence of the exact contribution of active and passive soft tissue structures to the dislocation process, whether intact, repaired or defected. This is especially the case when design and positioning parameters such as CCD angle or stem antetorsion change the geometric proportions of the skeletal system and hence overall musculoskeletal dynamics. Moreover, not all implant types such as tripolar, modular or revision systems have been subjected to thorough investigations.

1.2 Instability of Total Knee Replacements

Biomechanical complications after total knee arthroplasty comprise many different sources. The Swedish Knee Arthroplasty Register [375] considered about 2.800 revised subjects in a ten-year period identifying 19 % of the cases related to patellar problems, more than 13 % to instability and around 7 % to non-specified complications. A follow-up study including 909 revision procedures [195] listed 15.3 % patellar complications, 12.0 % malposition, 2.5 % dislocation and 35,2 % unspecified causes including instability. Schroer et al. [340] analyzed 844 revisions of six orthopedic institutions with 18.7 % of the cases due to instability, 6.6 % due to malalignment and 4.1 % due to patella revision. In accordance with Dalury et al. [79], the authors registered instability even as major cause of failure with 25.2 % by regarding only revisions less than two years after primary surgery. These findings underline that instability constitutes a predominant cause for TKR revision (Fig. 1.4), especially in an early stage. However, the various outcomes from study to study also illustrate that there is a high level of uncertainty to specify biomechanical causes for revision. One reason for these inconsistencies may arise from the fact that the TKR complications mentioned are strongly interconnected and lack of precise definition. Another reason why it is difficult to clearly categorize TKR failures may persist in the complexity of the knee joint per se and the changes present after surgery.

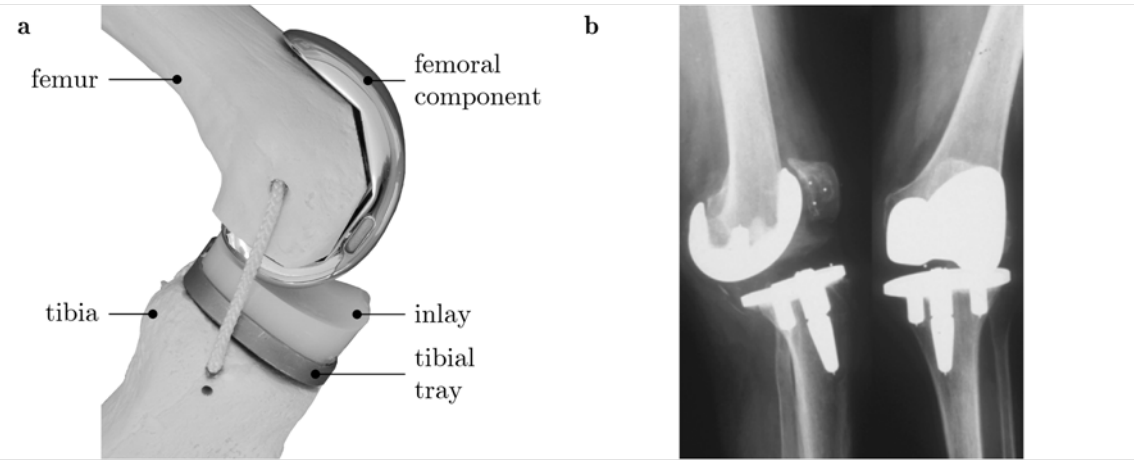

Fig. 1.4 Implanted bicondylar TKR. **a** Components of a posterior cruciate retaining TKR. **b** Radiographs of an unstable TKR, extracted from Bader et al. [14].

The native knee joint consists of three bone segments (tibia, femur and patella) and comprises two cartilaginous articulations [147, 341]. On the one hand, the patellofemoral joint characterizes the gliding contact between the retropatellar surface and the femoral trochlea situated between the femoral condyles. Due to the congruency of both contacting surfaces, the patella is geometrically guided along a translational path through the trochlear groove during tibiofemoral flexion/extension [2,176]. Medial and lateral soft tissue restraints further couple the patella to the femoral and tibial segment, the iliotibial tract and the menisci [72, 92, 264, 265, 294, 380]. As part of the extensor mechanism, the patella connects the quadriceps femoris muscle to the tibia via the patellar ligament. Due to the patellar deflection along the trochlear groove, the quadriceps muscle is able to apply an increased torque on the tibia to generate tibial extension.

On the other hand, the tibiofemoral joint describes the articulations between the medial and lateral condyles of the tibia and the femur, respectively, splitting the joint into two compartments. The contact surfaces of both femoral condyles are circular in shape with increasing curvature in anterior direction from a mediolateral view. Whereas the medial condyle of the tibia exhibits a slightly concave surface which appears to be somewhat congruent to its counterpart, the lateral condyle exhibits a convex form in the sagittal plane. Each compartment is filled with one meniscus attached to the tibial side which increases the contact area between the condyles. Due to the mismatch between the contacting surfaces in the two compartments, the relative mobility between the two bone segments are only constraint in one translational direction along the tibial shaft and one rotational as the two contact points impede tibial adduction/abduction.

A crucial part of the tibiofemoral joint is an intricate ligament apparatus reinforcing and enclosing the joint capsule [75, 143, 160, 169, 232–234, 380, 405]. Given the anatomic cir-

cumstances, it is essential for restraining and stabilizing relative motion in the tibiofemoral joint [11]: The primary resistance against anterior tibial displacement and drawer arises from the anterior cruciate ligament [53, 143, 334]. Other structures such as the iliotibial tract [53, 426] and the collateral ligaments [53, 325, 334, 372] limit larger anterior translation when the anterior cruciate ligament is deficient or absent. The posterior cruciate ligament is the primary restraint against posterior translation especially during flexion [53, 143, 145, 149]. If sectioned, all structures of the posterolateral corner [53, 145, 149, 391] as well as the posterior oblique ligament [309, 325] prevent larger posterior tibial displacements. Tight enclosure of the compartments by crucial and collateral ligaments minimize medial or lateral translations. Medial opening of the joint due to abduction (valgus) is mainly impeded by the medial collateral ligament [148, 325]. Tibial adduction (varus) is restricted by both the lateral collateral ligament and the structures of the posterolateral corner [145, 148, 149]. In this context, some researchers emphasize the importance of the popliteofibular ligament as major restraint [259, 391]. Furthermore, the combination of the anterior cruciate ligament, the lateral collateral ligament and the posterolateral structures governs internal rotation [145, 247]. External rotation is almost equally restrained by the lateral collateral ligament and the posterolateral corner [145, 149], especially the popliteofibular ligament [391]. Further loss of the posterior cruciate ligament increases external rotation [145, 149]. In full passive extension, the tibia is compulsory rotated externally due to tightening of the cruciate ligaments and the shape of the articulating surfaces [140]. This terminal rotation is reversed by activation of the popliteus muscle [169].

These considerations make clear that the ligamentous structures, single or in combination, play an important role in governing knee joint motion and guaranteeing its functionality. This means that passive ligament forces mainly contribute to patello- and tibiofemoral dynamics besides contact interactions, inertial and gravitational forces of the bone segments, and active muscle forces. As a result, the native knee joint shows particular kinematic characteristics. Pinskerova et al. [314] identified in both in vitro and in vivo analyses that posterior femoral translation with respect to the tibial plateau (so-called femoral rollback) mainly occurs in the lateral compartment and relates only to the movement of the contact points. As the medial femoral condyle rather tended to slide, they concluded that tibiofemoral motion is composed of flexion movements accompanied by femoral external rotation. Their findings were consistent to the studies of Blankevoort and co-workers [41, 42] who defined limits of internal/external rotation at each degree of flexion within which rather unconstrained motion is possible. Hence, the tibiofemoral joint may be considered as a joint with two degrees of freedom where adduction/abduction and the three translations are constrained directions with elastic compliance. Other studies [167, 387] documented that these joint characteristics also affect patellar kinematics and loading.

Total knee arthroplasty implicates several substantial changes compared to native knee characteristics. A bicondylar TKR consists of a femoral component, an inlay and a tibial tray. The design of the femoral component emulates the shape of the native proximal femur including the condyles and the trochlear groove, with design parameters such as condylar frontal, distal and posterior radii. The inlay (fixed or mobile bearing) is attached to the tibial tray and replicates the tibial plateau. Depending on the design its condyles conform more or less to the condylar radii of the femoral component. In general, surgeons can choose between four types of TKRs with varying component constraint [277]: Posterior cruciate retaining (PCR) TKRs where only the anterior cruciate ligament is sacrificed and which remain rather unconstrained; posterior stabilized (PS) implants where in addition the posterior cruciate ligament is replaced by a cam-post mechanism; varus-valgus constrained (VVC) implants with further limited rotational motion by a taller post guided along a deep femoral box; and rotating hinge implants which reduce the tibiofemoral joint to one degree-of-freedom in flexion/extension.

Although TKRs may vary in design and shape from brand to brand, the choice of the implant type already predefines the contact dynamics in both the patello- and tibiofemoral joint. Highly constrained implants may in fact substitute functionality of the ligament apparatus and therefore promise joint stability [260]. But they may provoke additional constraint forces at the implant-bone interface. Furthermore, standard surgical approaches such as the medial parapatellar approach require incision of patellar soft tissue restraints and the quadriceps tendon [336]. Despite excellent exposition of the surgical site they may entail patellar or other complications. Before TKR fixation, large bone resections on the femoral and tibial side are performed, defining the flexion and extension gaps into which the TKR components are to be placed [322]. They also predispose the orientation and alignment of the components and the joint line of the TKR [427]. During TKR implantation it is well accepted that ligament balancing plays a decisive role for a positive functional outcome. Any error during implant selection, bone resection as well as ligament balancing may contribute to ligament laxity or contracture, TKR malalignment and/or occurrence of additional space during flexion/extension movements. Moreover, all factors mentioned may inflict alterations in kinematics, muscle and joint loading within the lower limb.

Since TKR surgery represents a massive intervention to the knee, orthopedic surgeons are well aware of the challenges mentioned associated with a stable joint conjunction when using rather unconstrained implants. Nevertheless , instability phenomena still appear difficult to be clarified in daily clinical practice. Affected patients report from experiences such as a ”giving way” feeling or ”buckling” of their knee [122, 393]. Several instability patterns were described in retrospective studies [122, 263, 298, 342, 348, 383, 402, 403] reaching from subtle translational insufficiencies over severe valgus or hyperextension (genu recurvatum) positions to infrequent, complete dislocations. Pietsch et al. [313] summarized numerous influencing

factors including axial or rotational deviations, surgical errors in bone resection or soft tissue release and wrong choice of implant type or tibial inlay. Other clinicians [32,122,146,327,348, 356,393] listed several underlying causes besides ligamentous insufficiencies such as mismatch of the flexion/extension gaps, deficient extensor mechanism, malposition and malalignment of components and inadequate TKR design. Many of these causes also comprise patellofemoral complications [31, 48, 109]. Given these potential influencing factors and causes, instability phenomena were classified according to their occurrence into asymmetrical (varus-valgus) or symmetrical instability in extension, midflexion or anteroposterior instability in flexion and global instability [221, 276, 299, 327, 393, 427].

The clinical surveys and categorizations outlined above display a fundamental confusion arising with the term "instability". Ligamentous insufficiency, generally the cause of an unstable native knee joint, does not necessarily coincide with TKR instability. Nevertheless, it appears to be the basis of the clinical perception that instability is more related to kinematic indications than to mechanical stability [11, 286, 327]; such as larger translational and/or angular displacements in otherwise constrained directions with certain elastic compliance, or excessive motion along the free directions. Also, the term refers to phenomena on the artificial tibiofemoral rather than the patellofemoral joint; notwithstanding the fact that patellofemoral instability such as patellar subluxation or dislocation certainly compromises functionality of the extensor mechanism and, in return, tibiofemoral dynamics. This clinical perception, however, requires a deep understanding of how normal kinematics and loading of a stable TKR look like and where instability begins, in particular when using PCR or PS implants.

In this context, motion analyses revealed abnormal knee kinematics and muscular activity of TKR patients compared to healthy subjects [6, 30, 253, 262, 271, 371], despite functional improvement between pre and post surgery [184]. Since motion capturing systems are limited in illuminating the relative motion of the components in more detail, numerous studies placed emphasis on fluoroscopic techniques for in vivo investigations [157, 183]. Using fluoroscopy kinematic effects adverse to the normal knee were observed such as variable condylar lift-off [91,187,366] and opposite axial rotation patterns [21,90,366]. Stiehl et al. [368] recognized erratic and non-reproducible anteroposterior femoral translation as well as abnormal patellar mobility during flexion of PCR knees. This type of implant additionally showed a posterior position in extension, anterior translation during midflexion and a limited RoM, contrary to native knees [89, 368]. Bellemans et al. [29] detected impingement between the tibial inlay and the femoral back impeding larger flexion in the majority of their examined PCR patients. Aberrant kinematic patterns also persisted when using mobile bearing inlays instead of fixed inlays [66, 367, 404]. In contrast to that, PS implants with the cam-post mechanism generally indicated a more physiological performance [88,257], whereas further improvements were reported by using higher conformity between the articulating surfaces [9, 121], asymmetric

designs [55] or mobile bearing inlays [85]. Likewise, more physiological kinematics were observed in PCR knees with asymmetric designs of the femoral component [57,218] or the tibial inlay [269]. Although surgical factors such as tibial slope also influences tibiofemoral kinematics [56], these studies underscore that implant type and specific design features essentially contribute to overall TKR performance.

For a complete picture of TKR dynamics, researchers developed instrumented knee endoprostheses that enabled force measurements in vivo. Taylor and co-workers [376, 377] were the first to estimate forces and torques at the knee using a distal femoral replacement equipped with a rotating hinge joint. Based on cruciate retaining and sacrificing implants, a variety of daily and recreational activities were investigated with regard to axial forces [98, 99] or complete load data [96, 101, 168, 228]. The use of different implant types and designs, however, make the transfer from one study to the other difficult. Further studies examined the contact mechanics by including kinematic data, indicating greater contact forces in the medial compartment for several activities [281, 388, 438]. The load distribution was found to correlate with the TKR alignment in the frontal plane [154]. Apart from daily activities, intraoperative force measurements displayed that substantial soft tissue balancing, including recuts and soft tissue release, is required after the initial bone cuts to avoid imbalance [97].

Although in vivo measurements provided the groundwork on TKR dynamics, they are not suitable to consider instability scenarios due to ethical reasoning. Therefore, specimen-based testing has been widely used for assessing TKR kinematics and stability under the influence of surrounding soft tissue. Analogous to the fluoroscopic studies aforementioned, TKRs were analyzed with respect to kinematics of rotating and mobile bearings [102,370], effect of femoral and inlay design [50, 369, 408, 409] and functionality of the cam-post mechanism of PS implants [242, 243, 295]. Even though native knee mechanics may not be fully restored by PCR or PS designs, researchers [244, 280] stressed the essential role of a well-functioning posterior cruciate ligament or cam-post mechanism, respectively. According to Yildirim et al. [429] certain improvements could also be obtained by design features which affect the guidance of motion. Besides implant designs, it was substantiated that an internal rotated and/or a medial shifted femoral component deteriorates varus-valgus stability during flexion [8], and causes patellar maltracking [319, 320]. An external malrotated femoral component was seen to restrict rotations in the same direction [285]. Furthermore, elevation of the joint line was demonstrated to augment laxity during midflexion [256] and adversely affect patellofemoral contact mechanics [129]. Werner et al. [406] noted that variations in varus-valgus alignment of the tibial tray resulted in an unequal pressure distribution between the two compartments. The authors also noticed unacceptable adduction/abduction patterns with slightly lax collateral ligaments which highlights the importance of correct ligament tensioning to provide varus-valgus but also rotational stability [410]. Generally, TKR implantation led to different ligamentous strains [86, 251] and an increase of required quadriceps force [296],

compared to native knees. Several studies [198,258,333,411] considered soft tissue release to be an effective tool in treating ligament contractures if performed in consideration of their function on knee stability. Other analyses suggested that soft tissue tension could be reduced by an increased tibial slope [297], a thinner tibial inlay [251] or a PS implant [292], at least for larger flexion angles.

For deeper insights on relevant factors influencing TKRs dynamics other methods have been employed which allow analyses on a reproducible and comparable base. Distraction tests on rotating hinge TKRs confirmed the suspected risk of instability and dislocation for shorter stems with large tapers [401]. By using mechanical test setups researchers compared TKR functionality of varying implant types and designs quantifying significant differences in relative movements [93, 153, 397, 398]. Luger et al. [250] ascertained the tendency of a low conformity PCR design to anterior subluxation as well as immoderate external/internal rotation under low compressive loads without restraints. Likewise, multibody system (MBS) models based on standards for constraint testing were developed to assess the kinematic behavior of a PCR implant [275], and find an optimized PCR design under predefined load situations [416]. Piazza et al. [312] concluded from an analytical approach that posterior tibial slope diminishes femoral rollback in PS implants due to reduced cam-post interactions.

Beyond that, researchers developed MBS or FEM models validated against in vitro test setups. Whereas plenty of studies focused on describing the contact mechanics and dynamics of various implant types and designs [17, 18, 22, 100, 117, 123, 126, 155, 248, 433, 437], others investigated parameters impacting both joint mechanics and stability. Femoral malrotation was proven to cause patellar maltracking and hence malalignment of the extensor mechanism [71, 124, 204]. It also induces varus/valgus alignment during flexion elevating collateral ligament forces [382]. Sensitivity analyses on PS and rotating hinge TKRs [186, 310] demonstrated that TKR kinematics and contact forces can be easily altered by positioning and anatomical parameters, irrespective of the implant type. Fitzpatrick and co-workers [127,128] extended such common parameter variations by considering the impact of most conceivable design, surgical and subject-specific parameters on TKR mechanics. According to their probabilistic evaluations, the radii of the femoral condyle, the joint line position, tibial slope and varus-valgus alignment were most influential parameters besides subject-specific ones. They also pointed out that there is a strong correlation between surgical parameters and ligament forces, as widely accepted among surgeons. Zelle et al. [436] recognized in a couple of their FEM simulations the tibial inlay to anteriorly lift off from the tray, or the femoral component to subluxate by excessively rolling back and rotating internally; both phenomena were observed in simulations with an overtight posterior cruciate ligament. In cases of normal or low ligament tension, the authors even noticed anterior femoral translation as described earlier. This specific instability pattern could be attributed by Clary et al. [67] to PCR implant designs where the radii of the femoral condyles abruptly drop in posterior direction.

The same study also outlined that the amount of anteroposterior translation is governed by the conformity of the tibial inlay.

As for the hip joint, more and more musculoskeletal models have been established to evaluate tibiofemoral [5, 142, 164, 206, 210, 246, 249, 274, 311, 378, 381, 417] but also patellofemoral [349, 384] joint dynamics incorporating active muscular forces. The quoted models were generally validated against motion analysis, electromyogram (EMG) as well as contact force data derived from TKR patients. Heller et al. [173] demonstrated that extreme varus or valgus alignment elevated tibiofemoral joint reaction forces and shifted the adduction/abduction torque within their model-based study. Elevation of the joint line could be correlated to an increase in tibiofemoral and especially patellofemoral loading during daily activities [219]. By considering the load distribution between the two compartments, other studies [350, 417] revealed the role of muscle and ligament forces to counterbalance the adduction torque in the knee joint which would otherwise lead to unloading of the lateral compartment. In this way, quadriceps, hamstring and gastrocnemii muscles were shown to essentially contribute to knee stability in the frontal plane.

All these biomechanical studies highlight the tremendous effort spent to gain insights on TKR functionality and improvements in their overall performance. That way, kinematic patterns were detected, such as anterior femoral translation, opposite internal/ external rotation or condylar lift-off, erratic or adverse to the native knee. For obtaining comparable joint kinematics, it is well substantiated that several design and surgical factors have a deep impact on tibiofemoral dynamics. These include femoral radii and tibial conformity on the one hand, and varus-valgus alignment, femoral rotation, tibial slope and joint line position on the other hand. The same accounts for the imperative of well-balanced collateral ligaments, and a well-functioning posterior cruciate ligament for PCR implants. Apart from these investigations, however, there is almost no biomechanical evidence on instability phenomena and patterns seen clinically, let alone their quantification. One potential reason for this lies in the fact that deeper insights on these issues require analyses of instability-associated maneuvers with incorporation of passive and active soft tissue structures; a demand not yet addressed by present testing or simulation methods. In this sense, the exact contribution of ligaments and muscles remains rather unknown to the process leading to erratic or excessive motion, subluxation or frank dislocation, regardless of whether intact, incised or released. This is intensified by clinical notions that certain design and surgical parameters, known to influence TKR kinematics and loading, may provoke instability patterns in patients. Moreover, further constrained implant types such as VVC or rotating hinge implants have not been evaluated in-depth as regards their effect on joint stability.

1.3 Aims and Scope of the Work

Instability after total joint arthroplasty remains a challenging complication to deal with in daily clinical practice. Both the obscurity often related to this type of joint failure and the severe consequences for patients, especially in case of dislocation, make it difficult for clinicians to find appropriate countermeasures. As treatment of affected joints most commonly ends in revision surgery with further drawbacks and risks, it is of major interest to prevent instability phenomena in the first place. Prevention, however, requires comprehension of underlying mechanisms and decisive factors influencing the instability process. In order to obtain insights on these issues, biomechanical investigations are invaluable which at best cope with the demands of in vivo analyses. More precisely, this would mean to capture the dynamics of the replaced joint or the complete musculoskeletal system involved, respectively, even for maneuvers where instability phenomena are likely to occur. With this prerequisite it is clear that testing on TJR patients is out of question.

In fact, much has been achieved by means of test and simulation methods commonly accepted among biomechanical researchers. The major failure mechanisms related to THR dislocation were identified along with contributing factors such as specific motion patterns, implant design and positioning parameters (see chapter 1.1). Factors impacting TKR kinematics and loading have been highlighted in a series of diverse studies that are closely related to tibiofemoral joint stability. Potential TKR instability patterns were also spotted like paradoxical anteroposterior translation, adverse rotations or lift-off phenomena (see chapter 1.2). However, there is still little evidence on the dynamic interdependencies between the implant components and the anatomic environment during instability events in vivo. This especially applies on the response of surrounding soft tissues including passive ligament and capsular structures as well as active muscles. In this context, all studies and approaches on THR or TKR stability entail certain shortcomings, such that reliable and reproducible analyses are scarce meeting the demands mentioned.

The purpose of this work is to present a comprehensive approach which is capable of testing TJR stability under dynamic, reproducible and physiological conditions. The approach is based on a hardware-in-the-loop (HiL) simulation where a robotic physical setup interacts with a mathematical model. Functionality of the physical setup [119, 175] and appropriate control modes for use in HiL simulations [177, 196, 197] was verified in previous works. Therefore, the main objective within this work is the validation of the HiL test system. This includes the development of specific biomechanical models which define physiological test conditions with regard to THR and TKR testing. Certainly, there is no direct comparison possible to instability or even dislocation events of affected patients. On this account, an alternative validation strategy is followed within this work. For testing THRs, the HiL test system is validated against in vivo data retrieved from normal patient activities. Due to

the significant contribution of the ligaments to knee stability, the validation for TKR testing focuses primarily on a physiological replication of TKR dynamics compared to in vitro conditions.

Given these aims, the scope of this work comprises first the basic concept and underlying principles of the HiL simulation for testing TJRs, in extension to the compendious descriptions in previous works [175, 177, 196, 197]. This is followed by a brief overview of all components of the physical setup as well as the control mode and architecture used. The mathematical theory for biomechanical modeling is outlined in more detail based on a MBS formulation. The second part of the work is addressed to dynamic testing of THRs. It comprehends the functional principle of the HiL simulation used for THR testing and the establishment of a musculoskeletal model based on motion analyses. The chapter finalizes with HiL simulations that are validated against in vivo data derived from THR patients. In a similar manner, dynamic testing of TKRs is introduced in the third part, with representation of a MBS model of the artificial knee joint and validation of the HiL test system against data from an in vitro study. Finally, the application of HiL simulations as a novel testing tool is discussed in the light of common test and simulation methods. The discussion also illuminates the outcomes and limitations of the HiL simulations presented along with potential contributions to the current state of research concerning THR and TKR instability. Conclusions based on the HiL test system at this stage and an outlook on prospective projects complete this work.

2 HiL Simulation for Testing Total Joint Replacements

The underlying concept of how HiL simulations can be utilized for TJR testing is depicted at the beginning of this chapter. The description expands succinct presentations given in previous works [175, 177, 196, 197]. This is followed by an introduction of the physical setup including an industrial robot, along with the control strategy and architecture implemented. Concerning the mathematical model, rigid multibody systems are used to deliver the boundary conditions for the physical setup. Within this modeling approach, bones are treated as non-deformable bodies which are mutually linked by idealized joints. The approach is chosen as MBS models are particularly suitable for real-time applications such as HiL simulations [337], in contrast to FEM models. The MBS formulation presented is based on the theoretical background in the literature [338, 339, 420]. Emphasis is placed on its application on musculoskeletal modeling which allows for consideration of soft tissue structures.

2.1 Concept of HiL Simulations

Testing of real components requires boundary conditions which resemble at best the real environment of the components in situ. However, realistic boundary conditions may often be not applicable due to environmental complexity or lack of appropriate input data impeding real testing within an experimental setup alone. One way to overcome these difficulties is to follow a hardware-in-the-loop approach. During such an approach, the performance of real components is evaluated in a mathematically or often numerically described environment which is simulated on a process computer [188]. Both real component and process computer interact within closed control loops such that the in situ environment is approximated by the computed environment. In this manner, HiL simulations were successfully applied in automotive research using MBS models to simulate real-time vehicle dynamics [108, 210, 331]. In spacecraft engineering industrial robots were implemented into a HiL environment to investigate the contact dynamics during rendezvous and docking maneuvers of satellites [43, 223]. Other examples are given for testing of combustion engine control systems [189] and biomedical devices [156]. These applications illustrate that HiL simulations expand

the common repertoire of testing methods by implementing mathematical and numerical methods into the test environment.

One of the key problems in implant testing is how to adequately address soft tissue structures in an experimental setup. On the one hand, ligaments and capsular structures apply passive forces on bone segments when deflected. Experimental studies based on in vitro conditions normally provide these structures and their physiological response during testing. However, the outcomes of in vitro studies cannot be reproduced due to the decay of the human specimens. This means that in vitro testing does not render any comparative results under exactly the same boundary conditions. Other test approaches, which emulated ligaments by implementation of restraints into the test setup [93,250,397,398], reflect the anatomic environment only to a limited extend. On the other hand, muscle structures actuate bone segments by active forces which are governed by the input of the nervous system. As these structures are almost impossible to account for experimentally, most test approaches oversimplified muscular function by assuming constant [14, 119, 153, 250, 291, 397, 398] or prescribed [209, 252] load application.

In contrast to previous test approaches, evaluation of implant functionality and stability requires dynamic testing under reproducible and physiological conditions. The essential idea of the approach followed within the scope of this work is to extract the anatomic and physiological environment of the implant components into a mathematical model (Fig. 2.1). Actuator and sensor systems are required, in order to achieve interaction between the model and the real implant components. These form a physical setup where the implant components are attached to. The actuator system applies motion and forces onto the implant components according to the boundary conditions delivered by the model. The sensor systems measure the implant response which is transferred back to the model. Hence, both the physical setup and the model interact within a real-time environment forming a HiL simulation.

While the framework of the outlined HiL simulation remains the same, the specific configuration depends on the functionality of the artificial joint. In general, the mobility of segments are restricted by articulations to other segments. Considering these articulations as idealized joints, the relative mobility between adjacent segments is described by a complementary set of free and constraint spatial directions [197]. This means that motion between two segments

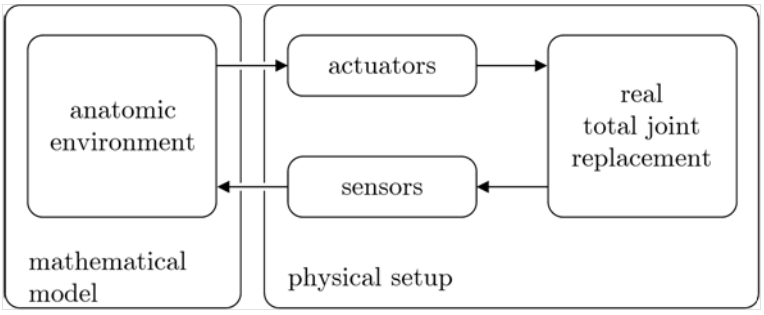

Fig. 2.1 Interactions between the real TJR embedded into the physical setup and the mathematical model that provides the anatomic environment form the HiL simulation.

is generated if forces/torques τ_i^{f} are applied along the free directions of the joint q_i as highlighted in the examples given in Fig. 2.2. On the contrary, the geometry of the joint inhibits relative movement which causes forces/torques f_i^{r} and l_i^{r}, respectively, in the constrained directions z_i. These joint characteristics of free and constraint directions are used to identify an appropriate control strategy for the actuator system.

The decision which strategy to take for a real artificial joint depends on the mechanical compliance of the contact along the six spatial directions. The compliance also predefines in which directions the mathematical model determines motion or force quantities. In general, high compliance or even free motion requires position control. Therefore, the model determines the relative displacements in directions with high compliance which the robot has to follow in position control mode. Contact forces along these directions are considered as applied forces within the model. On the contrary, low compliance to the point of rigid body contact favors force control. Hence, directions of low compliance are treated as constraints in the model. The model then calculates the coordinates of the corresponding reaction forces which are applied onto the artificial joint by the robot running in force control.

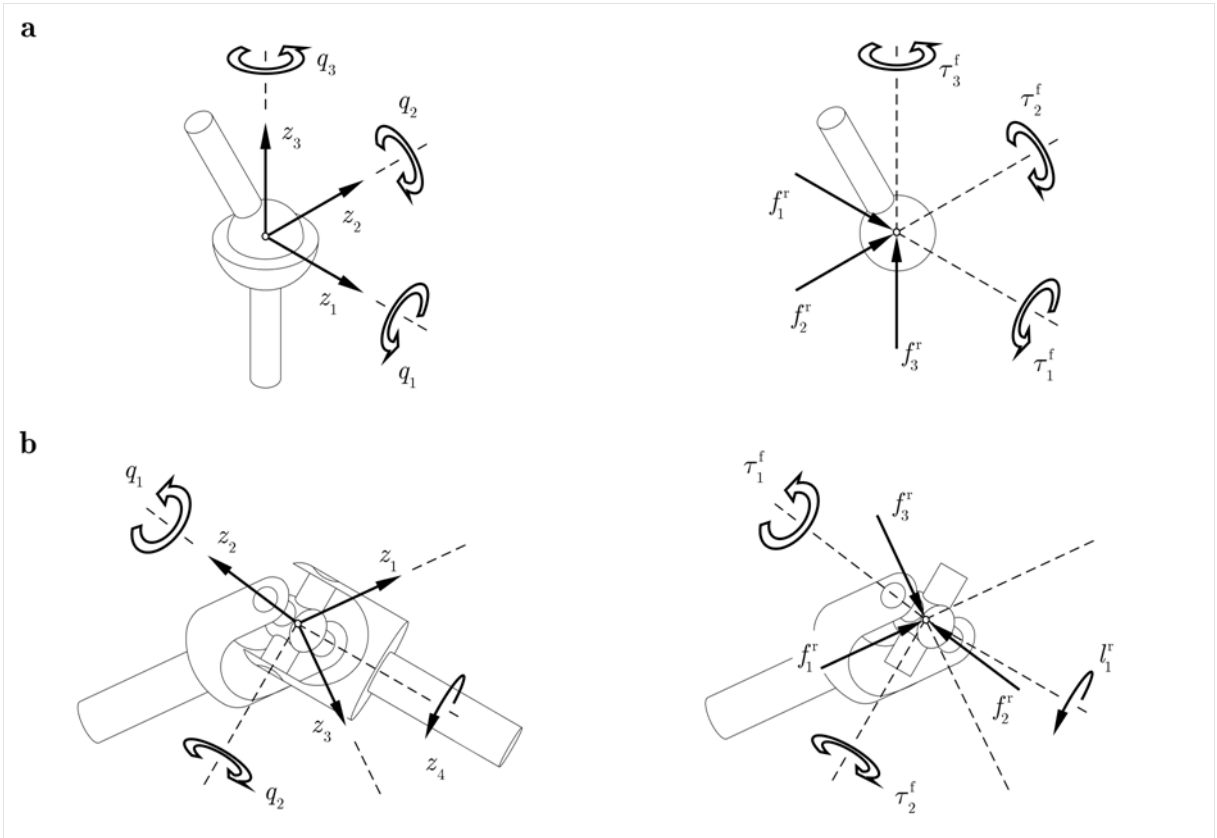

Fig. 2.2 Free and constraint directions on kinematic and force levels. Torques τ_i^{f} generate motion if applied along the joint coordinates q_i. The joint geometry defines reaction forces/torques f_i^{r} and l_i^{r}, respectively, in the constraint directions z_i. **a** Spherical joint, extracted from Kaehler et al. [197]. **b** Universal joint.

2.2 Physical Setup

2.2.1 Components and Hybrid Position-Force Control

The physical setup has two major components (Fig. 2.3). On the one hand, there is a six-axis industrial robot (TX200, Stäubli Tec-Systems GmbH, Bayreuth, Germany) which is equipped with a six degree-of-freedom force-torque sensor (Omega 160, ATI Industrial Automation, Apex, North Carolina, USA). The robot serves as actuator system of the physical setup and is capable of generating both force and range of motion required for various implant types. On the other hand, there is a compliant support mounted on a ground-fixed framework. It consists of three serially arranged prismatic joints with orthogonal axes. Springs restrain the displacements along these axes providing elastic compliance in the three translational directions which are recorded by displacement sensors (MSK 5000, SIKO, Buchenbach, Germany). Mounting devices were attached to both the end-effector of the robot and the compliant support such that the real implant components (with or without bone geometries) can be attached to the physical setup.

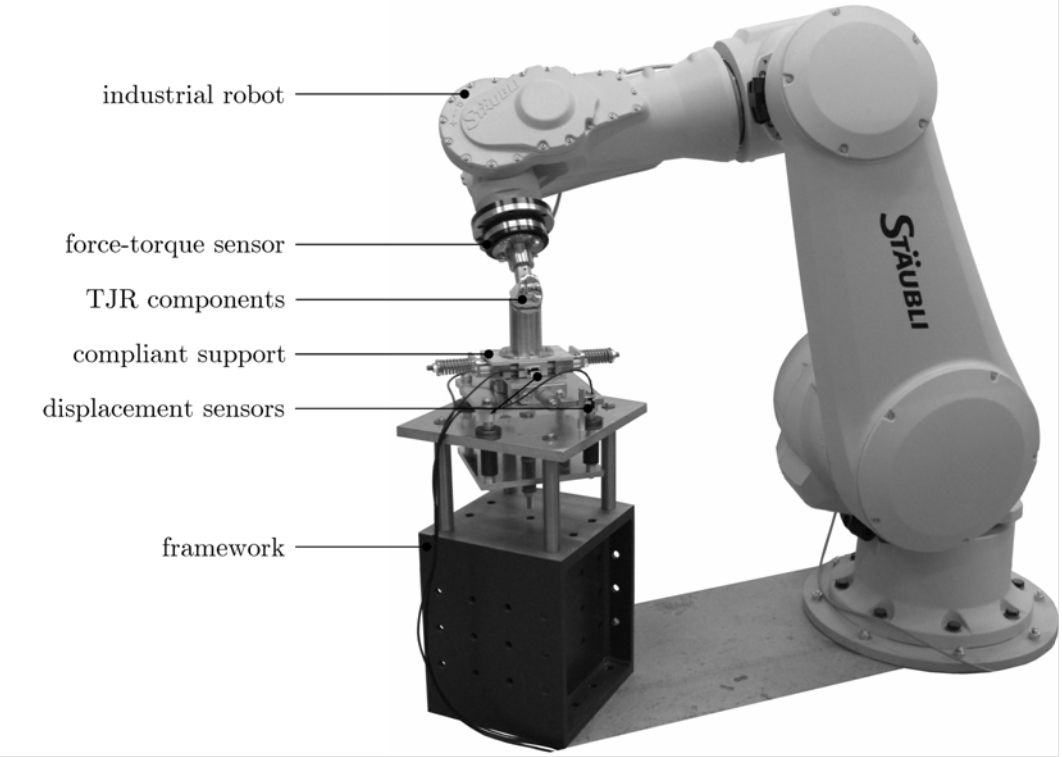

Fig. 2.3 Physical setup consisting of an industrial robot and a compliant support mounted on a framework. The TJR components are fixed on mounting devices attached to the end-effector and the compliant support. Measurements are taken via the force-torque sensor and displacement sensors.

In order to move and load an artificial joint according to its free and constraint directions (compare 2.1), the robot runs in hybrid position-force control. Implementation of this control strategy and its functionality within a HiL simulation are described elsewhere [177,197]. The position control is achieved by the robot controller (CS8C HP, Stäubli Tec-Systems GmbH, Bayreuth, Germany) running with a control cycle of 4 ms in its standard configuration. Outer force regulating control loops are used for force control generating the control input for the inner position and velocity controllers. This means that the robot moves in the constrained direction until the force, applied onto the compliant support and measured by the force-torque sensor, coincide with the corresponding desired value [352]. Relative displacements between implant components are estimated by comparing the position of the end-effector with respect to the compliant support. Moreover, occurring torques along the free directions are measured by the force-torque sensor.

2.2.2 Control Architecture

During HiL simulations the physical setup and the mathematical model are embedded into a control system [175, 177] which enables the information transfer between all components involved (Fig. 2.4). Within the control system, robot, sensors and the model communicate in the same time frame based on the control cycle of the robot controller. The step size of the solver in the model corresponds to the control cycle, or a fraction of it if a scaling factor is introduced between real time and simulation time. The robot controller accounts for synchronization between the continuous-time integrator and the discrete-time controller in the robot hardware in cases where numerical integration is used in the model.

All information are exchanged between model and robot before the beginning of a new time step. The robot receives the desired values from the last computational step of the model and sends current measurements. During computation of the next time step, the robot moves and loads the attached implant components according to the desired values received.

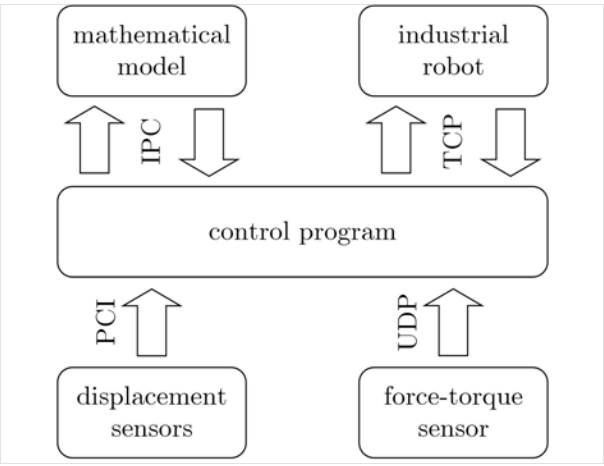

Fig. 2.4 Control system connecting all components of the HiL simulation via interfaces, extracted from Herrmann and co-workers [175, 177]. Interprocess communication (IPC) protocol, transmission control protocol (TCP), peripheral component interconnect (PCI) bus and user datagram protocol (UDP) are used as interfaces.

2.3 Modeling of Musculoskeletal Systems

2.3.1 Kinematics of Skeletal Systems

The mathematical description of musculoskeletal systems is based on a MBS formulation which has been proven to be suitable for real-time applications such as HiL simulations [337]. Within this approach, bone segments are treated as rigid bodies. These are mutually linked by idealized joints. In general, the topology of MBS models can be differentiated into open systems with chain-like or tree-like structures, and closed systems containing kinematic loops.

At first, a tree-structured topology is considered. The skeletal system accounted for in the modeling task consists of p bone segments. The segments are constrained by joints along the kinematic chain of the system that are mathematically described by b holonomic constraints. The overall degrees of freedom f of the system is then given by

$$f = 6p - b. \tag{2.1}$$

This includes b_z constraints of the artificial joint being of interest within the HiL simulation, where $b_\mathrm{z} \subseteq b$. Accordingly, the spatial motion is described by f joint coordinates $\boldsymbol{q} \in \mathbb{R}^f$ and b_z coordinates in constrained directions of the artificial joint $\boldsymbol{z} \in \mathbb{R}^{b_\mathrm{z}}$,

$$\boldsymbol{q} = [q_1 \dots q_f]^\mathrm{T} \qquad \text{and} \qquad \boldsymbol{z} = [z_1 \dots z_{b_\mathrm{z}}]^\mathrm{T}. \tag{2.2}$$

Hence, the position and orientation of the i-th segment along the kinematic chain can be explicitly expressed in terms of the coordinates $\boldsymbol{q}$ and $\boldsymbol{z}$,

$$\boldsymbol{r}_i = \boldsymbol{r}_i(\boldsymbol{q}, \boldsymbol{z}) \qquad \text{and} \qquad \boldsymbol{S}_i = \boldsymbol{S}_i(\boldsymbol{q}, \boldsymbol{z}), \tag{2.3}$$

where $\boldsymbol{r}_i \in \mathbb{R}^3$ denotes the position vector and $\boldsymbol{S}_i \in \mathbb{R}^{3,3}$ the rotation matrix [338, 339] with respect to the inertial frame. The translational and rotational velocities of the i-th segment are given by

$$\boldsymbol{v}_i = \boldsymbol{J}_{\mathrm{T}i}(\boldsymbol{q}, \boldsymbol{z})\, \dot{\boldsymbol{q}} \qquad \text{with} \qquad \boldsymbol{J}_{\mathrm{T}i} = \frac{\partial \boldsymbol{v}_i}{\partial \dot{\boldsymbol{q}}}, \tag{2.4}$$

$$\boldsymbol{\omega}_i = \boldsymbol{J}_{\mathrm{R}i}(\boldsymbol{q}, \boldsymbol{z})\, \dot{\boldsymbol{q}} \qquad \text{with} \qquad \boldsymbol{J}_{\mathrm{R}i} = \frac{\partial \boldsymbol{\omega}_i}{\partial \dot{\boldsymbol{q}}}, \tag{2.5}$$

with the translational and rotational Jacobian matrices $\boldsymbol{J}_{\mathrm{T}i} \in \mathbb{R}^{3,f}$ and $\boldsymbol{J}_{\mathrm{R}i} \in \mathbb{R}^{3,f}$, respectively. The time derivatives of the coordinates $\boldsymbol{z}$ are neglected, i.e. $\dot{\boldsymbol{z}} = \ddot{\boldsymbol{z}} = \boldsymbol{0}$. By further differentiation with respect to the inertial frame, the translational and rotational

accelerations of the i-th segment are obtained as

$$\dot{\boldsymbol{v}}_i = \boldsymbol{J}_{\mathrm{T}i}(\boldsymbol{q}, \boldsymbol{z})\, \ddot{\boldsymbol{q}} + \bar{\boldsymbol{a}}_i \qquad \text{with} \qquad \bar{\boldsymbol{a}}_i = \dot{\boldsymbol{J}}_{\mathrm{T}i}(\boldsymbol{q}, \dot{\boldsymbol{q}}, \boldsymbol{z})\, \dot{\boldsymbol{q}}, \tag{2.6}$$

$$\dot{\boldsymbol{\omega}}_i = \boldsymbol{J}_{\mathrm{R}i}(\boldsymbol{q}, \boldsymbol{z})\, \ddot{\boldsymbol{q}} + \bar{\boldsymbol{\alpha}}_i \qquad \text{with} \qquad \bar{\boldsymbol{\alpha}}_i = \dot{\boldsymbol{J}}_{\mathrm{R}i}(\boldsymbol{q}, \dot{\boldsymbol{q}}, \boldsymbol{z})\, \dot{\boldsymbol{q}}. \tag{2.7}$$

Under certain circumstances the motion of the system is further constrained by kinematic loops [420]. Such constraints are given when, for instance, more than one extremity is in contact with the ground leading to a closed kinematic chain [389]. The result are interdependencies among the joint coordinates $\boldsymbol{q}$ reducing the degrees of freedom from Eq. (2.1) to

$$f_{\mathrm{c}} = f - b_{\mathrm{c}}, \tag{2.8}$$

where b_{c} denotes the number of loop closure constraints. Eq. (2.8) represents the Chebychev-Grübler-Kutzbach criterion [420] for only one kinematic loop. The b_{c} constraints are implicitly written in terms of the coordinates $\boldsymbol{q}$ and $\boldsymbol{z}$ as

$$\boldsymbol{g}(\boldsymbol{q}, \boldsymbol{z}) = \boldsymbol{0}, \tag{2.9}$$

$$\dot{\boldsymbol{g}}(\boldsymbol{q}, \boldsymbol{z}) = \boldsymbol{G}(\boldsymbol{q}, \boldsymbol{z})\, \dot{\boldsymbol{q}} = \boldsymbol{0} \qquad \text{with} \qquad \boldsymbol{G} = \frac{\partial \boldsymbol{g}}{\partial \dot{\boldsymbol{q}}}, \tag{2.10}$$

$$\ddot{\boldsymbol{g}}(\boldsymbol{q}, \boldsymbol{z}) = \boldsymbol{G}(\boldsymbol{q}, \boldsymbol{z})\, \ddot{\boldsymbol{q}} + \bar{\boldsymbol{\eta}} = \boldsymbol{0} \qquad \text{with} \qquad \bar{\boldsymbol{\eta}} = \dot{\boldsymbol{G}}(\boldsymbol{q}, \dot{\boldsymbol{q}}, \boldsymbol{z})\, \dot{\boldsymbol{q}}, \tag{2.11}$$

at the position, velocity and acceleration levels. The rows of the derivative matrix $\boldsymbol{G} \in \mathbb{R}^{b_{\mathrm{c}}, f}$ indicate the constrained directions of the the loop closure constraints.

2.3.2 Musculoskeletal Dynamics

The skeletal system is set in motion when forces and torques are applied onto the bone segments. Defined by their geometry, joints constrain the relative mobility between linked segments causing reaction forces and torques. These interactions between motion and acting forces and torques constitute the dynamic behavior of the skeletal system.
For a given rigid segment i with the mass m_i and the inertia tensor $\boldsymbol{I}_i \in \mathbb{R}^{3,3}$, the translational and rotational interactions are mathematically described by Newton's and Euler's equation, respectively. The equations are written with respect to the segment's center of gravity as

$$m_i \dot{\boldsymbol{v}}_i = \boldsymbol{f}_i^{\mathrm{e}} + \boldsymbol{f}_i^{\mathrm{r}}, \tag{2.12}$$

$$m_i \dot{\boldsymbol{\omega}}_i + \widetilde{\boldsymbol{\omega}}_i \boldsymbol{I}_i \boldsymbol{\omega}_i = \boldsymbol{l}_i^{\mathrm{e}} + \boldsymbol{l}_i^{\mathrm{r}}, \tag{2.13}$$

with the applied forces $\boldsymbol{f}_i^{\mathrm{e}} \in \mathbb{R}^3$ and torques $\boldsymbol{l}_i^{\mathrm{e}} \in \mathbb{R}^3$, and the reaction forces $\boldsymbol{f}_i^{\mathrm{r}} \in \mathbb{R}^3$ and torques $\boldsymbol{l}_i^{\mathrm{r}} \in \mathbb{R}^3$. The left side of Eqs. (2.12) and (2.13) characterize the inertial forces and torques, respectively, which arise during acceleration of the segment.

For a tree-structured multibody system with p segments, Eqs. (2.12) and (2.13) yield a system of $6p$ equations. Describing the velocities and accelerations in terms of the coordinates $\boldsymbol{q}$ and $\boldsymbol{z}$ according to Eqs. (2.4) to (2.7), the global Newton-Euler equations are expressed in matrix notation with respect to the inertial frame as

$$\underbrace{\begin{bmatrix} m_i\boldsymbol{E} & & \boldsymbol{0} & \boldsymbol{0} & & \boldsymbol{0} \\ & \ddots & & & \ddots & \\ \boldsymbol{0} & & m_p\boldsymbol{E} & \boldsymbol{0} & & \boldsymbol{0} \\ \boldsymbol{0} & & \boldsymbol{0} & \boldsymbol{I}_i & & \boldsymbol{0} \\ & \ddots & & & \ddots & \\ \boldsymbol{0} & & \boldsymbol{0} & \boldsymbol{0} & & \boldsymbol{I}_p \end{bmatrix}}_{\widehat{\boldsymbol{M}}(\boldsymbol{q},\boldsymbol{z})} \underbrace{\begin{bmatrix} \boldsymbol{J}_{\mathrm{T}i} \\ \vdots \\ \boldsymbol{J}_{\mathrm{T}p} \\ \boldsymbol{J}_{\mathrm{R}i} \\ \vdots \\ \boldsymbol{J}_{\mathrm{R}p} \end{bmatrix}}_{\boldsymbol{J}(\boldsymbol{q},\boldsymbol{z})} \ddot{\boldsymbol{q}} + \underbrace{\begin{bmatrix} m_i\bar{\boldsymbol{a}}_i \\ \vdots \\ m_p\bar{\boldsymbol{a}}_p \\ \boldsymbol{I}_i\bar{\boldsymbol{\alpha}}_i + \widetilde{\boldsymbol{\omega}}_i\boldsymbol{I}_i\boldsymbol{\omega}_i \\ \vdots \\ \boldsymbol{I}_p\bar{\boldsymbol{\alpha}}_p + \widetilde{\boldsymbol{\omega}}_p\boldsymbol{I}_p\boldsymbol{\omega}_p \end{bmatrix}}_{\hat{\boldsymbol{\tau}}^{\mathrm{c}}(\boldsymbol{q},\dot{\boldsymbol{q}},\boldsymbol{z})} = \underbrace{\begin{bmatrix} \boldsymbol{f}_i^{\mathrm{e}} \\ \vdots \\ \boldsymbol{f}_p^{\mathrm{e}} \\ \boldsymbol{l}_i^{\mathrm{e}} \\ \vdots \\ \boldsymbol{l}_p^{\mathrm{e}} \end{bmatrix}}_{\hat{\boldsymbol{\tau}}^{\mathrm{e}}(\boldsymbol{q},\dot{\boldsymbol{q}},\boldsymbol{z},\boldsymbol{a})} + \underbrace{\begin{bmatrix} \boldsymbol{f}_i^{\mathrm{r}} \\ \vdots \\ \boldsymbol{f}_p^{\mathrm{r}} \\ \boldsymbol{l}_i^{\mathrm{r}} \\ \vdots \\ \boldsymbol{l}_p^{\mathrm{r}} \end{bmatrix}}_{\hat{\boldsymbol{\tau}}^{\mathrm{r}}(\boldsymbol{q},\boldsymbol{z})} \tag{2.14}$$

with the unit matrix $\boldsymbol{E} \in \mathbb{R}^{3,3}$, the global Jacobian matrix $\boldsymbol{J} \in \mathbb{R}^{6p,f}$ and the mass matrix $\widehat{\boldsymbol{M}} \in \mathbb{R}^{6p,6p}$ containing the inertial properties of the segments. Coriolis and centrifugal forces as well as gyroscopic torques are summarized in vector $\hat{\boldsymbol{\tau}}^{\mathrm{c}} \in \mathbb{R}^{6p}$. Applied forces and torques are merged in vector $\hat{\boldsymbol{\tau}}^{\mathrm{e}} \in \mathbb{R}^{6p}$. Moreover, vector $\hat{\boldsymbol{\tau}}^{\mathrm{r}} \in \mathbb{R}^{6p}$ contains the reaction forces and torques of the joints along the kinematic chain which are defined as

$$\hat{\boldsymbol{\tau}}^{\mathrm{r}} = \boldsymbol{Q}(\boldsymbol{q},\boldsymbol{z})\boldsymbol{\lambda}^{\mathrm{r}}, \tag{2.15}$$

where the columns of matrix $\boldsymbol{Q} \in \mathbb{R}^{6p,b}$ indicate the constrained directions of the joints and vector $\boldsymbol{\lambda}^{\mathrm{r}} \in \mathbb{R}^{b}$ reaction force coordinates along these directions [339]. Matrix $\boldsymbol{Q}$ can be obtained from the b holonomic constraints of the joints written in implicit form [420].

In case of tree-structured systems, the Newton-Euler equations can be further reduced to a minimal set of equations where the motion of the kinematic chain can be directly evaluated with respect to the applied forces. According to the principle of virtual work, the virtual work of reaction forces vanishes as virtual movement and reaction forces are orthogonal [339, 420]. Given the reaction forces and torques according to (2.15) and the virtual movement in terms of the coordinates $\boldsymbol{q}$ and $\boldsymbol{z}$, evaluation of the principle of virtual work results into

$$\boldsymbol{Q}^{\mathrm{T}}\boldsymbol{J} = \boldsymbol{J}^{\mathrm{T}}\boldsymbol{Q} = \boldsymbol{0}, \tag{2.16}$$

that constitutes the orthogonality between free and constrained directions (compare Fig. 2.2). Thus, the reaction forces and torques $\hat{\boldsymbol{\tau}}^{\mathrm{r}}$ are also eliminated in the Newton-Euler equations when pre-multiplying Eq. (2.14) with the transpose of the global Jacobian $\boldsymbol{J}^{\mathrm{T}} \in \mathbb{R}^{f,6p}$. This

leads to a set of f ordinary differential equations,

$$\boldsymbol{M}(\boldsymbol{q},\boldsymbol{z})\,\ddot{\boldsymbol{q}} + \boldsymbol{\tau}^{\mathrm{c}}(\boldsymbol{q},\dot{\boldsymbol{q}},\boldsymbol{z}) = \boldsymbol{\tau}^{\mathrm{e}}(\boldsymbol{q},\dot{\boldsymbol{q}},\boldsymbol{z},\boldsymbol{a}), \tag{2.17}$$

which represent the equations of motion of a tree-structured system with the mass matrix $\boldsymbol{M} = \boldsymbol{J}^{\mathrm{T}}\widehat{\boldsymbol{M}}\boldsymbol{J} \in \mathbb{R}^{f,f}$. Vector $\boldsymbol{\tau}^{\mathrm{c}} = \boldsymbol{J}^{\mathrm{T}}\hat{\boldsymbol{\tau}}^{\mathrm{c}} \in \mathbb{R}^{f}$ contains the torques of the centrifugal and Coriolis forces as well as gyroscopic torques with respect to the joint axes. Furthermore, the vector $\boldsymbol{\tau}^{\mathrm{e}} = \boldsymbol{J}^{\mathrm{T}}\hat{\boldsymbol{\tau}}^{\mathrm{e}} \in \mathbb{R}^{f}$ includes the resulting torques of the applied forces which can be further divided into passive and active parts,

$$\boldsymbol{\tau}^{\mathrm{e}} = \boldsymbol{\tau}^{\mathrm{p}}(\boldsymbol{q},\dot{\boldsymbol{q}},\boldsymbol{z}) + \boldsymbol{\tau}^{\mathrm{m}}(\boldsymbol{q},\dot{\boldsymbol{q}},\boldsymbol{z},\boldsymbol{a}). \tag{2.18}$$

The passive torques $\boldsymbol{\tau}^{\mathrm{p}} = \boldsymbol{J}^{\mathrm{T}}\hat{\boldsymbol{\tau}}^{\mathrm{p}} \in \mathbb{R}^{f}$ usually arise from gravitational forces, forces due to interactions with the environment and forces from soft tissue structures depending on a nonlinear, viscoelastic material behavior [139]. Torques generated from active muscle structures $\boldsymbol{\tau}^{\mathrm{m}} = \boldsymbol{J}^{\mathrm{T}}\hat{\boldsymbol{\tau}}^{\mathrm{m}} \in \mathbb{R}^{f}$ also depend on muscle activation levels $\boldsymbol{a}$ [5], if included in the modeling task.

In case that kinematic loops are introduced according to Eqs. (2.9) to (2.11), the motion of the system is further constrained leading to a reduction of the degrees of freedom (see Eq. (2.8)). As a consequence, additional constraint forces/torques act on the segments at the cut loops. These are taken into account in the equations of motion of the spanning tree by extending Eq. (2.17) with the transpose of the derivative matrix from Eq. (2.10), $\boldsymbol{G}^{\mathrm{T}} \in \mathbb{R}^{f,b_{\mathrm{c}}}$, and additional constraint force coordinates summarized in vector $\boldsymbol{\lambda}^{\mathrm{c}} \in \mathbb{R}^{b_{\mathrm{c}}}$. This results into

$$\boldsymbol{M}(\boldsymbol{q},\boldsymbol{z})\,\ddot{\boldsymbol{q}} + \boldsymbol{\tau}^{\mathrm{c}}(\boldsymbol{q},\dot{\boldsymbol{q}},\boldsymbol{z}) = \boldsymbol{\tau}^{\mathrm{e}}(\boldsymbol{q},\dot{\boldsymbol{q}},\boldsymbol{z},\boldsymbol{a}) + \boldsymbol{G}^{\mathrm{T}}(\boldsymbol{q},\boldsymbol{z})\boldsymbol{\lambda}^{\mathrm{c}}. \tag{2.19}$$

The equations of motion of the closed-loop system then consists of a differential-algebraic set of equations composed of Eq. (2.19), and the the loop closure constraints from Eq. (2.9).

2.3.3 Inverse and Forward Dynamics Approach

One of the key problems in musculoskeletal modeling consists of integrating active muscular structures that serve as actuators for the skeletal system. Active muscle forces $\boldsymbol{f}^{\mathrm{m}}$ depend on the mechanical behavior of muscle structures which are described by force-length and force-velocity characteristics [181, 321, 415]. These characteristics vary from muscle to muscle depending on the functional architecture such as physiological cross section area and fiber length [137, 213, 245, 399, 412]. Furthermore, the input of the nervous system governs muscle force application by regulating muscle excitation $\boldsymbol{u}$ and hence their activation levels $\boldsymbol{a}$ [434].

The transmission from muscle activation $\boldsymbol{a}$ to muscle force $\boldsymbol{f}^{\mathrm{m}}$ is formulated microscopically in Huxley-type or macroscopically in Hill-type muscle models [419] which are frequently implemented into musculoskeletal models.

In general, there are two approaches in order to determine muscle forces $\boldsymbol{f}^{\mathrm{m}}$ (Fig. 2.5a). The most common approach used in biomechanical research is inverse dynamics, which was successfully used by many researchers to predict physiological joint loading during human motion [5, 46, 171, 210, 246, 249, 254, 273, 274, 303, 349, 358]. The basic idea of this approach is to estimate the driving muscle torques $\boldsymbol{\tau}^{\mathrm{m}}$ acting at the joints for given motion patterns $\boldsymbol{q}(t)$ often derived from motion analyses. Hence, the equations of motion of a tree-structured system according to Eq. (2.17) with Eq. (2.18) are evaluated as

$$\boldsymbol{\tau}^{\mathrm{m}} = \boldsymbol{M}(\boldsymbol{q}, \boldsymbol{z})\, \ddot{\boldsymbol{q}} + \boldsymbol{\tau}^{\mathrm{c}}(\boldsymbol{q}, \dot{\boldsymbol{q}}, \boldsymbol{z}) - \boldsymbol{\tau}^{\mathrm{p}}(\boldsymbol{q}, \dot{\boldsymbol{q}}, \boldsymbol{z}). \tag{2.20}$$

Resolving the muscle torques $\boldsymbol{\tau}^{\mathrm{m}}$ obtained from Eq. (2.20) with respect to active muscle forces $\boldsymbol{f}^{\mathrm{m}}$ leads to the distribution problem of muscle forces [307, 346]. The problem occurs as there are usually more actuators within musculoskeletal systems than required to produce specific motion patterns. As a result, active muscle forces $\boldsymbol{f}^{\mathrm{m}}$ cannot be uniquely determined from the muscle torques $\boldsymbol{\tau}^{\mathrm{m}}$ by using standard algebraic techniques. A general approach to solve the distribution problem is to define a physiological cost function which is minimized by means of static optimization techniques [307, 346]. Implementation of muscle mechanics as mentioned above also allows to resolve the distribution problem with respect to activation levels $\boldsymbol{a}$ [5]. This approach implies that the nervous system pursues an optimum activation pattern during muscle force control for a specific motor task [199].

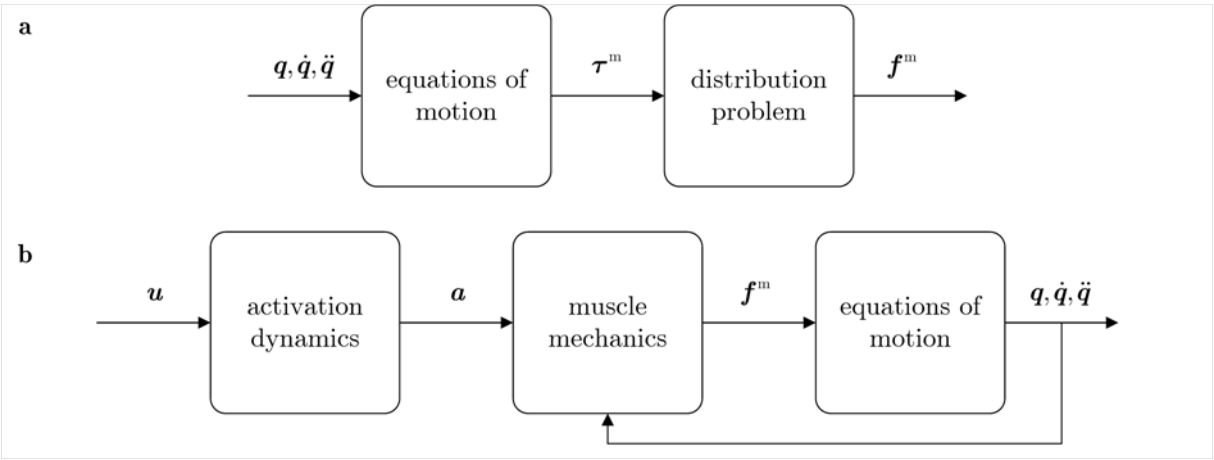

Fig. 2.5 Estimation of muscle forces $\boldsymbol{f}^{\mathrm{m}}$ within musculoskeletal models. **a** Inverse dynamics. **b** Forward dynamics.

Another source of redundancy is given when kinematic loops are included in the musculoskeletal model representing, for example, human motions with both feet placed on the ground [389]. Evaluation of the equations of motion from Eq. (2.19) along with Eq. (2.18) yields

$$\boldsymbol{\tau}^{\mathrm{m}} + \boldsymbol{G}^{\mathrm{T}}(\boldsymbol{q}, \boldsymbol{z})\boldsymbol{\lambda}^{\mathrm{c}} = \boldsymbol{M}(\boldsymbol{q}, \boldsymbol{z})\, \ddot{\boldsymbol{q}} + \boldsymbol{\tau}^{\mathrm{c}}(\boldsymbol{q}, \dot{\boldsymbol{q}}, \boldsymbol{z}) - \boldsymbol{\tau}^{\mathrm{p}}(\boldsymbol{q}, \dot{\boldsymbol{q}}, \boldsymbol{z}). \tag{2.21}$$

with two unknowns, the muscle torques $\boldsymbol{\tau}^{\mathrm{m}}$ and the additional constraint force coordinates $\boldsymbol{\lambda}^{\mathrm{c}}$. In the same way as the distribution problem of muscle forces, Eq. (2.21) may be treated as equality constraint to a static optimization problem [390], complying with the loop closure constraints Eqs. (2.9) to (2.11). This method is further developed in Chapter 3.3.

The second approach used in biomechanics consists of directly computing the skeletal motion according to forces applied onto the segments which is often referred to as direct or forward dynamics (Fig. 2.5b). In this approach, muscle structures are represented by muscle models which generate muscle forces $\boldsymbol{f}^{\mathrm{m}}$ depending on muscle mechanics and their activation levels $\boldsymbol{a}$. In order to determine muscle excitation patterns $\boldsymbol{u}$ for a specific motor task, researchers generally use experimental EMG data, data tracking or dynamic optimization procedures following a physiological cost function [116]. Muscle activations $\boldsymbol{a}$ are then obtained from the excitation patterns $\boldsymbol{u}$ by evaluating activation dynamics. Hence, the equations of motion of a tree-structured system from Eq. (2.17) with (2.18) delivers the accelerations, i.e.

$$\ddot{\boldsymbol{q}} = \boldsymbol{M}(\boldsymbol{q}, \boldsymbol{z})^{-1}(\boldsymbol{\tau}^{\mathrm{p}}(\boldsymbol{q}, \dot{\boldsymbol{q}}, \boldsymbol{z}) + \boldsymbol{\tau}^{\mathrm{m}}(\boldsymbol{q}, \dot{\boldsymbol{q}}, \boldsymbol{z}, \boldsymbol{a}) - \boldsymbol{\tau}^{\mathrm{c}}(\boldsymbol{q}, \dot{\boldsymbol{q}}, \boldsymbol{z})). \tag{2.22}$$

The velocities $\dot{\boldsymbol{q}}$ and the joint angles $\boldsymbol{q}$ are calculated by numerical integration.

In case of kinematic loops within the system, the equations of motion from Eq. (2.19) with (2.18) can be represented by a set of $f + b_{\mathrm{c}}$ linear equations along with the loop closure constraints on acceleration level Eq. (2.11),

$$\begin{bmatrix} \boldsymbol{M}(\boldsymbol{q}, \boldsymbol{z}) & -\boldsymbol{G}^{\mathrm{T}}(\boldsymbol{q}, \boldsymbol{z}) \\ -\boldsymbol{G}(\boldsymbol{q}, \boldsymbol{z}) & \boldsymbol{0} \end{bmatrix} \begin{bmatrix} \ddot{\boldsymbol{q}} \\ \boldsymbol{\lambda}^{\mathrm{c}} \end{bmatrix} = \begin{bmatrix} \boldsymbol{\tau}^{\mathrm{p}}(\boldsymbol{q}, \dot{\boldsymbol{q}}, \boldsymbol{z}) + \boldsymbol{\tau}^{\mathrm{m}}(\boldsymbol{q}, \dot{\boldsymbol{q}}, \boldsymbol{z}, \boldsymbol{a}) - \boldsymbol{\tau}^{\mathrm{c}}(\boldsymbol{q}, \dot{\boldsymbol{q}}, \boldsymbol{z}) \\ \bar{\boldsymbol{\eta}}(\boldsymbol{q}, \dot{\boldsymbol{q}}, \boldsymbol{z}) \end{bmatrix}. \tag{2.23}$$

As the determination of the velocities $\dot{\boldsymbol{q}}$ and the joint angles $\boldsymbol{q}$ from Eq. (2.23) in compliance with the loop closure constraints at the position and velocity levels Eqs. (2.9) and (2.10) entails computational difficulties [420], researchers usually circumvent the problem by introducing measured contact forces [164,381] or appropriate contact models [5,206]. In doing so, the additional constraints arising from interaction with the system's environment are treated as passive applied forces reducing the equations of motion to Eq. (2.22). Within the scope of this work, however, forward dynamics is followed in a simplified manner in Chapter 4.3 without consideration of kinematic loops and active muscle forces.

3 Dynamic Testing of Total Hip Replacements

In the following the HiL test system introduced in the previous chapter is adopted for testing THRs. First, the underlying concept of the HiL simulation is translated into a functional principle according to the characteristics of artificial hip joints. A strategy widely accepted in the musculoskeletal field of research [171, 254, 273, 358] is pursued for validating the test system in this configuration. That includes the comparison of the outcomes of the HiL simulations to data derived from instrumented patients for normal daily activities. Hence, motion analyses of a single subject were performed for two normal maneuvers to obtain kinematic data as input for the musculoskeletal model. An inverse dynamics approach is developed based on the equations described in chapter 2.3 that allows for calculation of the hip joint reaction forces while incorporating displacements and torques measured by the physical setup. The model is then implemented into a multibody software suitable for real-time applications. Finally, the results of the validation are presented.

3.1 Functional Principle of Testing Total Hip Replacements

In artificial hip joints the motion of the femur relative to the pelvis is constrained in translational directions due to the contact between the femoral head and the acetabular cup. On the contrary, relative movements in rotational directions are free within the technical range of motion. Given these joint characteristics THRs are commonly regarded as spherical joints as illustrated in Fig. 2.2a. Hence, an appropriate control strategy for the robot is to apply force in the constrained translational and to move the femoral stem in the free rotational directions using hybrid position-force control [197].

This control strategy defines the interactions between the physical setup and the implemented musculoskeletal model (Fig. 3.1). For the spatial load case, the free directions are specified as the rotations of the femur with respect to the pelvis with the angles q_1 (adduction/abduction), q_2 (internal/external rotation) and q_3 (flexion/extension). At a current time instant t the model delivers values of the angles q_1, q_2 and q_3 which are transferred to

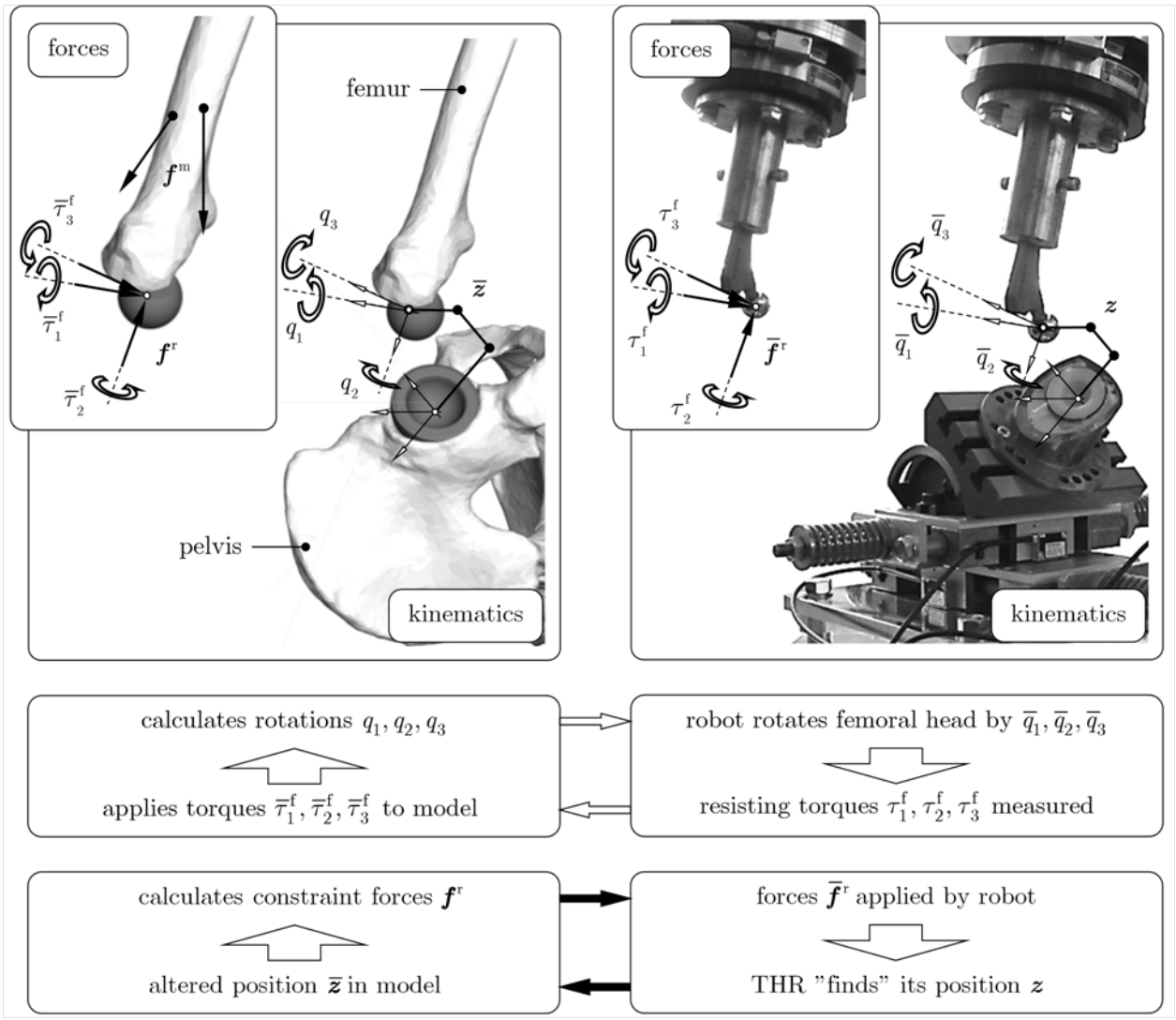

Fig. 3.1 Functional principle of the HiL simulation for testing THRs with respect to joint stability. Transfer between the musculoskeletal model and the physical setup is illustrated within the two control loops on kinematic and force level.

the robot controller. Accordingly, the femoral component of the THR is rotated into the position, $\bar{q}_1$, $\bar{q}_2$ and $\bar{q}_3$, by the robot using position control. Resisting torques $\boldsymbol{\tau}^{\mathrm{f}}$, usually due to friction, are measured along the coordinates $\bar{q}_1$, $\bar{q}_2$ and $\bar{q}_3$ as a consequence of the movement, and fed back to the model closing the first control loop of the HiL simulation. The transferred values denoted by bars normally differ from the original values without bars due to signal delays and the limited dynamic bandwidth of the controlled robot.

Another control loop is given by considering the three translations treated as constrained directions. At the same time instant t the corresponding components of the reaction forces $\boldsymbol{f}^{\mathrm{r}}$ are calculated by the model which mainly depend on active muscle forces $\boldsymbol{f}^{\mathrm{m}}$ besides gravitational and dynamic forces. After transmission to the robot controller, the robot applies the

reaction forces $\bar{\boldsymbol{f}}^{\mathrm{r}}$ onto the THR using force control. As long as the THR bears the applied forces, only minor relative displacements are recorded between the femoral head and the cup. Separation of the joint partners and hence instability is indicated by increasing relative displacements. This is also accompanied by rising values of the measured resisting torques $\boldsymbol{\tau}^{\mathrm{f}}$ in case of impingement [14, 291, 344]. The values of the measured resisting torques $\boldsymbol{\tau}^{\mathrm{f}}$ as well as the displacements $\boldsymbol{z}$ are fed back into the model having an impact on soft tissue elongation and muscle lever arms in the next time instant.

3.2 Experimental Data

Approval of an ethical review committee and the consent of one healthy subject (male, 24 a, 1.81 m, 80 kg) were obtained to perform motion analyses of dislocation-associated maneuvers. During the analyses, kinematic data of attached skin markers were recorded using an ultrasound measuring system (CMS-HS Measuring System, zebris Medical GmbH, Isny im Allgäu, Germany). Ground reaction forces were measured by a force plate (Typ 9287B, Kistler Group, Winterthur, Switzerland). Also, electrical activity was deduced from EMG data of main thigh and shank muscles.

For validation purposes of the test system, two normal maneuvers were considered which are associated with posterior dislocation if executed excessively [217, 284]: knee bending and seating-to-rising. Both maneuvers were repeated five times with a seat height of 48 cm. Averaged data sets were gained for each maneuver by normalizing the time scale and averaging the five motion cycles. Down sampling, spline interpolation and numerical differentiation were performed using the Curve Fitting Toolbox in MATLAB (Version 7.11, MathWorks, Ismaning, Germany) to achieve smooth kinematic data of the skin markers from the averaged data sets on position, velocity and acceleration levels. MRI data of the lower extremities were recorded along with the attached skin markers after the motion analyses.

In order to validate the test system, a similar strategy was sought within the scope of this work as presented by other researchers in the musculoskeletal field [171, 254, 273, 358]. Hence, hip joint contact forces were derived from in vivo data of routine activities [33]. These included comparable load cases from three male patients such as knee bending, sitting down and standing up (chair height 50 cm), whereas the last two were summarized to one load case. Averaged hip contact and ground reaction force components of each load case and patient were transformed to a standardized global reference frame [423] and normalized with respect to the time. This allowed comparison of calculated forces against the derived in vivo data (see Chapter 3.4).

3.3 Musculoskeletal Model of the Lower Limb

3.3.1 Multibody Topology

The musculoskeletal model consists of a multibody system with overall $p = 4$ moving segments modeled as rigid bodies (Fig. 3.2). The kinematic chain starts at the right foot assumed to be ground-fixed and continues with the tibia and fibula summarized as one segment, the femur, the pelvis and the upper body including the head and the upper extremities. Both ankle and knee joint are modeled as universal joints with two rotational degrees of freedom each. The upper body is attached to the pelvis at the sacrum endplate center by a revolute joint. A kinematic subchain represents the hip joint consisting of three orthogonal prismatic joints and three revolute joints with co-intersecting axes. The $b_z = 3$ coordinates of the prismatic joints are constrained by the measurements $\bar{\boldsymbol{z}}$ which are transferred to the model. The three revolute joints correspond to the free rotations defined by the Cardan angles q_1, q_2 and q_3. Moreover, the kinematic chain is closed by means of a fictive planar joint consisting of one revolute and two prismatic joints. It is established in the sagittal plane and connects the pelvis with the ground. This way the left body part is taken into account allowing symmetric human movements with both feet attached to the ground.

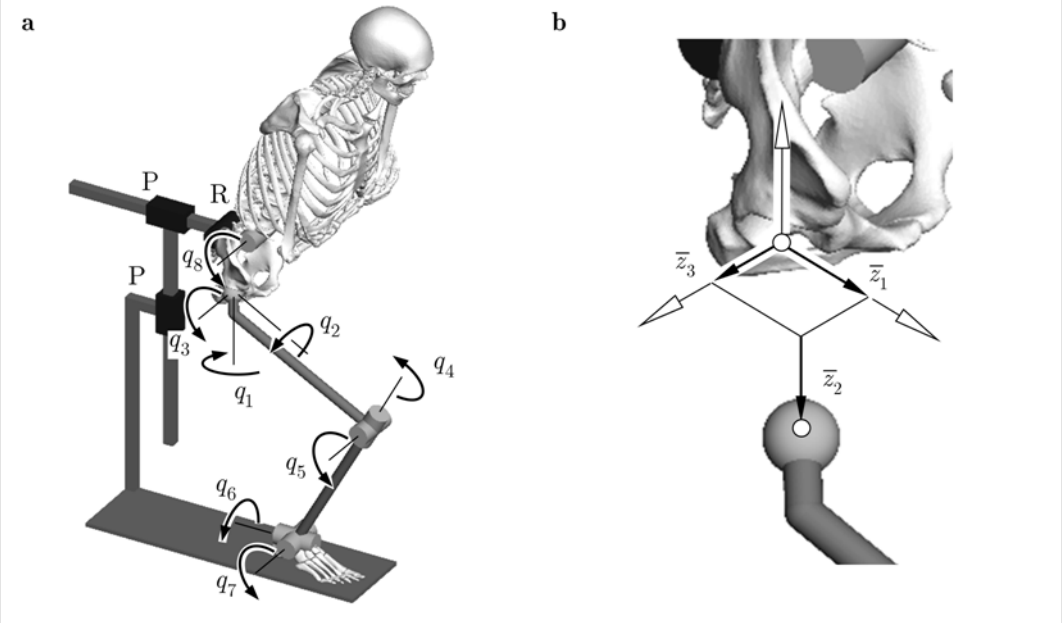

Fig. 3.2 Multibody system of the lower extremity for testing THRs. **a** Multibody topology with illustration of the joint coordinates and the fictive planar joint in the sagittal plane indicated as one revolute (R) and two prismatic (P) joints. **b** Measured and transferred coordinates in constrained directions of the THR.

The motion of the spanning tree obtained by cutting the loop at the fictive planar joint is described by $f = 8$ joint coordinates $\boldsymbol{q} \in \mathbb{R}^8$ and $b_\mathrm{z} = 3$ measured coordinates $\bar{\boldsymbol{z}} \in \mathbb{R}^3$ of the THR,

$$\boldsymbol{q} = [q_1 \dots q_8]^\mathrm{T} \qquad \text{and} \qquad \bar{\boldsymbol{z}} = [\bar{z}_1 \dots \bar{z}_3]^\mathrm{T}. \tag{3.1}$$

Thus, the position and orientation of the i-th segment can be written in terms of the joint coordinates $\boldsymbol{q}$ and the measurements $\bar{\boldsymbol{z}}$,

$$\boldsymbol{r}_i = \boldsymbol{r}_i(\boldsymbol{q}, \bar{\boldsymbol{z}}) \qquad \text{and} \qquad \boldsymbol{S}_i = \boldsymbol{S}_i(\boldsymbol{q}), \tag{3.2}$$

where $\boldsymbol{r}_i \in \mathbb{R}^3$ denotes the position vector of the mass center and $\boldsymbol{S}_i \in \mathbb{R}^{3,3}$ the rotation matrix. The translational and rotational velocities of the i-th segment are then expressed as

$$\boldsymbol{v}_i = \boldsymbol{J}_{\mathrm{T}i}(\boldsymbol{q}, \bar{\boldsymbol{z}})\, \dot{\boldsymbol{q}} \qquad \text{with} \qquad \boldsymbol{J}_{\mathrm{T}i} = \frac{\partial \boldsymbol{v}_i}{\partial \dot{\boldsymbol{q}}}, \tag{3.3}$$

$$\boldsymbol{\omega}_i = \boldsymbol{J}_{\mathrm{R}i}(\boldsymbol{q})\, \dot{\boldsymbol{q}} \qquad \text{with} \qquad \boldsymbol{J}_{\mathrm{R}i} = \frac{\partial \boldsymbol{\omega}_i}{\partial \dot{\boldsymbol{q}}}, \tag{3.4}$$

with the translational and rotational Jacobian matrices, $\boldsymbol{J}_{\mathrm{T}i} \in \mathbb{R}^{3,8}$ and $\boldsymbol{J}_{\mathrm{R}i} \in \mathbb{R}^{3,8}$, respectively. By further differentiation with respect to the global reference frame, the translational and rotational accelerations of the i-th segment are given by

$$\dot{\boldsymbol{v}}_i = \boldsymbol{J}_{\mathrm{T}i}(\boldsymbol{q}, \bar{\boldsymbol{z}})\, \ddot{\boldsymbol{q}} + \bar{\boldsymbol{a}}_i \qquad \text{with} \qquad \bar{\boldsymbol{a}}_i = \dot{\boldsymbol{J}}_{\mathrm{T}i}(\boldsymbol{q}, \dot{\boldsymbol{q}}, \bar{\boldsymbol{z}})\, \dot{\boldsymbol{q}}, \tag{3.5}$$

$$\dot{\boldsymbol{\omega}}_i = \boldsymbol{J}_{\mathrm{R}i}(\boldsymbol{q})\, \ddot{\boldsymbol{q}} + \bar{\boldsymbol{\alpha}}_i \qquad \text{with} \qquad \bar{\boldsymbol{\alpha}}_i = \dot{\boldsymbol{J}}_{\mathrm{R}i}(\boldsymbol{q}, \dot{\boldsymbol{q}})\, \dot{\boldsymbol{q}}. \tag{3.6}$$

As the dynamics of the displacements in the constrained directions is based on the settings of the force controller of the robot, the time derivatives of the measured coordinates $\bar{\boldsymbol{z}}$ are neglected, i.e $\dot{\bar{\boldsymbol{z}}} = \ddot{\bar{\boldsymbol{z}}} = \boldsymbol{0}$.

Due to the replacement of the left counterpart, the joint coordinates $\boldsymbol{q}$ of the spanning tree are constrained by the fictive planar joint closing the kinematic chain. The corresponding symmetry conditions with respect to the sagittal plane are described by $b_\mathrm{c} = 3$ additional implicit loop closure constraints that reduce the degrees of freedom of the system to $f_\mathrm{c} = 5$. The constraints are written as

$$\boldsymbol{g}(\boldsymbol{q}, \bar{\boldsymbol{z}}) = \boldsymbol{0}, \tag{3.7}$$

$$\dot{\boldsymbol{g}}(\boldsymbol{q}, \bar{\boldsymbol{z}}) = \boldsymbol{G}(\boldsymbol{q}, \bar{\boldsymbol{z}})\, \dot{\boldsymbol{q}} = \boldsymbol{0} \qquad \text{with} \qquad \boldsymbol{G} = \hat{\boldsymbol{G}}\boldsymbol{J}(\boldsymbol{q}, \bar{\boldsymbol{z}}), \tag{3.8}$$

$$\ddot{\boldsymbol{g}}(\boldsymbol{q}, \bar{\boldsymbol{z}}) = \boldsymbol{G}(\boldsymbol{q}, \bar{\boldsymbol{z}})\, \ddot{\boldsymbol{q}} + \bar{\boldsymbol{\eta}} = \boldsymbol{0} \qquad \text{with} \qquad \bar{\boldsymbol{\eta}} = \dot{\boldsymbol{G}}(\boldsymbol{q}, \dot{\boldsymbol{q}}, \bar{\boldsymbol{z}})\, \dot{\boldsymbol{q}}, \tag{3.9}$$

at the position, velocity and acceleration levels (compare Eqs. (2.9) to (2.11)). The three

constrained directions of the pelvis, the translation perpendicular to the sagittal plane and the two out-of-plane rotations, are indicated by corresponding non-zero entries in the rows of matrix $\hat{\boldsymbol{G}} \in \mathbb{R}^{3,24}$. Matrix $\boldsymbol{J} = [\boldsymbol{J}_{\mathrm{T1}} \dots \boldsymbol{J}_{\mathrm{T4}}\, \boldsymbol{J}_{\mathrm{R1}} \dots \boldsymbol{J}_{\mathrm{R4}}]^{\mathrm{T}}$ describes the global Jacobian matrix of the system.

3.3.2 Estimation of Hip Joint Reaction Forces

Due to the consideration of muscle structures the applied forces considered in the model arise from both passive and active forces. Hence, the applied forces according to Eq. (2.18) are summarized to

$$\boldsymbol{\tau}^{\mathrm{e}} = \underbrace{\boldsymbol{\tau}^{\mathrm{g}}(\boldsymbol{q}, \bar{\boldsymbol{z}}) + \boldsymbol{\tau}^{\mathrm{l}}(\boldsymbol{q}, \dot{\boldsymbol{q}}, \bar{\boldsymbol{z}}) + \bar{\boldsymbol{\tau}}^{\mathrm{f}}(\boldsymbol{q}, \bar{\boldsymbol{z}})}_{\boldsymbol{\tau}^{\mathrm{p}}(\boldsymbol{q}, \dot{\boldsymbol{q}}, \bar{\boldsymbol{z}})} + \boldsymbol{\tau}^{\mathrm{m}}(\boldsymbol{q}, \bar{\boldsymbol{z}}, \boldsymbol{a}), \tag{3.10}$$

where vector $\boldsymbol{\tau}^{\mathrm{g}} = \boldsymbol{J}^{\mathrm{T}} \hat{\boldsymbol{\tau}}^{\mathrm{g}} \in \mathbb{R}^8$ describes the torques due to gravitational forces and vector $\boldsymbol{\tau}^{\mathrm{l}} = \boldsymbol{J}^{\mathrm{T}} \hat{\boldsymbol{\tau}}^{\mathrm{l}} \in \mathbb{R}^8$ the torques due to ligament and capsular forces adjacent to the modeled joints. The measured and transferred torques, $\bar{\tau}_1^{\mathrm{f}}$, $\bar{\tau}_2^{\mathrm{f}}$ and $\bar{\tau}_3^{\mathrm{f}}$ given in local reference frames, are included in vector $\bar{\boldsymbol{\tau}}^{\mathrm{f}} = \boldsymbol{J}^{\mathrm{T}} \hat{\boldsymbol{\tau}}^{\mathrm{f}} \in \mathbb{R}^8$. Furthermore, vector $\boldsymbol{\tau}^{\mathrm{m}} = \boldsymbol{J}^{\mathrm{T}} \hat{\boldsymbol{\tau}}^{\mathrm{m}} \in \mathbb{R}^8$ contains the torques of active muscle forces incorporated in the model.

Considering the closed-loop topology of the musculoskeletal model the equations of motion are then formulated in terms of the joint coordinates $\boldsymbol{q}$ and the measured displacements $\bar{\boldsymbol{z}}$ as

$$\boldsymbol{M}(\boldsymbol{q}, \bar{\boldsymbol{z}})\, \ddot{\boldsymbol{q}} + \boldsymbol{\tau}^{\mathrm{c}}(\boldsymbol{q}, \dot{\boldsymbol{q}}, \bar{\boldsymbol{z}}) = \boldsymbol{\tau}^{\mathrm{g}}(\boldsymbol{q}, \bar{\boldsymbol{z}}) + \boldsymbol{\tau}^{\mathrm{l}}(\boldsymbol{q}, \dot{\boldsymbol{q}}, \bar{\boldsymbol{z}}) + \bar{\boldsymbol{\tau}}^{\mathrm{f}}(\boldsymbol{q}, \bar{\boldsymbol{z}}) + \boldsymbol{\tau}^{\mathrm{m}}(\boldsymbol{q}, \bar{\boldsymbol{z}}, \boldsymbol{a}) + \boldsymbol{G}^{\mathrm{T}}(\boldsymbol{q}, \bar{\boldsymbol{z}}) \boldsymbol{\lambda}^{\mathrm{c}}, \tag{3.11}$$

according to Eq. (2.19) with Eq. (3.10). The mass matrix $\boldsymbol{M} = \boldsymbol{J}^{\mathrm{T}} \widehat{\boldsymbol{M}} \boldsymbol{J} \in \mathbb{R}^{8,8}$ includes the masses of the bone segments and the corresponding soft tissue. Vector $\boldsymbol{\tau}^{\mathrm{c}} = \boldsymbol{J}^{\mathrm{T}} \hat{\boldsymbol{\tau}}^{\mathrm{c}} \in \mathbb{R}^8$ denotes the torques of the Coriolis and centrifugal forces as well as gyroscopic torques. In addition, the equations of motion are extended by the constraint forces in the sagittal plane as outlined in Eq. (2.19). These are expressed in terms of the transpose matrix $\boldsymbol{G}^{\mathrm{T}} = \boldsymbol{J}^{\mathrm{T}} \hat{\boldsymbol{G}}^{\mathrm{T}} \in \mathbb{R}^{8,3}$ from Eq. (3.8) and $b_{\mathrm{c}} = 3$ constraint force coordinates $\boldsymbol{\lambda}^{\mathrm{c}} \in \mathbb{R}^3$.

The equations of motion described in Eq. (3.11) implies two sources of redundancy in the musculoskeletal system. The first is due to the closed kinematic chain of the model representing human motions with both feet attached to the ground [389]. This means physically that the skeletal system can be internally loaded by active muscle forces without generating motion. The second is due to the distribution problem of muscle forces as generally more muscle structures are available than required to produce muscle torques for a specific motor task [307, 346].

For a given motion $\boldsymbol{q}(t)$ and its time derivatives satisfying the loop closure constraints, Eqs. (3.7) to (3.9), the first redundancy problem is addressed by evaluating the equations of motion with respect to the $f = 8$ muscle torques $\boldsymbol{\tau}^{\mathrm{m}}$ and the $b_{\mathrm{c}} = 3$ constraint force coordinates $\boldsymbol{\lambda}^{\mathrm{c}}$. This leads to an under-determined system of $f = 8$ linear equations,

$$\begin{bmatrix} \boldsymbol{E} & \boldsymbol{G}^{\mathrm{T}}(\boldsymbol{q}, \bar{\boldsymbol{z}}) \end{bmatrix} \begin{bmatrix} \boldsymbol{\tau}^{\mathrm{m}} \\ \boldsymbol{\lambda}^{\mathrm{c}} \end{bmatrix} = \boldsymbol{\tau}^{\mathrm{g}}(\boldsymbol{q}, \bar{\boldsymbol{z}}) + \boldsymbol{\tau}^{\mathrm{l}}(\boldsymbol{q}, \dot{\boldsymbol{q}}, \bar{\boldsymbol{z}}) + \bar{\boldsymbol{\tau}}^{\mathrm{f}}(\boldsymbol{q}, \bar{\boldsymbol{z}}) - \boldsymbol{M}(\boldsymbol{q}, \bar{\boldsymbol{z}})\, \ddot{\boldsymbol{q}} - \boldsymbol{\tau}^{\mathrm{c}}(\boldsymbol{q}, \dot{\boldsymbol{q}}, \bar{\boldsymbol{z}}) \tag{3.12}$$

with the unit matrix $\boldsymbol{E} \in \mathbb{R}^{8,8}$. The redundancy problem is resolved by regarding Eq. (3.12) as equality constraint of a static optimization problem minimizing the quadratic cost function

$$\boldsymbol{I}_{\mathrm{c}}(\boldsymbol{x}) \equiv \boldsymbol{x}^{\mathrm{T}} \boldsymbol{P} \boldsymbol{x} = \min_{\boldsymbol{x}} \qquad \text{with} \qquad \boldsymbol{x} = \begin{bmatrix} \boldsymbol{\tau}^{\mathrm{m}} \\ \boldsymbol{\lambda}^{\mathrm{c}} \end{bmatrix} \text{ subjected to Eq. (3.12)}, \tag{3.13}$$

with a diagonal weighting matrix $\boldsymbol{P} \in \mathbb{R}^{11,11}$ [390]. Within this work matrix $\boldsymbol{P}$ is identified with the unit matrix.

The second redundancy problem has to be solved for estimating n individual muscle forces from the muscle torques $\boldsymbol{\tau}^{\mathrm{m}}$. In order to incorporate muscle mechanics [181, 321, 415] and architecture [137, 213, 245, 399, 412], the absolute muscle forces $\boldsymbol{f}^{\mathrm{m}} \in \mathbb{R}^n$ are considered in terms of their muscle activation levels $\boldsymbol{a} \in \mathbb{R}^n$. These are used to scale the physiological force of each muscle [5, 199, 200]. Thus,

$$\boldsymbol{f}^{\mathrm{m}} = \boldsymbol{C}(\boldsymbol{q}, \dot{\boldsymbol{q}}, \bar{\boldsymbol{z}})\boldsymbol{a} \qquad \text{with} \qquad C_j = f_j^{\mathrm{lv}}(\boldsymbol{q}, \dot{\boldsymbol{q}}, \bar{\boldsymbol{z}}) A_j \sigma_j \tag{3.14}$$

where the diagonal matrix $\boldsymbol{C} \in \mathbb{R}^{n,n}$ contains the physiological muscle forces C_j defined each as the product of factor f_j^{lv} addressing the muscle's force-length and force-velocity properties, respectively, and the isometric muscle force, estimated by the physiological cross section area A_j and the physiological muscle stress σ_j [4].

As previously shown by Anderson and Pandy [5], properties of activated muscle structures and the activation dynamics have little impact on the prediction of muscle and hip joint reaction forces. Hence, muscle mechanics is neglected within this work, i.e. $f_j^{\mathrm{lv}} = 1$. Moreover, forces due to passive muscle tissue are assumed to be marginal and therefore negligible [395]. The distribution problem of muscle forces is then expressed as an under-determined system of $f = 8$ linear equations for $n > f$ muscle activation levels $\boldsymbol{a}$,

$$\boldsymbol{\tau}^{\mathrm{m}} = \boldsymbol{J}^{\mathrm{T}}(\boldsymbol{q}, \bar{\boldsymbol{z}}) \boldsymbol{B}(\boldsymbol{q}, \bar{\boldsymbol{z}}) \boldsymbol{C} \boldsymbol{a}, \tag{3.15}$$

with the muscle torques $\boldsymbol{\tau}^{\mathrm{m}}$ obtained from Eq. (3.13). Matrix $\boldsymbol{B} \in \mathbb{R}^{24,n}$ summarizes the normalized force and torque directions of each muscle with respect to the mass centers of the segments [386]. A common way to find a solution is to regard Eq. (3.15) as an equality

constraint to a static optimization problem [307, 346]. Here, a quadratic cost function is utilized

$$\boldsymbol{I}_{\mathrm{m}}(\boldsymbol{a}) \equiv \boldsymbol{a}^{\mathrm{T}}\boldsymbol{O}\boldsymbol{a} = \min_{\boldsymbol{a}} \qquad \text{subjected to Eq. (3.15) and } 0 \leq a_j \leq 1, \tag{3.16}$$

with a diagonal weighting matrix $\boldsymbol{O} \in \mathbb{R}^{n,n}$ identified with the unit matrix [5].
Given the constraint force coordinates $\boldsymbol{\lambda}^{\mathrm{c}}$ from Eq. (3.13) and the muscle activation levels $\boldsymbol{a}$ from Eq. (3.16), the reaction forces $\boldsymbol{f}^{\mathrm{r}}$ required for the HiL simulation are calculated using the Newton-Euler equations (compare Eq. (2.14)) for the four rigid segments. After extending these equations by the constraint forces and torques $\hat{\boldsymbol{G}}^{\mathrm{T}}\boldsymbol{\lambda}^{\mathrm{c}}$ in the sagittal plane, the reaction forces/torques of the four segments $\hat{\boldsymbol{\tau}}^{\mathrm{r}} \in \mathbb{R}^{24}$ are given with respect to the inertia frame as

$$\hat{\boldsymbol{\tau}}^{\mathrm{r}} = \widehat{\boldsymbol{M}}(\boldsymbol{q})\boldsymbol{J}(\boldsymbol{q},\bar{\boldsymbol{z}})\ddot{\boldsymbol{q}} + \hat{\boldsymbol{\tau}}^{\mathrm{c}}(\boldsymbol{q},\dot{\boldsymbol{q}},\bar{\boldsymbol{z}}) - \hat{\boldsymbol{\tau}}^{\mathrm{g}} - \hat{\boldsymbol{\tau}}^{\mathrm{l}}(\boldsymbol{q},\dot{\boldsymbol{q}},\bar{\boldsymbol{z}}) - \hat{\boldsymbol{\tau}}^{\mathrm{f}}(\boldsymbol{q}) - \hat{\boldsymbol{\tau}}^{\mathrm{m}}(\boldsymbol{q},\bar{\boldsymbol{z}},\boldsymbol{a}) - \hat{\boldsymbol{G}}^{\mathrm{T}}\boldsymbol{\lambda}^{\mathrm{c}}. \tag{3.17}$$

Matrix $\widehat{\boldsymbol{M}} \in \mathbb{R}^{24,24}$ denotes the mass matrix with respect to absolute velocities of the bone segments and the corresponding soft tissue. Likewise, vector $\hat{\boldsymbol{\tau}}^{\mathrm{g}} \in \mathbb{R}^{24}$ contains the gravitational forces/torques, vector $\hat{\boldsymbol{\tau}}^{\mathrm{l}} \in \mathbb{R}^{24}$ the ligament and capsular forces/torques, vector $\hat{\boldsymbol{\tau}}^{\mathrm{f}} \in \mathbb{R}^{24}$ the measured and transferred torques, vector $\hat{\boldsymbol{\tau}}^{\mathrm{m}} = \boldsymbol{B}\boldsymbol{C}\boldsymbol{a} \in \mathbb{R}^{24}$ the muscle forces/torques, and vector $\hat{\boldsymbol{\tau}}^{\mathrm{c}} \in \mathbb{R}^{24}$ the Coriolis and centrifugal forces/torques as well as gyroscopic torques, all given with respect to absolute velocities. Evaluation of Eq. (3.17) then delivers the reaction forces $\boldsymbol{f}^{\mathrm{r}}$ at the hip joint which are transferred to the robot controller.

3.3.3 Implementation of the Musculoskeletal Model

The musculoskeletal model is based on osseous geometries derived from a human male computed tomography dataset [357] using segmentation and reconstructing techniques [216] (Fig. 3.3a). Reconstructed geometries were transformed into local reference frames [16, 424, 425]. Joint rotation centers were obtained by fitting spheres or cylinders into articulating surfaces of the geometries. Subsequently, the kinematic chain described above was composed in the multibody software SIMPACK (v8.9, Simpack AG, Gilching, Germany) [330] starting with the foot attached to the global reference frame [423].
One segment generally consists of bone and soft tissue structures. The overall segment masses m_i were formulated as functions of the subject's mass using regression equations [418] which were further differentiated into bone and soft tissue masses. A linear regression equation correlating effective bone density to Hounsfield units [379] was used to estimate an average bone density ρ_{b} from the histogram of the segmented femoral bone, where $\rho_{\mathrm{b}} = 1.69 \cdot 10^3$ kg/m^3. Along with the volumes of the reconstructed geometries, the bone masses were calculated. Soft tissue masses were then obtained by subtracting the bone masses

Fig. 3.3 Musculoskeletal model of the lower right extremity with the upper body attached as one rigid segment and an implanted THR.

from the overall segment masses. Mass moments of inertia were derived from full cylinders representing bone structures fitted into the proportions of the osseous geometries. Hollow cylinders aligned to the full cylinders embodied soft tissue structures assuming a soft tissue density $\rho_s = 1.056 \cdot 10^3$ kg/m^3 [400]. Bone mass centers were identified with the volume centers of the reconstructed bone geometries. Mass centers of the soft tissue were placed into the centers of the hollow cylinders. The overall segment mass moments of inertia $\boldsymbol{I}_i$ and mass centers were determined from the inertia properties of bone and soft tissue structures. Within this work, the segments for the pelvis and the upper body were considered with only half the overall segment mass as only the right body part is concerned.

As implantation of THR components may alter the geometric proportions within the kinematic chain, both the acetabular cup and the femoral stem were virtually implanted into the bone geometries introducing implant positioning and design parameters. On the one hand, the cup was placed according to radiographic angles (inclination ι, anteversion β) with respect to the pelvic reference frame [214, 282] preserving the hip joint rotation center on the pelvic side. On the other hand, the stem was positioned along the long axis of the proximal femur shaft whereas the neck-shaft intersections of both implant and bone served as reference points for implant setting s. Femoral antetorsion ϑ was defined as rotation around the implant shaft axis aligned to the long axis of the proximal femur shaft. At $\vartheta = 0°$ antetorsion, the implant neck axis fell into a plane spanned by the most posterior points of the two condyles and the greater trochanter. For given design parameters (neck-to-shaft angle ν, neck length l, head offset h and head diameter d), the hip joint rotation center was defined with respect to the femoral reference frame which does not necessarily coincide with the center of the native femoral head.

Passive forces from capsule and ligament structures were neglected, i.e. $\boldsymbol{\tau}^{\mathrm{l}} = \mathbf{0}$. Active muscle forces were assumed to act along straight lines [45, 346]. Hence, overall $n = 70$ muscle elements were implemented according to anatomic attachment sites [147, 341] whereas larger muscles were split into several elements (Fig. 3.3b). Muscle wrapping and curvature was taken into account by using segment-fixed via-points [171]. Likewise, deflection of the quadriceps apparatus was modeled by femur-fixed via-points along the trochlear groove gained from a patellofemoral model [176]. Physiological cross section areas A_j were derived from the literature [213, 399]. Physiological muscle stresses were assumed to be $\sigma_j = 1.0$ MPa [4] for all muscle force elements. A quadratic programming algorithm [236] was implemented into the model to resolve both redundancy problems given in Eq. (3.13) and Eq. (3.16), respectively. Input and output interfaces were integrated to enable the data transfer between the model and the control system.

Subsequently, the musculoskeletal model was scaled onto the subject from the motion analyses (see chapter 3.2) according to his osseous anatomic structure derived from the MRI data recorded and body weight. Likewise, segment-fixed points were generated in the model based on the position of the skin markers relative to the bones. The measured maneuvers were transferred onto the joint coordinates of the model $\boldsymbol{q}$ by means of a model-based least squares fit where the distances between skin markers and related segment-fixed points were minimized by coupled springs. The cost function of this procedure can be interpreted as potential of virtual springs between trajectories of the skin markers and compliant trajectories of the segment-fixed points. This resulted in one set of joint coordinates $\boldsymbol{q}(t)$ for each maneuver from the averaged and smoothed kinematic data (compare Chapter 3.2) leading to two model variations. A smooth contact [439] was implemented for the seating-to-rising maneuver between the global reference frame at seat height and the tuber ischiadicum. CAD data of the femoral stem (SL-Plus, size 6, Smith & Nephew Orthopaedics AG, Baar, Switzerland) were virtually implanted into both model variations with a neck-to-shaft angle $\nu = 131°$, a neck length $l = 53.9$ mm, a head offset $h = 0$ mm and a head diameter $d = 28$ mm. The stem was placed at $\vartheta = 25°$ antetorsion with an implant setting of $s = -5$ mm such that the rotation center of the implant coincided with the center of the subject's femoral head. A reconstructed acetabular cup was orientated at $\iota = 45°$ inclination and $\beta = 0°$ anteversion.

3.4 Validation of the HiL Simulation

3.4.1 Configuration of the HiL test system

The real femoral stem (SL-Plus, size 6, cone 12/14, CCD angle 131°, Smith & Nephew Orthopaedics AG, Baar, Switzerland) with a metallic head (size 28/M) was fixed with polyurethane casting resin into the mounting device attached to the endeffector of the robot.

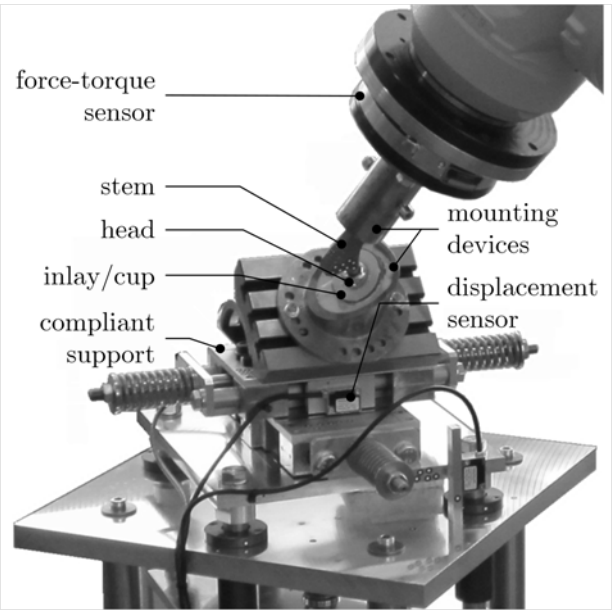

Fig. 3.4 Configuration of the physical setup for testing THRs. The THR components are attached to mounting devices which are fixed to the endeffector of the robot and the compliant support, respectively.

Likewise, the acetabular cup (Alloclassic CSF, size 52, with a polyethylene inlay, size 52/58, Zimmer GmbH, Freiburg, Germany) was mounted on the compliant support (Fig. 3.4). Cup orientation corresponded to cup positioning in the model variations. Relative displacements $\boldsymbol{z}$ between the femoral head and the cup are obtained by subtracting the data recorded by the displacement sensors from the position of the endeffector. This approach suffers from deviations due to small elastic deformation of the femoral component which were diminished by an error model implemented into the control program. The error model was adjusted for each model variation such that dislocation was indicated beyond 3 mm displacement between head and cup. No lubrication was used during testing.

Both model variations were exported into real-time capable machine code as an ordinary-differential-equations formulation using the explicit Euler integrator scheme [107] with 1 ms as fixed step size. This way, a scaling factor was introduced between simulation time and real time as a control cycle of 8 ms was used for the robot controller. The exported model variations were embedded into the control system to allow interactions with the physical setup (see chapter 2.2). Before each HiL simulation, the force-torque sensor was calibrated for the given joint motion by subtracting the resulting torque due the endeffector's weight at the femoral head. Both initial angular position and force was applied by the robot according to the initial values of the model. At this position, all values of the relative displacements measured $\boldsymbol{z}$ were reset to zero. Finally, the HiL simulation was initialized by the model.

During simulation all transferred quantities between model variations and physical setup were recorded. Calculated hip joint reaction forces were also transformed into the global reference frame. The force components were reflected along the sagittal plane to allow comparison to the force data of the patients [33] which were given with respect to the left hip joint. Moreover, ground reaction forces were obtained. All outcomes were normalized

with respect to time to gain one complete motion cycle from a two-legged stance position and back. These results were used to asses validity of the HiL simulation for each maneuver against the data derived from the in vivo study [33].

3.4.2 Results of the HiL simulations

At each time instant the musculoskeletal model calculated the joint reaction forces according to the joint angles given. By transferring corresponding values for the hip joint to the robot controller, the robot adjusted current orientation and loading of the real implant components. Fed back torques measured along the free directions influenced muscle force calculation at the next instant of time. Each HiL simulation was stopped after finishing one complete motion cycle (Fig. 3.5).

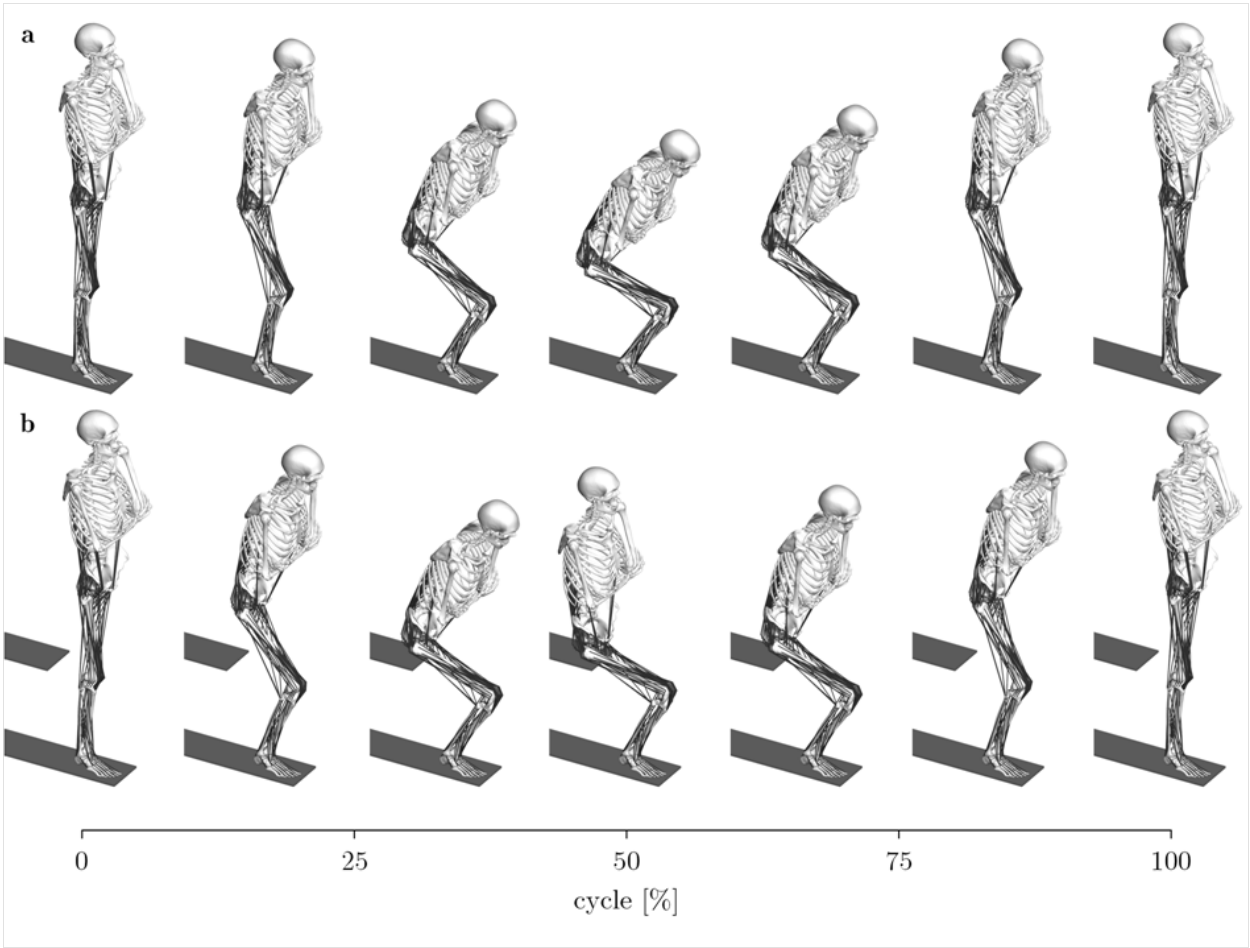

Fig. 3.5 Complete cycles of subject-specific maneuvers during the two HiL simulations. **a** Knee bending. **b** Seating-to-rising.

The knee bending maneuver consisted of large flexion movements ranging from 0° to over 83° flexion in the hip joint (Fig. 3.6a). Low external rotations up to 9° were registered at the beginning and end of the cycle. Only minor abduction movements were noted at higher flexion. Rising and descending of the flexion angle was consistent with an increasing and decreasing reaction force calculated in the hip joint (Fig. 3.6b). The major force component with respect to the pelvic reference frame was estimated in x-direction with about -188 % of subject's body weight (%BW) at 65 % of the motion cycle. Absolute values varied from 57 %BW to 268 %BW. No dislocation process occurred during the HiL simulation as only minor relative displacements were measured (Fig. 3.6c). Moreover, the friction torque was recorded with peak values around 0.4 %BWm during squatting which increased up to 0.67 %BWm during coming out of the squat (Fig. 3.6d).

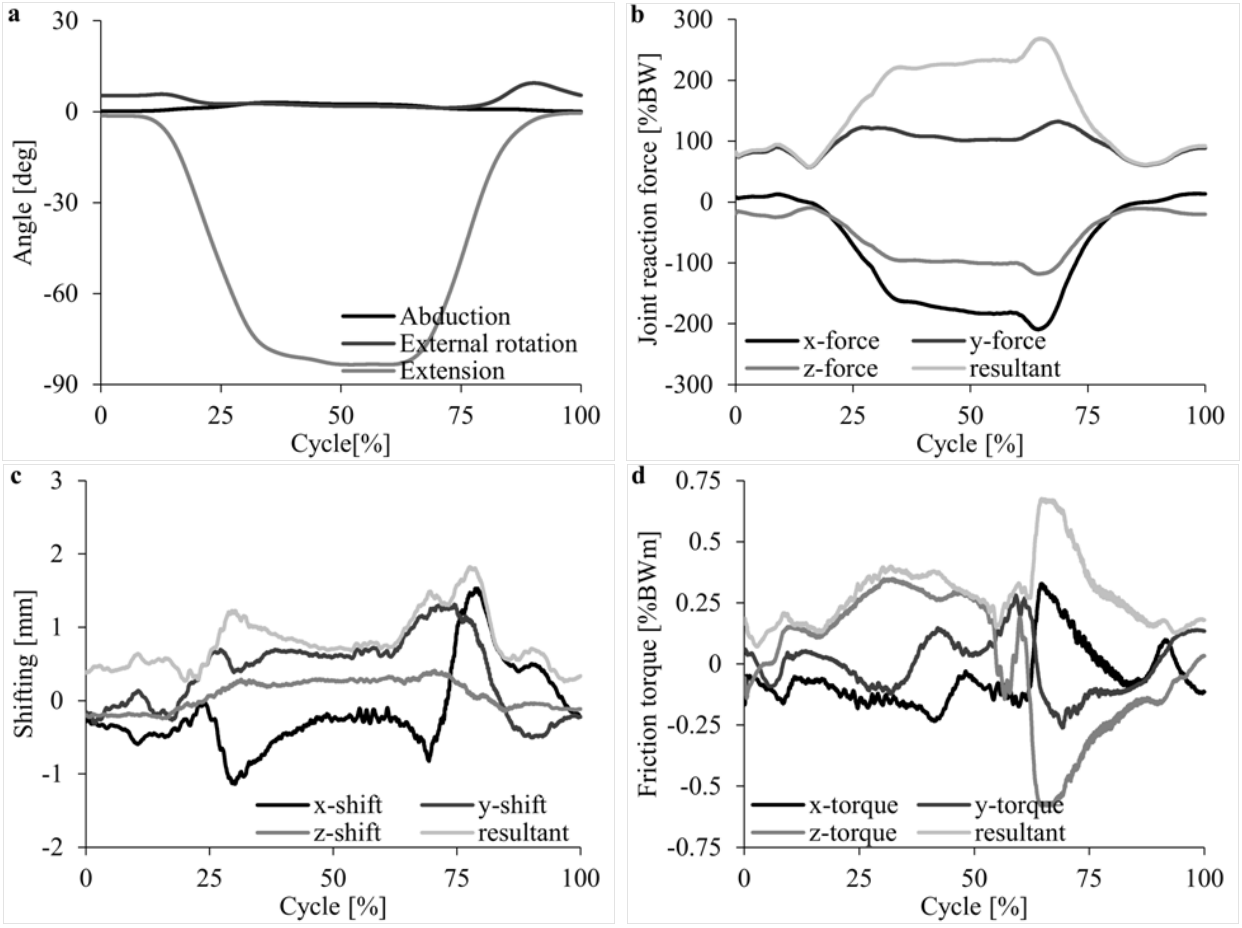

Fig. 3.6 Outcomes of the HiL simulation for the knee bending maneuver given with respect to one complete motion cycle. Unfiltered data. **a** Hip joint angles describing pelvic rotation with respect to the femur in Cardan angles. **b** Hip joint reaction force predicted by the musculoskeletal model given in the pelvic reference frame. **c** Measured shifting of the femoral head with respect to the pelvic reference frame. **d** Friction torque measured by the force-torque sensor with respect to the pelvic reference frame.

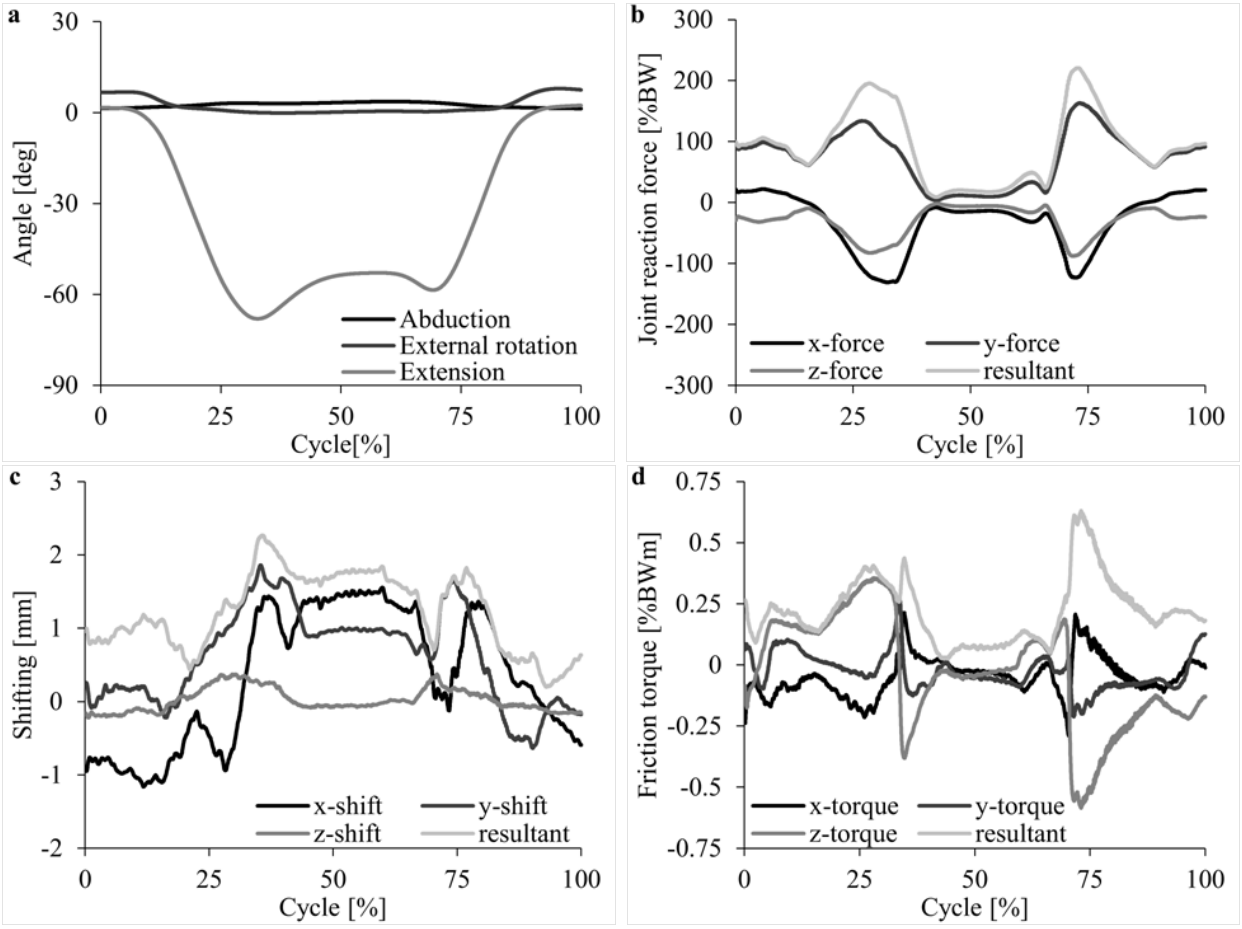

Fig. 3.7 Outcomes of the HiL simulation for the seating-to-rising maneuver given with respect to one complete motion cycle. Unfiltered data. **a** Hip joint angles describing pelvic rotation with respect to the femur in Cardan angles. **b** Hip joint reaction force predicted by the musculoskeletal model given in the pelvic reference frame. **c** Measured shifting of the femoral head with respect to the pelvic reference frame. **d** Friction torque measured by the force-torque sensor with respect to the pelvic reference frame.

As far as the seating-to-rising maneuver is concerned the flexion movement reached 68° in contrast to low abduction and external rotation angles (Fig. 3.7a). Seating and rising phases were accompanied by increase of the hip joint reaction force (Fig. 3.7b). The major force component was recorded around 159 %BW in y-direction with respect to the pelvic reference frame. Absolute force values showed peaks with 195 %BW during sitting down and 220 %BW during standing up. Throughout the duration of actual sitting, between 40 % and 60 % of the motion cycle, the absolute force decreased below 10 %BW. With maximum displacements around 2 mm, no dislocation was indicated during the HiL simulation (Fig. 3.7c). The absolute friction torque reached peak values around 0.43 %BWm during seating and 0.63 %BWm during rising (Fig. 3.7d).

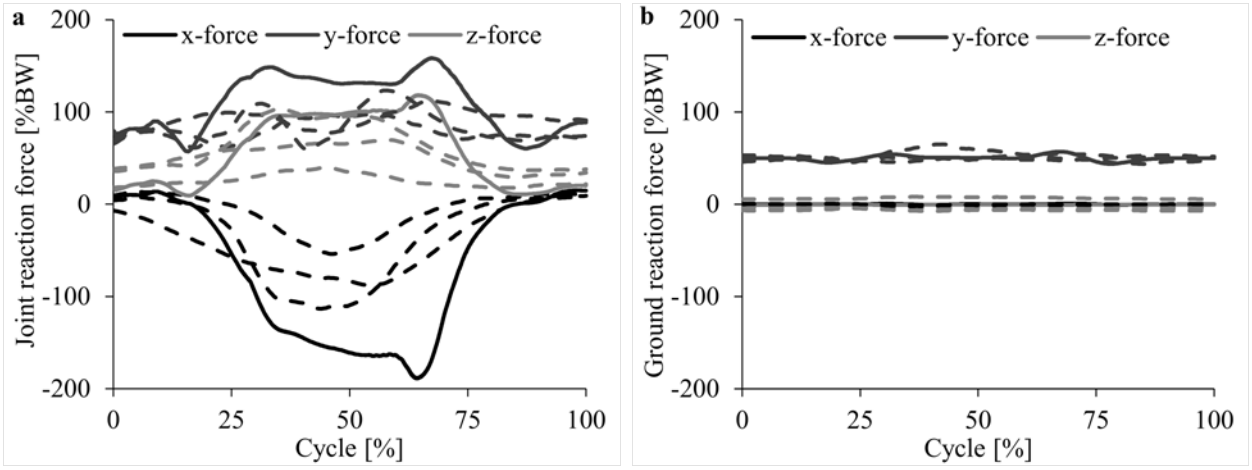

Fig. 3.8 Force components calculated during HiL simulation (solid lines) compared to averaged in vivo data (dashed lines) derived from three male patients [33] for the knee bending maneuver. All data are given with respect to the global reference frame [423] and the left side of the body. **a** Hip joint reaction force. **b** Ground reaction force.

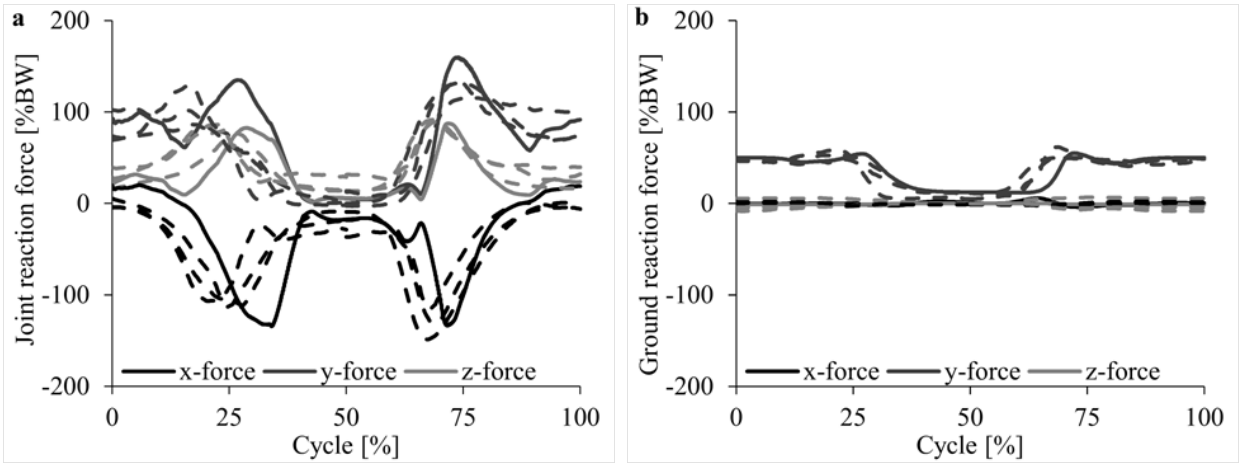

Fig. 3.9 Force components calculated during HiL simulation (solid lines) compared to averaged in vivo data (dashed lines) derived from three male patients [33] for the seating-to-rising maneuver. All data are given with respect to the global reference frame [423] and the left side of the body. **a** Hip joint reaction force. **b** Ground reaction force.

Calculation of the hip joint and the ground reaction force enabled comparison to the in vivo data derived from three male patients [33]. The knee bending maneuver revealed overestimation of the force components compared to the patients' data (Fig. 3.8a). However, the model predicted well major trends along the three directions for this load case. Regarding the seating-to-rising maneuver (Fig. 3.9a), all force components agreed well in trend and magnitude with the patients' data, apart from the subject's timing. Estimated ground reaction

forces correlated adequately for both maneuvers which especially applies for the y-component vertical to the ground (Fig. 3.8b) and Fig. 3.9b). As a result, the HiL test system is capable of simulating comparable THR load cases as given under in vivo conditions.

4 Dynamic Testing of Total Knee Replacements

As for THRs the HiL test system is adopted for TKR testing. First, a functional principle is developed from the underlying HiL concept for an unconstrained artificial knee joint. Since the ligament apparatus plays a decisive role for TKR stability, the configuration considered here focuses on the replication of TKR dynamics with physiological representation of major ligament structures. For validation purposes, tibiofemoral load data were retrieved from a study on knee extension movements of instrumented human knee specimens. The multibody model required follows a forward dynamics approach with incorporation of displacement and torque measurements from the physical setup. It is implemented into a multibody software suitable for real-time applications in order to reproduce the same load conditions as during in vitro testing. At the end of the chapter, the validity of the test system is assessed by comparing the outcomes of the HiL simulation to the in vitro derived data.

4.1 Functional Principle of Testing Total Knee Replacements

Considering native knee joints, the relative mobility between adjacent bone segments is generally less constrained than for hip joints. Depending on the TKR type implanted, however, the relative mobility varies after total knee arthroplasty. For instance, rotating hinge implants restrict all translational and rotational directions except of flexion/extension movements as the tibial and femoral components are linked by a hinge joint. Unconstrained, posterior cruciate retaining TKRs replace the articulating surfaces of the native knee without direct linkage between the femoral and tibial components. For this type of implant the three translations and the adduction/abduction rotation are restricted due to soft tissue restraints and contact between the components, similar to the native knee joint [41, 42, 314]. These directions are defined as constrained directions in the following control strategy comparable to a universal joint as shown in Fig. 2.2b. The remaining flexion/extension and internal/external rotations are treated as free directions within the technical range of motion.

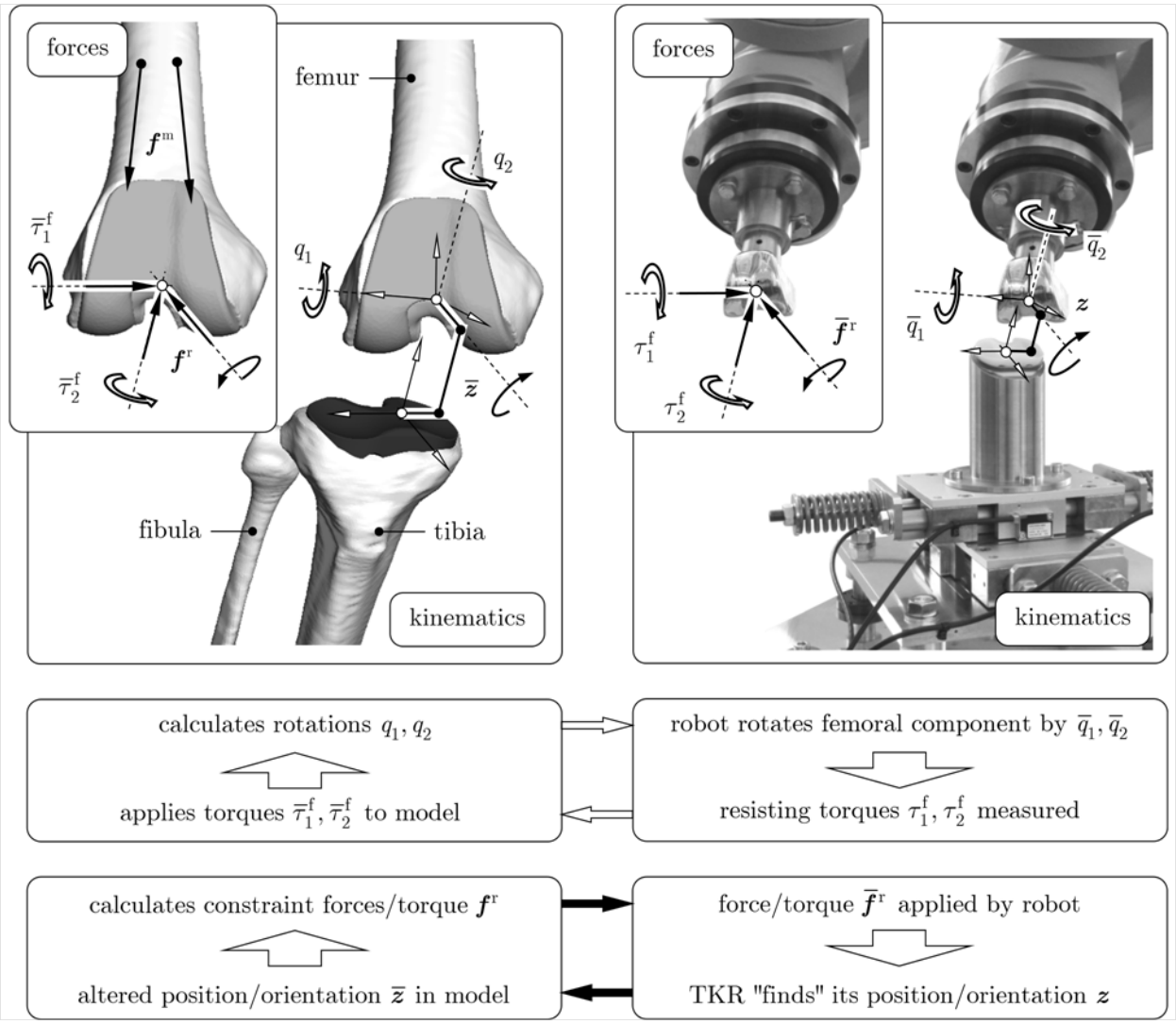

Fig. 4.1 Functional principle of the HiL simulation for testing TKRs with respect to joint stability. Transfer between the multibody model and the physical setup is illustrated within the two control loops on kinematic and force level.

Regarding the spatial load case according to Fig. 4.1, the free directions are given by the angles q_1 (flexion/extension) and q_2 (internal/external rotation). The three translational directions and the remaining rotational direction of the tibiofemoral joint are summarized in the vector $\boldsymbol{z}$ as constrained directions. For an actual time instant t the multibody model delivers values of the coordinates q_1 and q_2 in the free directions and reaction forces/torque in the four constrained directions, summarized in the vector $\boldsymbol{f}^r$. Soft tissue forces are also taken into account besides the patellar contact force, gravitational and inertial forces. Both coordinates q_1, q_2 and reaction forces/torque $\boldsymbol{f}^r$ are transferred to the robot controller. Hence, the robot rotates the femoral component into the position $\bar{q}_1$, $\bar{q}_2$ and applies the reaction forces/torque $\bar{\boldsymbol{f}}^r$ onto the TKR. The quantities with bar denote again transferred

values from the model to the physical setup and vice versa. In the case of ideal transmission the transferred robot values $\bar{q}_1$, $\bar{q}_2$ and $\bar{\boldsymbol{f}}^{\mathrm{r}}$ are identical with the corresponding values q_1, q_2 and $\boldsymbol{f}^{\mathrm{r}}$ of the model.

In order to close the HiL control loop the three displacements and one rotation, summarized in vector $\boldsymbol{z}$, are measured and fed back to the multibody model. Another loop closure is achieved by the torques τ_1^{f} and τ_2^{f} along the coordinates q_1 and q_2, which are also measured and fed back into the model. These torques could be caused by friction forces in the TKR. Again disturbances of the measurements and the signal transmissions cause differences between the actual robot values τ_1^{f}, τ_2^{f}, $\boldsymbol{z}$ and the corresponding transferred values $\bar{\tau}_1^{\mathrm{f}}$, $\bar{\tau}_2^{\mathrm{f}}$, $\bar{\boldsymbol{z}}$. The robot is able to apply the reaction forces/torque $\bar{\boldsymbol{f}}^{\mathrm{r}}$ as long as the TKR components bear these loads in the corresponding directions. This is generally accompanied by increasing relative displacements and rotation $\boldsymbol{z}$ that influence soft tissue elongation during the next time instant. Furthermore, abnormal relative movement between the components may indicate an unstable TKR conjunction.

4.2 Experimental Data

Validation of the HiL simulation is based on the in vitro study conducted by Kessler et al. [204]. Within their experimental work, a single radius posterior cruciate retaining TKR (Scorpio CR, Stryker Orthopaedics, Mahwah, New Jersey, USA) with patellar resurfacing was implanted into six human specimens of the lower extremity using a medial surgical approach. Each specimen was resected midway of the femoral bone and horizontally attached to a custom-made experimental setup (Fig. 4.2). All proximal muscle tissue such as the hamstrings and the quadriceps muscles were also removed. The quadriceps tendon was actuated by an electric motor in order to simulate knee extension from 90° to 0° at a rate of 1° per second.

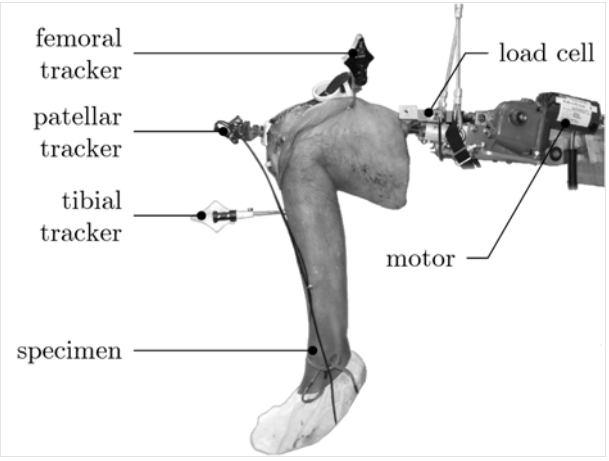

Fig. 4.2 Experimental setup for testing human knee specimens regarding flexion/extension movements with an instrumented TKR, extracted from Kessler et al. [204].

During their testing both patellar and tibial kinematics were recorded with respect to the femur by means of a navigation system. The rotations followed a rotation sequence with flexion/extension about the mediolateral axis of the femur, adduction/abduction about the anteroposterior axis and internal/external rotation about the superoinferior axis of the tibia. Femoral anteroposterior translation (femoral rollback) was measured as translation of the center of the femoral transepicondylar line with respect to the center of the anteroposterior and mediolateral extents of the tibia. Furthermore, the implanted tibial tray was equipped with force transducers [201]. This allowed measurement of the contact force between the implant components along the tibial shaft perpendicular to the inlay. Both kinematic and force data recorded are used in the following to validate the HiL simulation for testing the same TKR system.

4.3 Multibody Model of the Artificial Knee Joint

4.3.1 Multibody Topology

For validation purposes, the multibody model replicates the test conditions as present in the experimental setup according to Fig. 4.2. Hence, it comprises $p = 2$ moving bone segments within an open-chain topology. The kinematic chain is composed of the femur assumed to be ground-fixed, the patella and the tibia along with the fibula modeled as one rigid body (Fig. 4.3). In addition, the foot is rigidly attached to the tibia with a flexion angle of 90°. Modeled as a kinematic subchain the tibiofemoral joint is represented by three orthogonal prismatic joints and three revolute joints with co-intersecting axes describing a

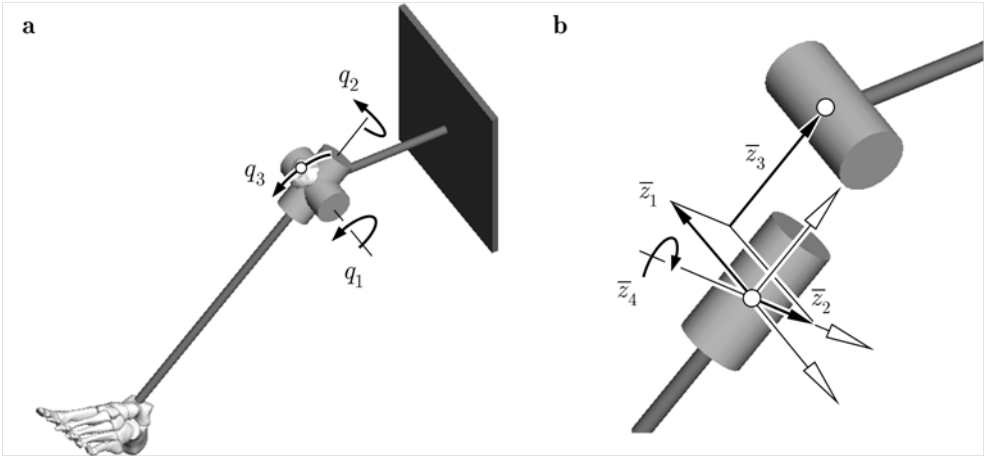

Fig. 4.3 Multibody model of the artificial knee joint for testing TKRs. **a** Multibody topology showing the minimal coordinates of the tibiofemoral and patellofemoral joint. **b** Measured and transferred coordinates in constrained directions of the TKR.

rotation sequence based on Cardan angles. Two revolute joints correspond to the free flexion/extension and internal/external rotations described by the rotation angles q_1 and q_2, respectively. The coordinates of the $b_z = 4$ other joints are constrained by the measurements $\bar{\boldsymbol{z}}$ provided by the robot. The patella is linked to the femur by a generalized, one-degree-of-freedom joint given in terms of one independent coordinate q_3. In this way the deflection of the patella is taken into account along the femoral trochlea.
The motion of the skeletal system is described by $f = 3$ independent coordinates $\boldsymbol{q} \in \mathbb{R}^3$ with $b_z = 4$ measured constraint coordinates $\bar{\boldsymbol{z}} \in \mathbb{R}^4$ of the artificial knee joint, i.e.

$$\boldsymbol{q} = [q_1\, q_2\, q_3]^{\mathrm{T}} \qquad \text{and} \qquad \bar{\boldsymbol{z}} = [\bar{z}_1 \ldots \bar{z}_4]^{\mathrm{T}}\,. \tag{4.1}$$

Vector $\boldsymbol{q}$ summarizes the free coordinates of the tibiofemoral joint, q_1 and q_2, and the patellofemoral joint, q_3. Hence, the position and orientation of the i-th segment (tibia or patella, respectively) is expressed in terms of the independent coordinates $\boldsymbol{q}$ and the measurements $\bar{\boldsymbol{z}}$ as

$$\boldsymbol{r}_i = \boldsymbol{r}_i(\boldsymbol{q}, \bar{\boldsymbol{z}}) \qquad \text{and} \qquad \boldsymbol{S}_i = \boldsymbol{S}_i(\boldsymbol{q}, \bar{\boldsymbol{z}}), \tag{4.2}$$

where $\boldsymbol{r}_i \in \mathbb{R}^3$ denotes the position vector of the mass center and $\boldsymbol{S}_i \in \mathbb{R}^{3,3}$ the rotation matrix (compare chapters 2.3.1 and 3.3.1). The translational and rotational velocities of the i-th segment are then given by

$$\boldsymbol{v}_i = \boldsymbol{J}_{\mathrm{T}i}(\boldsymbol{q}, \bar{\boldsymbol{z}})\, \dot{\boldsymbol{q}} \qquad \text{with} \qquad \boldsymbol{J}_{\mathrm{T}i} = \frac{\partial \boldsymbol{v}_i}{\partial \dot{\boldsymbol{q}}}, \tag{4.3}$$

$$\boldsymbol{\omega}_i = \boldsymbol{J}_{\mathrm{R}i}(\boldsymbol{q}, \bar{\boldsymbol{z}})\, \dot{\boldsymbol{q}} \qquad \text{with} \qquad \boldsymbol{J}_{\mathrm{R}i} = \frac{\partial \boldsymbol{\omega}_i}{\partial \dot{\boldsymbol{q}}}, \tag{4.4}$$

with the translational and rotational Jacobian matrices, $\boldsymbol{J}_{\mathrm{T}i} \in \mathbb{R}^{3,3}$ and $\boldsymbol{J}_{\mathrm{R}i} \in \mathbb{R}^{3,3}$, respectively. By further differentiation with respect to the inertial frame, the translational and rotational accelerations of the i-th segment are obtained as

$$\dot{\boldsymbol{v}}_i = \boldsymbol{J}_{\mathrm{T}i}(\boldsymbol{q}, \bar{\boldsymbol{z}})\, \ddot{\boldsymbol{q}} + \bar{\boldsymbol{a}}_i \qquad \text{with} \qquad \bar{\boldsymbol{a}}_i = \dot{\boldsymbol{J}}_{\mathrm{T}i}(\boldsymbol{q}, \dot{\boldsymbol{q}}, \bar{\boldsymbol{z}})\, \dot{\boldsymbol{q}}, \tag{4.5}$$

$$\dot{\boldsymbol{\omega}}_i = \boldsymbol{J}_{\mathrm{R}i}(\boldsymbol{q}, \bar{\boldsymbol{z}})\, \ddot{\boldsymbol{q}} + \bar{\boldsymbol{\alpha}}_i \qquad \text{with} \qquad \bar{\boldsymbol{\alpha}}_i = \dot{\boldsymbol{J}}_{\mathrm{R}i}(\boldsymbol{q}, \dot{\boldsymbol{q}}, \bar{\boldsymbol{z}})\, \dot{\boldsymbol{q}}. \tag{4.6}$$

The time derivatives of the measured coordinates $\bar{\boldsymbol{z}}$ are neglected, $\dot{\bar{\boldsymbol{z}}} = \ddot{\bar{\boldsymbol{z}}} = \boldsymbol{0}$, as the dynamics of the displacements in the constrained directions is based on the settings of the force controller of the robot.

4.3.2 Estimation of Knee Joint Reaction Forces

As all relevant muscle structures were resected within the experimental work [204], the forces considered in the multibody model arise from passive forces only. With $\boldsymbol{\tau}^{\mathrm{m}} = \boldsymbol{0}$, the applied

forces according to Eq. (2.18) are summarized to

$$\boldsymbol{\tau}^{\mathrm{e}} = \underbrace{\boldsymbol{\tau}^{\mathrm{g}}(\boldsymbol{q}, \bar{\boldsymbol{z}}) + \boldsymbol{\tau}^{\mathrm{l}}(\boldsymbol{q}, \dot{\boldsymbol{q}}, \bar{\boldsymbol{z}}) + \bar{\boldsymbol{\tau}}^{\mathrm{f}}(\boldsymbol{q}, \bar{\boldsymbol{z}})}_{\boldsymbol{\tau}^{\mathrm{p}}(\boldsymbol{q}, \dot{\boldsymbol{q}}, \bar{\boldsymbol{z}})}, \tag{4.7}$$

where vector $\boldsymbol{\tau}^{\mathrm{g}} = \boldsymbol{J}^{\mathrm{T}} \hat{\boldsymbol{\tau}}^{\mathrm{g}} \in \mathbb{R}^3$ denotes the torques due to gravitational forces and vector $\boldsymbol{\tau}^{\mathrm{l}} = \boldsymbol{J}^{\mathrm{T}} \hat{\boldsymbol{\tau}}^{\mathrm{l}} \in \mathbb{R}^3$ the torques due to ligament forces spanning the tibio- and patellofemoral joints. The measured and transferred torques $\bar{\tau}_1^{\mathrm{f}}$ and $\bar{\tau}_2^{\mathrm{f}}$, given in local reference frames, are included in vector $\bar{\boldsymbol{\tau}}^{\mathrm{f}} = \boldsymbol{J}^{\mathrm{T}} \hat{\boldsymbol{\tau}}^{\mathrm{f}} \in \mathbb{R}^3$.

Given the applied forces, the equations of motion for the open kinematic chain are formulated in terms of the coordinates $\boldsymbol{q}$ and $\bar{\boldsymbol{z}}$ (compare Eq. (2.17)) as

$$\boldsymbol{M}(\boldsymbol{q}, \bar{\boldsymbol{z}})\, \ddot{\boldsymbol{q}} + \boldsymbol{\tau}^{\mathrm{c}}(\boldsymbol{q}, \dot{\boldsymbol{q}}, \bar{\boldsymbol{z}}) = \boldsymbol{\tau}^{\mathrm{g}}(\boldsymbol{q}, \bar{\boldsymbol{z}}) + \boldsymbol{\tau}^{\mathrm{l}}(\boldsymbol{q}, \dot{\boldsymbol{q}}, \bar{\boldsymbol{z}}) + \bar{\boldsymbol{\tau}}^{\mathrm{f}}(\boldsymbol{q}, \bar{\boldsymbol{z}}). \tag{4.8}$$

The mass matrix $\boldsymbol{M} = \boldsymbol{J}^{\mathrm{T}} \widehat{\boldsymbol{M}} \boldsymbol{J} \in \mathbb{R}^{3,3}$ is obtained under the assumption that the soft tissue masses are added to the masses of the corresponding skeletal segments. The vector $\boldsymbol{\tau}^{\mathrm{c}} = \boldsymbol{J}^{\mathrm{T}} \hat{\boldsymbol{\tau}}^{\mathrm{c}} \in \mathbb{R}^3$ contains the torques of the centrifugal and Coriolis forces as well as gyroscopic torques. Hence, the motion of the system is estimated by evaluating Eq. (4.8) with respect to the accelerations

$$\ddot{\boldsymbol{q}} = \boldsymbol{M}(\boldsymbol{q}, \bar{\boldsymbol{z}})^{-1} (\boldsymbol{\tau}^{\mathrm{g}}(\boldsymbol{q}, \bar{\boldsymbol{z}}) + \boldsymbol{\tau}^{\mathrm{l}}(\boldsymbol{q}, \dot{\boldsymbol{q}}, \bar{\boldsymbol{z}}) + \bar{\boldsymbol{\tau}}^{\mathrm{f}}(\boldsymbol{q}, \bar{\boldsymbol{z}}) - \boldsymbol{\tau}^{\mathrm{c}}(\boldsymbol{q}, \dot{\boldsymbol{q}}, \bar{\boldsymbol{z}})). \tag{4.9}$$

Numerical integration delivers the velocities $\dot{\boldsymbol{q}}$ and the joint angles $\boldsymbol{q}$ for the next time instant.

The reaction forces/torque $\boldsymbol{f}^{\mathrm{r}}$ required for the HiL simulation are obtained for the estimated motion by considering the Newton-Euler equations (compare Eq. (2.14)) for the two rigid segments. Rearrangement of these equations yields the reaction forces/torques $\hat{\boldsymbol{\tau}}^{\mathrm{r}} \in \mathbb{R}^{12}$ given in the inertia frame as

$$\hat{\boldsymbol{\tau}}^{\mathrm{r}} = \widehat{\boldsymbol{M}}(\boldsymbol{q}, \bar{\boldsymbol{z}}) \boldsymbol{J}(\boldsymbol{q}, \bar{\boldsymbol{z}}) \ddot{\boldsymbol{q}} + \hat{\boldsymbol{\tau}}^{\mathrm{c}}(\boldsymbol{q}, \dot{\boldsymbol{q}}, \bar{\boldsymbol{z}}) - \hat{\boldsymbol{\tau}}^{\mathrm{g}} - \hat{\boldsymbol{\tau}}^{\mathrm{l}}(\boldsymbol{q}, \dot{\boldsymbol{q}}, \bar{\boldsymbol{z}}) - \hat{\boldsymbol{\tau}}^{\mathrm{f}}(\boldsymbol{q}, \bar{\boldsymbol{z}}). \tag{4.10}$$

Here, matrix $\widehat{\boldsymbol{M}} \in \mathbb{R}^{12,12}$ describes the mass matrix with respect to absolute velocities of the bone segments and the corresponding soft tissue. Likewise, vector $\hat{\boldsymbol{\tau}}^{\mathrm{g}} \in \mathbb{R}^{12}$ contains the gravitational forces/torques, vector $\hat{\boldsymbol{\tau}}^{\mathrm{l}} \in \mathbb{R}^{12}$ the ligament forces/torques, vector $\hat{\boldsymbol{\tau}}^{\mathrm{f}} \in \mathbb{R}^{12}$ the measured and transferred torques, and vector $\hat{\boldsymbol{\tau}}^{\mathrm{c}} \in \mathbb{R}^{12}$ the Coriolis and centrifugal forces/torques as well as gyroscopic torques, all given with respect to absolute velocities. Evaluation of Eq. (4.10) then provides the reaction forces/torque $\boldsymbol{f}^{\mathrm{r}}$ at the knee joint which are transferred to the robot controller.

4.3.3 Implementation of the Multibody Model

The multibody model was implemented using the simulation package SIMPACK (v8.9, Simpack AG, Gilching, Germany) including all relevant bone and ligament structures (Fig. 4.4). Local reference frames, averaged segment masses, centers of gravity and ligament attachment points were derived from the model description of Kessler et al. [204]. CAD data of the TKR components were aligned with respect to the local reference frames with no angular and translation displacement. Bone segments were extracted from the CT dataset of one left knee specimen with subsequent three-dimensional reconstructions [216] and fitted into the local reference frames. Both femoral and tibial condyles as well as the retropatellar surface were resected after reconstruction such that the TKR components matched the virtual bony contours. Mass moments of inertia were obtained from cylinders fitted into the geometric proportions of the bone segments.

Ligament structures were represented as straight line elements spanning between the corresponding attachment points. These included one bundle of the posterior cruciate, lateral and medial collateral ligaments as well as four bundles of the patellar tendon. The anterior cruciate ligament was not considered as it is generally resected during implantation of a PCR TKR. Each element was modeled as parallel spring-damper combination following non-linear force-displacement characteristics [40] with parameters from the literature [237,241]. For this investigation the translational and rotational path of the patella is based on the averaged kinematic data measured from the six knee specimens [204]. Furthermore, the movement of the patella joint was defined by a rheonomic constraint describing a smooth sinusoidal motion along the joint coordinate q_3. That way tibiofemoral motion was generated governed by gravitational and ligament forces.

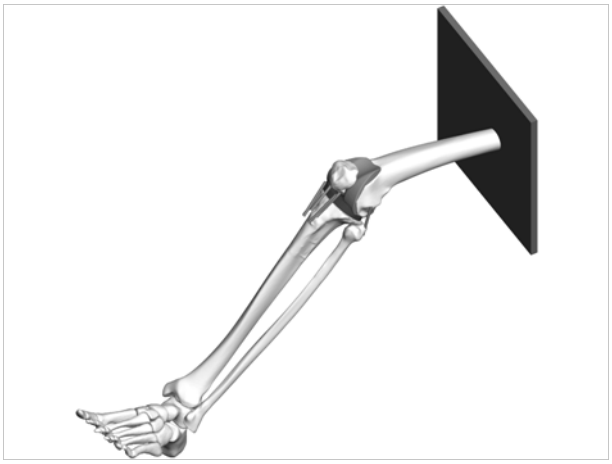

Fig. 4.4 Multibody model of the artificial knee joint with incorporation of bone and ligament structures.

4.4 Validation of the HiL Simulation

4.4.1 Configuration of the HiL test system

After implementation the multibody model described above was exported into real-time capable machine code as an ordinary-differential-equations formulation using the explicit Euler integrator scheme [107] with 1 ms as fixed step size. In this manner a scaling factor was introduced between simulation time and real time as the standard control cycle of 4 ms was used for the robot controller. The exported model was embedded into the control system to allow interactions with the physical setup (see chapter 2.2). The real femoral component (Scorpio CR, size 9, Stryker Orthopaedics, Mahwah, New Jersey, USA) was fixed with polyurethane casting resin into the mounting device attached to the endeffector of the robot (Fig. 4.5). Similarly, the real tibial tray (Scorpio CR, size 9, with a tibial inlay, size 7, thickness 5, Stryker Orthopaedics, Mahwah, New Jersey, USA) was mounted on the compliant support. No lubrication was used during testing.

Before the actual HiL simulation started, the force-torque sensor was calibrated for a flexion motion over 90° by subtracting the resulting torque due the endeffector's weight. The initial position of the femoral component with respect to the tibial inlay was adjusted using force control in the constrained directions. At this position all values of the measurements $\boldsymbol{z}$ were reset to zero. Finally, the HiL simulation was initialized by the model. Measurements were taken from the model and robot including the tibial internal/external rotation, tibial abduction/adduction, anteroposterior translation of the femoral component with respect to the tibial inlay and the force along the tibial shaft. These data were used to asses the validity of the HiL simulation against the in vitro results [204].

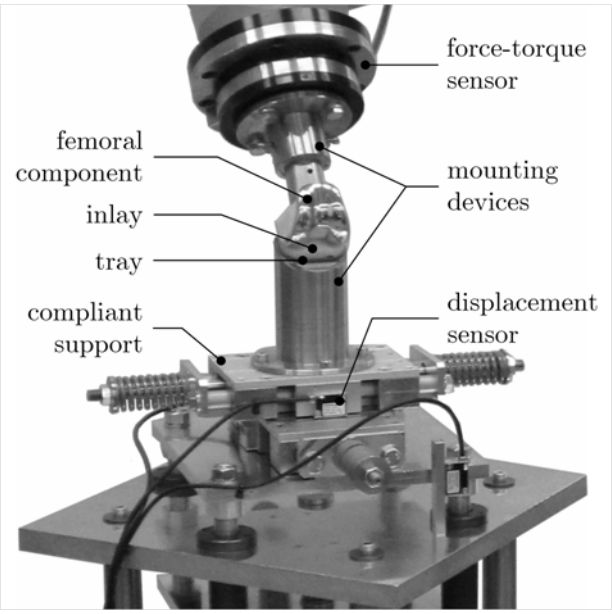

Fig. 4.5 Configuration of the physical setup for testing TKRs. The TKR components are attached to mounting devices which are fixed to the endeffector of the robot and the compliant support, respectively.

4.4.2 Results of the HiL simulation

During the HiL simulation the model determined tibial flexion and internal/external rotation governed by the prescribed patellar path and the applied forces. Along with the reaction forces/torque, the data was sent to the robot controller within the control cycle. The robot rotated the femoral component and loaded the TKR according to the desired values adjusting its current position and orientation. By feeding back the measured relative displacements and rotation, the tibia was shifted and orientated in the constrained directions within the model (Fig. 4.6). This influenced elongation of the incorporated ligaments altering the load situation of the next time instant.

Starting at 5° the simulation was stopped after 90° knee flexion (Fig. 4.7a). The flexion motion was accompanied by minor adduction and external rotation angles. The major force component was estimated perpendicular to the tibial inlay (Fig. 4.7b). Lower shear forces were recorded along the mediolateral and anteroposterior axes corresponding to tibial x- and y directions with values below ± 100 N. Throughout the simulation the femoral component shifted in posteromedial direction with respect to the inlay, with an overall displacement of about 7 mm (Fig. 4.7c). Furthermore, the torque estimated due to contact interactions reached absolute peak values up to 6 Nm (Fig. 4.7d). Oscillating values at the beginning of the simulation, observed especially in the torque data, indicate that the initial position of the real implant components were not exactly in accordance with the model.

According to the results the tibia was gradually rotated with respect to the femoral component from 4° external to about −6° internal rotation at 90° knee flexion (Fig. 4.8a). This differs from the outcomes of the human knee specimens which started between 0° and −15° internal rotation. However, the model followed the general trend of increasing internal rotation at higher knee flexion. Tibial adduction remained around 0° throughout the range of knee flexion reproducing well the behavior of the specimens (Fig. 4.8b). Regarding an-

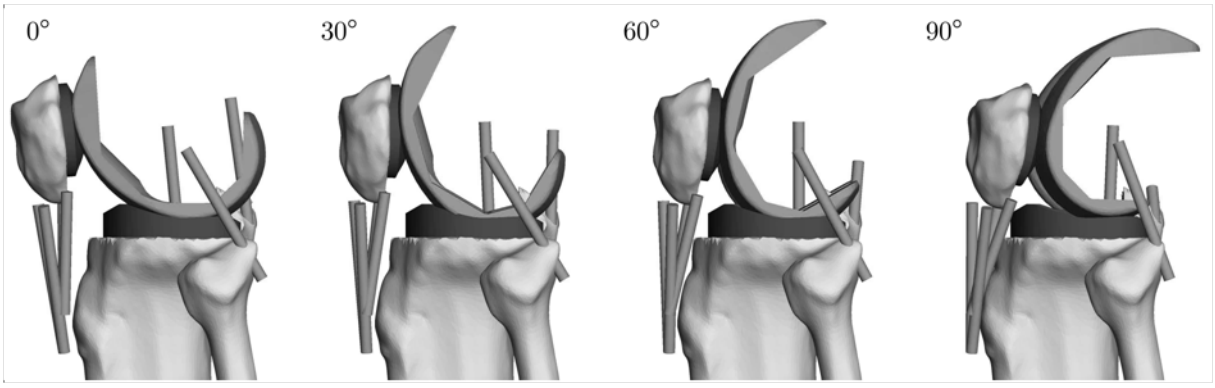

Fig. 4.6 Positioning of the femoral component with respect to the tibial inlay during the HiL Simulation.

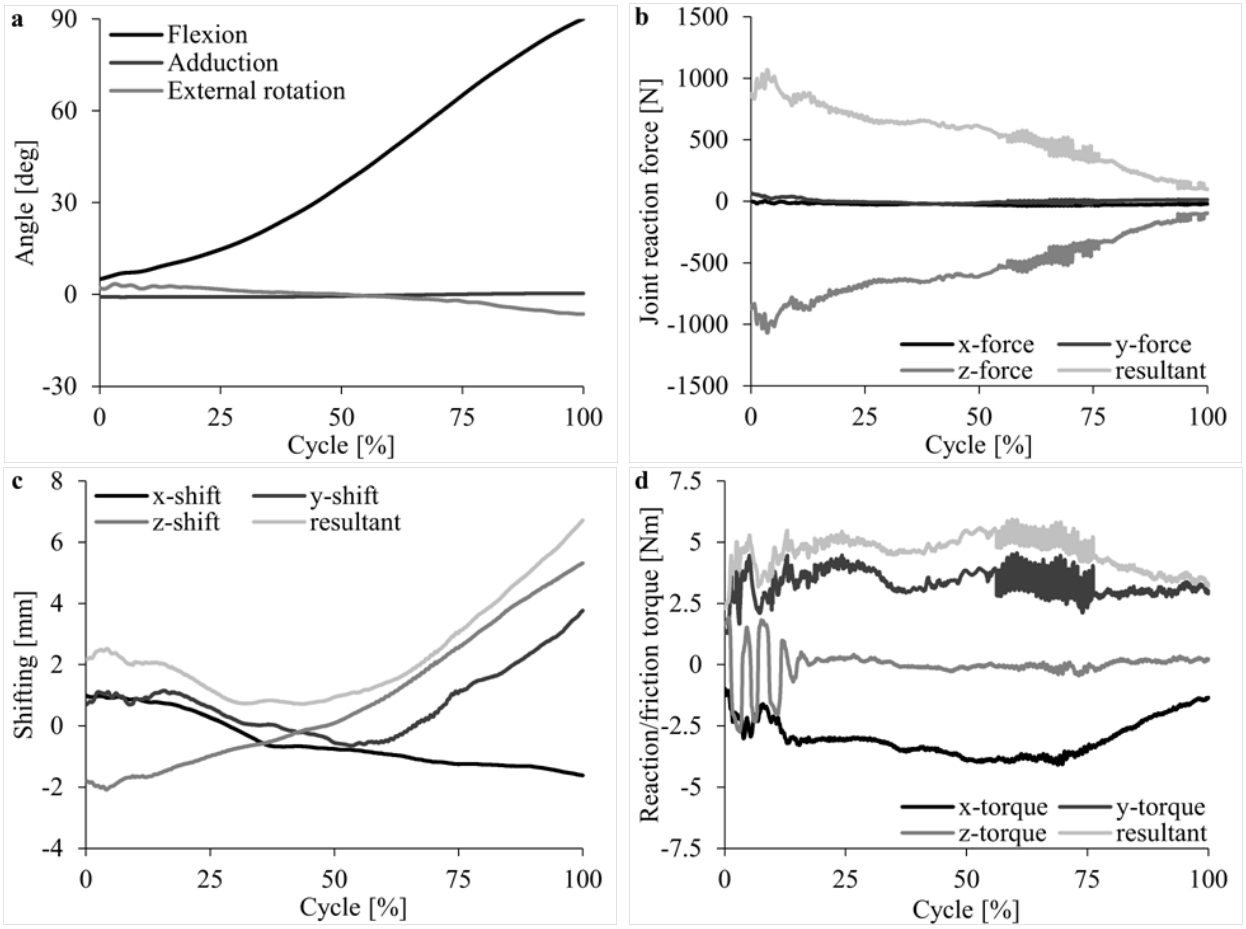

Fig. 4.7 Outcomes of the HiL simulation for the knee flexion movement. **a** Tibial rotation with respect to the femur described by Cardan angles. **b** Tibial knee joint reaction force predicted by the model given in the tibial reference frame. **c** Measured displacement of the femoral component with respect to the tibial reference frame. **d** Estimated reaction/friction torque given in the tibial reference frame.

teroposterior translation (Fig. 4.8c), the femoral component initially moved anterior with respect to the tibial inlay. After 30° knee flexion the femoral component shifted about 4 mm posterior pursuant to femoral rollback at higher knee flexion. This agrees well with the outcomes of the specimens which revealed no up to large femoral rollback. At the beginning of the simulation the tibia was loaded by the robot with a contact force perpendicular to the tibial inlay of about 1000 N (Fig. 4.8d). The loading largely dropped before 30° reaching 100 N at 90° knee flexion. Hence, the contact force recorded described well magnitude and trend compared to the experimental data.

Overall, the results of the HiL simulation were in good agreement with the outcomes of the in vitro study [204]. All results fell within the envelopes of the in vitro data, except of tibial internal/external rotation which, however, reproduced the general trend of the specimens.

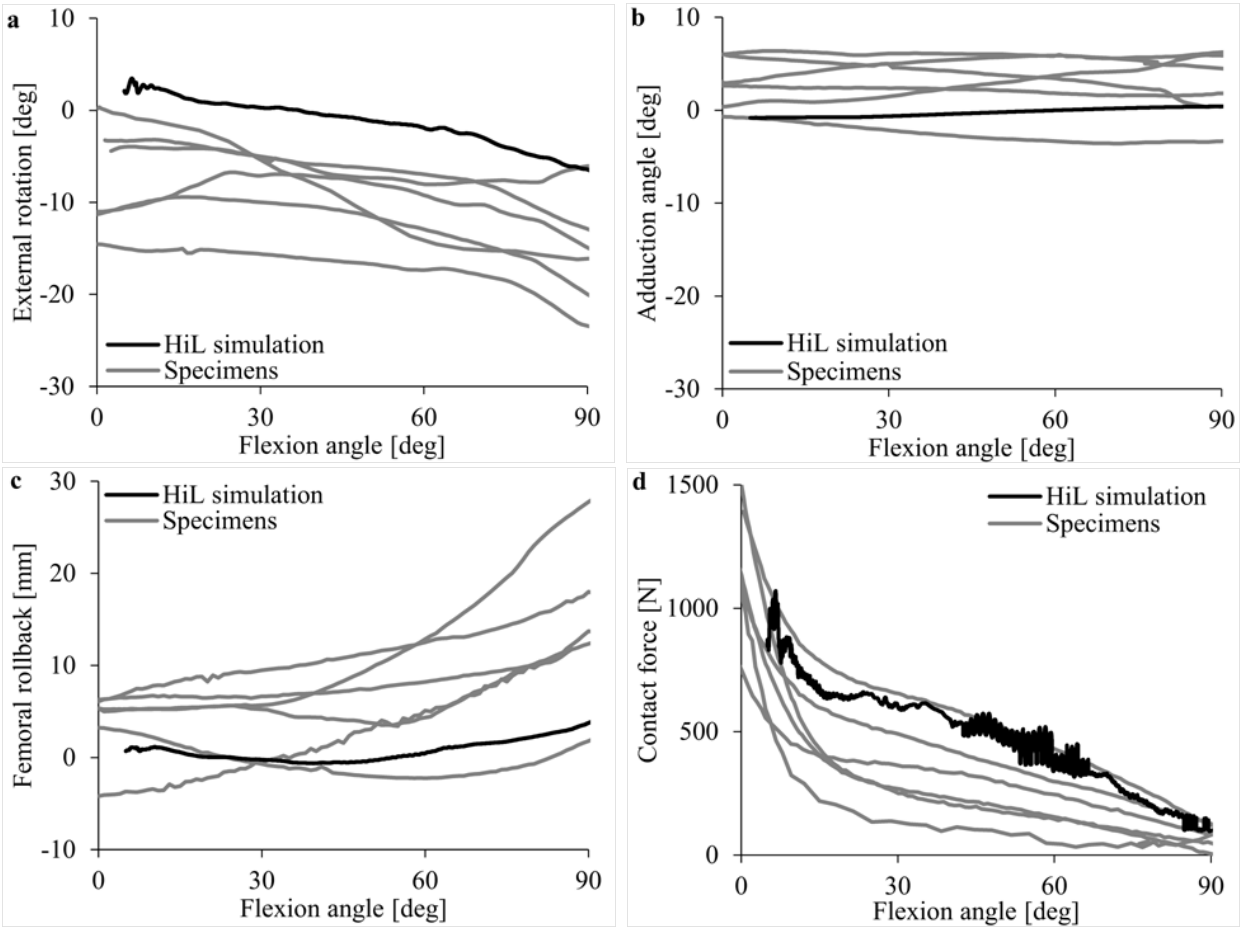

Fig. 4.8 Outcomes of the HiL simulation compared to data derived from six human knee specimens [204]. **a** Tibial external rotation with respect to the femoral component. **b** Tibial adduction with respect to the femoral component. **c** Anteroposterior translation of the femoral component with respect to the tibial inlay. **d** Contact force perpendicular to the tibial inlay.

As a result, the HiL test system is capable of predicting comparable TKR movement and loading as derived under in vitro conditions.

5 Discussion

Comparable testing of various TJRs with respect to their dynamic behavior requires reproducible and physiological test conditions. In the light of this prerequisite, the application of HiL simulations is contrasted with common test and simulation methods as novel testing tool in the field of biomechanical research. This is followed by a review under which conditions THR dislocation and TKR instability, respectively, are tested. The discussion also elucidates the outcomes and limitations of the current configurations of the HiL test system, along with potential contributions to the state of research concerning THR and TKR stability.

5.1 HiL Simulation as Testing Tool

From a biomechanical point of view, the ultimate goal for TJRs implanted into patients is to ensure long-term survival in the in vivo environment. This goal constitutes the basic prerequisite for restoring joint functionality and giving pain relief to suffering patient. In order to satisfy this demand, certain requirements were appointed in national or international standards which implants have to comply with prior to federal approval [73]. The requirements normally address TJR properties such as structural resistance, material behavior and biocompatibility. In this manner testing of components and material provides a solid basis to determine their suitability. In the light of all failure mechanisms reported in patients, however, current standardized testing procedures may not be able to reflect all aspects of joint biomechanics prevailing in vivo. This especially applies for mechanisms where the impact of active and passive soft tissue structures is not yet fully understood.

Concerning joint specific failure mechanisms such as instability and dislocation, researchers in the orthopedic field generally follow three approaches for their investigations: retrospective clinical studies, testing of real components or computer simulations using mathematical models. Whereas clinical studies are primarily limited as many crucial factors cannot be maintained on a constant and independent level, the two other are suitable approaches for illuminating cause and effect on a systematic basis. But both also entail certain limitations. The first experimental test setups in orthopedic research were predominately used to study joint kinematics [3,52,65,151,159,224–226,261,401]. Actuated along one or more directions, mechanical setups allowed for application of constant [14,153,291] or prescribed load patterns

[119,209,252] onto TJRs components. Although a few researchers even implemented passive restraints [93, 250, 397, 398], it remains an open question how passive and active soft tissue structures can be adequately accounted for in a realistic manner.

In contrast to that, specimen-based testing promises incorporation of real soft tissue, such as ligaments and capsular structures, including their mechanical response [86, 114, 258, 268, 280, 292, 355]. Muscle forces were often emulated statically by cable and pulley systems [24, 129, 244, 251, 319, 345, 410] or actively by actuators attached to specific tendons [50, 102, 204, 252, 370, 429] within those experimental setups. Unfortunately, the muscle forces applied using these methods may not reproduce in vivo conditions, let alone consideration of all relevant muscle structures spanning the joint to be tested. Moreover, human specimens do not permit reproducible and comparable evaluation of various parameters under exactly the same boundary conditions due to their decay after extraction.

In addition to testing procedures, mathematical models have been established to be useful tools for biomechanical investigations. Once deployed, simulations can be almost infinitely repeated and parameters arbitrarily varied. Several analytic [103, 182, 214, 217, 312, 413, 414, 431, 432] and MBS [275, 416] approaches assisted to study joint kinematics with respect to their technical RoM. Although MBS modeling implies several idealization and assumptions concerning muscle force estimation, a number of musculoskeletal models [5, 46, 142, 164, 171, 206, 210, 246, 249, 254, 273, 274, 303, 311, 349, 350, 358, 381, 417] were able to reflect in vivo joint loading and presumably physiological muscle force patterns. Other MBS [71, 117, 186, 204, 248, 382, 433] or FEM [17, 18, 124, 127, 128, 155, 437] models enabled investigation of TKR dynamics under in vitro conditions with incorporation of passive soft tissue structures. In addition, researchers evaluated stresses and strains experienced by TJR components and adjacent osseous structures by using FEM analysis [22,100,114,126,215,283,304,343–345]. These studies document that both MBS and FEM modeling approaches (considered separately or coupled) are able to reproduce physiological-like conditions and implement contact mechanics along articulating surfaces. However, models based on specimen-based test setups still inhere the same boundary conditions which especially applies on the lack of active muscle structures. Moreover, simulations including contact mechanics are afflicted with persistent uncertainties concerning the contact conditions. The quality of their results strongly depend on the discretization of surfaces and bodies, the mathematical contact formulation, and proper descriptions of friction and material behavior. Contact modeling therefore represents an intricate task which does not meet all aspects of the real contact situation as, for instance, found in mechanical or experimental testing.

The general problem in examining joint stability and functionality lies in the fact that comprehensive knowledge is required about TJR dynamics for abnormal maneuvers undertaken by patients. Evidence on the process of such events have been merely given by reports of

affected patients [122, 304, 323, 393] or damage found in retrievals [235, 313, 351]. Due to measurements performed in vivo for common activities in THR [33–35, 80, 81, 115, 220, 332] and TKR [96,98,99,101,168,228,376,377] patients, it is well known that joint motion and especially its compliant loading rely mostly on muscle forces, besides inertial, gravitational and ligament/capsular forces. These dependencies on soft tissue structures still persist in cases of abnormal events whereas alterations within the dynamic equilibrium can be expected. Hence, the challenge for TJR testing is to incorporate an environment which reproduces the joint dynamics while accounting for muscle activity and passive response of ligament and capsular structures. As outlined above, it seems impossible to comply with these demands within an experimental test setup alone. Mathematical models may approximate in vivo conditions to a valid extent, though complex contact modeling is limited. These trade-offs led to consideration of alternative approaches which resulted into the HiL test system presented within this work. This approach combines the advantages of real TJR testing and model-based simulation.

There are two essential components of the HiL test systems apart from the control and sensory system. On the one hand, an actuator system is required within the physical setup that guarantees large joint angles with sufficient load bearing capacity in any direction. For investigations on the native and artificial knee joint, several specimen-based test setups were established using robotic systems as actuators. Fuji et al. [138] extended a five-axis, articulated manipulator by a position-controlled translation axis to study anterior-posterior displacements in the knee joint under various force-controlled modes. Similarly, Rudy et al. [329] combined a six-joint serial-articulated manipulator with the force-torque feedback of a universal force sensor. This way, the robot was able to detect a translational and rotational path along the knee joint by means of force-torque control and retrace it under position control. Frey et al. [136] expanded a high-precision robot to an optimized test system by implementation of a quasi-continuous closed-loop controller for hybrid position-force control. In THR research, Kiguchi et al. [209] developed a mechanical test setup consisting of a hexapod platform with hybrid position-force control to investigate scenarios of joint dislocation. These studies prove that robot-based actuator systems are powerful tools for testing complex joint dynamics, especially in combination with a hybrid position-force control.

On the other hand, the purpose of the mathematical model is to determine TJR dynamics within a physiological environment while implementing current measurements of the physical setup. The model performance has to meet the requirements of a real-time simulation such that the dynamics of the real implant components embedded into the physical setup corresponds to the TJR dynamics in the model-based simulation. In a practical sense this means that model calculation and data exchange have to be performed fast enough within one fixed time interval [107], which is limited according to the control cycle of the actuator system.

As a consequence, non-stiff ordinary differential equations are expected from the model formulation which are evaluated by fixed time step numerical solvers [107, 331], typically the explicit Euler method. Stiff ordinary differential equations due to high spring constants and differential-algebraic equations due to kinematic closed loops may also be treated within one fixed time step by introducing linear implicit integration and non-iterative projection methods [10,51]; though these methods were not needed here. The time limit given would be difficult to hold by a FEM based model where generally a large number of equations have to be resolved. In contrast to FEM, the MBS approach is suitable to satisfy the mentioned requirements as already shown in several HiL applications [43,108,211,223,331]. Furthermore, commercial software is available to generate real-time capable machine code [107] which was used in the scope of this work.

Apart from more model-specific implications as highlighted in the following chapters (see chapter 5.2 and 5.3, respectively), the HiL test system entails several limitations in the current state. First, integration of force control along constrained directions of TJRs means that the dynamics of the respective movements are not governed by the equations of motion of the embedded MBS model. Instead, they are based on the settings of the force controller and the constraint stabilization method [197]. This assumption is considered to be acceptable for minor displacements/rotations compared to the motion in the free directions. That is especially the case as long as the robot is able to apply the desired force values onto the TJR components, for instance during subluxation of a dislocating joint. One way to avoid the issue mentioned is to introduce a flexible position-force control where the decision between free and constrained direction is made according to the level of compliance during the simulation rather than defining them a priori.

Second, during preliminary testing it was observed that the THR stem was elastically deformed under increasing loads as the stem could not be completely enclosed with polyurethane casting resin in the mounting device. This leads to additional displacements of the femoral head with respect to the acetabular cup, differing from in vivo conditions where the entire stem is implanted into the femoral bone. Thus, an error model was implemented and calibrated by using a contactless stereo camera system (PONTOS, GOM mbH, Braunschweig, Germany) in each model variation. The purpose of the error model was to estimate the displacements of the femoral head due to linear elastic deformations as a function of the applied forces. The estimated values were then subtracted from the measurements such that dislocation was reliably indicated beyond a 3 mm tolerance range. Furthermore, exchange of relative displacements and rotations require exactly the same position of reference points and orientation of the reference frame in the model simulation and the real actuated components. In contrast to the concentric alignment of THRs, the complex shape of TKR components make it difficult to accurately determine reference points and frames once attached to the robot's endeffector as specified in the MBS model. This inevitably leads to constant devi-

ations due to different initial positions, what was sought to be diminished manually within this work. In order to compensate the drawbacks mentioned for both THR and TKR testing, the relative position of the contacting partners should be identified in a direct manner. This may be achieved by implementing a real-time capable camera system attached to the physical setup which enables precise registration of the components' positioning by using image processing.

Third, the implementation of a robotic actuator system into the HiL control loops implies further demands on the testing procedure. Krenn and Schäfer [223] evaluated the stability of HiL simulations using an industrial robot to emulate the dynamic behavior of a manipulator during contact operations with a real object in space. After varying influencing parameters within a theoretical example, they concluded that large dead times and low sampling rate may cause instabilities of the HiL simulation. In a similar context, Boge and Ma [43] specified two conditions required for high fidelity of contact maneuvers within a robot-based HiL simulation: fast response of the robot to the control command, and same dynamic behavior of the robot's endeffector and the embedded MBS model during contact. The time between command and execution is given by the robot's responding time which was between four to eight times the control cycles in their study. They also stated that industrial robots would not completely conform to the second condition for their HiL application due to their high stiffness.

As all issues concerning dead times, sampling rate and potential instability of the HiL control loops specifically depend on the industrial robot and its control system, the functionality of the HiL test system presented here was verified in previous studies. Kaehler et al. [197] tested both position and force control modes by embedding a simulated spring-damper oscillator with one degree of freedom into the HiL environment. Their comparison between HiL simulation and analytical solution indicated that the position-controlled HiL simulation tended to be less damped and phase-delayed due to the time discretization and parasitic time constants. In force-controlled mode, their HiL simulation was disturbed by a time constant which occurred due the time needed to build-up contact forces. As the force controller governs the dynamic transition, they stated that the dynamics of the MBS model should be lower than that of the force controller. Within another study [175], the functionality of the hybrid position-force control was assured by simulating the dislocation process of a standard THR under prescribed boundary conditions. The outcomes of the study showed overall superior performance compared to results of a mechanical setup [14] in terms of measuring sensitivity and reproducibility. Using the same operation mode, Fabry et al. [119] reproduced physiological loading conditions to evaluate the dynamics of tripolar THR systems. Last but not least, the functional principle of the HiL approach was proven for testing a standard THR [196] and a PCR TKR [177]. The standard control cycle of 4 ms (corresponding to a sampling rate of 250 Hz) proved to work well for position control within these studies,

but may not be sufficient for force control in further HiL applications. In both cases this difficulty was addressed by introducing a scaling factor between simulation and real time as recommended earlier [197]. The outcomes of the THR study [196] showed an altered load situation during the dislocation process in case of changed cup positioning. The TKR study [177] demonstrated that a change in ligament structures within the implemented MBS model results into altered knee kinematics. In the light of these studies, the HiL test system constitutes a unique testing method capable of considering various TJR implants under complex dynamic load conditions.

5.2 Dislocation of Total Hip Replacements under Physiological Conditions

Despite considerable clinical success of THR procedures, dislocation prevails as a fundamental complication after total joint arthroplasty, besides infection and aseptic loosening. Given the clinical relevance researchers have urged to gain further insights on causes and factors influencing the dislocation process which is needed in order to take appropriate countermeasures. As a result of previous biomechanical studies, it is well known that design and positioning parameters predefine the technical RoM and therefore prosthetic impingement. After the first instant of impingement, additional angular motion evokes subluxation, where the femoral head is levered out of the acetabular cup until final dislocation. Moreover, traction forces were observed to pull out the femoral head from the cup leading to spontaneous separation. Although these mechanisms and several interrelations to risk factors have been identified yet, little is known about the actual dynamic behavior of THRs during instability events suffered by patients.

One of the key issues for generating realistic THR dynamics is how to adequately address muscle and capsular forces such that anatomic and physiological conditions are met in a testing environment. Loading and motion were investigated for routine activities [33], but in vivo testing of excessive load cases are not permissible. Bartz et al. [24] implemented a cable and pulley system into their specimen-based experimental setup to apply static muscle loading during idealized joint movements. However, their approach remains too idealized to simulate realistic load cases which incorporate active muscle forces. Higa et al. [180] considered only passive movements as performed intraoperatively with no active muscle forces. Moreover, they detected dislocation by impingement (component-to-component or bone-to-bone) or spontaneous separation by an outwardly directed vector of the joint reaction force from the cup's entry surface. Given these shortcomings, there is unfortunately no way to know whether a given impingement event or traction force will or will not presage dislocation based on their approach.

Unlike these two approaches, Nadzadi and co-workers [283,284] obtained hip joint kinematics of several subjects and corresponding force data derived form a previously validated musculoskeletal model [46]. As proposed earlier by Heller er al. [171], the data served as boundary conditions for FEM analyses included in their study which aimed to evaluate dislocation risk for realistic maneuvers. Pedersen et al. [304] analyzed the effect of cup placement on dislocation for realistic load cases based on Nadzazi et al.'s dataset and FEM approach [284]. Comparable to Higa et al. [180], they defined spontaneous separation by an outwardly directed joint reaction force where FEM simulations were stopped due to numerical singularities. In the same manner, Elkins et al. [114] used a dataset for a sit-to-stand maneuver derived from Nadzadi et al. [284] to compare their FEM model of a THR with intact capsule against test data obtained from a specimen-based hip simulator. After validation, they determined instability resistance using variations of damaged, repaired and intact capsule only by decrease or increase of the resisting torque during impingement-driven dislocation. They unfortunately missed to show whether a repaired or even intact capsule is able to actually inhibit the dislocation process or not as claimed by clinicians [185, 229, 306, 353, 407]. Based on the same FEM model and approach, Elkins and co-workers [110–113] conducted several subsequent analyses illuminating the risk of dislocations under varying influencing parameters.

All these approaches [110–114,283,284,304], however, bear a major shortcoming. Prescribed motion as well as loading used as boundary conditions imply the assumption that femoral head and acetabular cup remain concentrically aligned throughout the entire simulation of a dislocation-associated maneuver. This means that no interdependency between motion and forces is taken into account during events of instability which may potentially change the subluxation process investigated. Consequently, it remains unclear whether rising resisting torques or soft tissue forces can actually prevent the head from dislocating, which especially applies for spontaneous separation. Elkins and co-workers [111, 112] even disregarded the fact that alterations in femoral parameters such as neck length and stem antetorsion entail changes in overall musculoskeletal dynamics and hence the load situation at the hip joint as outlined by several researchers [83, 84, 170, 238, 239].

In this context, the HiL approach presented in this work broadens the use of musculoskeletal models by providing a physiological environment for the real THR to be tested. Whilst the HiL simulation is in progress, data such as relative displacements and measured torques of the artificial hip joint are fed back into the implemented model. Due to the consideration of the displacements as constraints in the model topology the assumption of concentric alignment declared by other researchers is avoided. This may provoke changes in magnitude and direction of the joint reaction force due to cutback or overcoming of additional joint torques, alterations in muscle lever arms or lengthening/shortening of capsule structures, if included. In return relative motion may vary in the further course. As it is an ongoing process the dynamic behavior of the THR tested is reproduced even during instability processes.

Several annotations need to be mentioned concerning model implementation and muscle force estimation implemented in the HiL environment. First of all, musculoskeletal modeling as followed here rests upon a MBS approach which always involves idealizations and simplifications of the real mechanical system being of interest [68, 69, 166, 337–339, 420]. The real musculoskeletal system was discretized into rigid segments based on the bones present in the human body (compare Fig. 3.3). This means that interconnected soft tissue were notionally separated and attached to nearby bone structures. To allow full scalability of the model, inertia properties were based on geometric bodies fitted into the segments ignoring anthropometric data [82]. Both deformation of segments or implant components and dynamic wobbling of soft tissue were neglected. As simulation studies [238, 239] underlined the impact of subject-specific modeling of the hip joint geometry including the definition of the hip joint rotation center, local reference frames and joint rotation centers were based on ossous geometries extracted from a reconstructed human male computed tomography dataset [357]. The subject's bone geometries derived from MRI scans turned out to have marginal difference compared to the reconstructed data such that minor scaling approximated well the subject's hip joint geometry. Moreover, a CAD model of the THR stem was implanted into the femoral geometry introducing design and positioning parameters which were shown to influence hip joint loading [83,170]. All joint articulations were represented as idealized joints characterized by well-defined joint rotation centers, stationary rotational axes and no friction torque. These joint characteristics have to be considered as approximation since native ankle and knee joint motions are rather described by translations along and rotations about screw axes [28, 42, 266]. Furthermore, researchers [144, 192] pointed out that a model has to reflect the geometry as well as the rotational degrees of freedom of the real system, in order to obtain reasonable outcomes on the distribution problem of muscle forces. Therefore, both native ankle and knee joint were modeled as Cardan joints with two degrees-of-freedom, the artificial hip joint as a kinematic subchain with three degrees-of-freedom.

Active muscle structures modeled as muscle elements were assumed to act along straight lines neglecting volumetric effects [45, 346]. The three-dimensional model topology enabled implementation of bi-articular muscles in a global manner which positively contributes to human body stabilization and metabolic costs [133, 150]. As force predictions are sensitive to origin and insertion points chosen [54], all attachment sites were mapped on the osseous contours according to anatomic descriptions [147, 341]. Resulting forces from summarized muscle fibers normally exert additional torques on the attachment sites which especially applies on muscles with large surface insertions [386]. To account for this mechanical effect, line and surface shaped attachment sites were further divided into several areas whose centroids served as attachment points. This approach was assumed to be acceptable for the lower extremity which contains muscles with parallel fibers and smaller insertions in contrast to other body parts [386]. Besides bone wrapping, additional via-points were incorporated to

gain a more realistic representation of curved muscle paths especially adjacent to the hip joint. This has been suggested to improve predictions of the reaction force components [272]. According to Vrahas et al. [395] passive tissue contribute less than 10 % to intersegmental torques during gait and stair climbing. Consequently, passive forces arising from muscular or capsular structures were not considered. While this simplification may hold true for common activities as considered in this work, their implementation should be reevaluated for extreme dislocation-associated maneuvers which especially applies to the hip capsule.

Estimation of muscle forces was based on an inverse dynamics analysis in order to gather hip joint reaction forces. Due to ethical reasoning, the required motion data was obtained from a male subject in general good health assuming that the maneuvers performed would be common tasks among both healthy subjects and THR patients [283, 284]. Whereas inverse dynamics provides valid net torques along the free directions of the joints, there is no way of determining precise neural control inputs for active muscles based on algebraic techniques [165]. To obtain at least the contribution of muscle forces to the joint torques, it is a common way to treat the redundancy problem following from inverse dynamics as static optimization problem [307, 346, 390]. However, optimization techniques are subject to the assumption that muscle functionality and neural control strategies can be summarized into plausible cost functions [49]. This assumption generally remains difficult to justify as further prerequisites due to muscle or activation dynamics and neural controls are often neglected or impossible to implement.

The current model formulation comprises two redundancy problems. Both maneuvers considered in this work were motions with both feet attached to the ground. The additional chair constraint within the seating-to-rising maneuver was dealt with by a contact force [439]. Hence, the model topology underlying both maneuvers contains one kinematic closed loop leading to dependencies among the joint coordinates [389]. In order to reduce modeling complexity and computational costs, the closed loop was accounted for by defining symmetry conditions with respect to the pelvic sagittal plane. These conditions allowed omitting the contralateral limb. However, Lamontagne et al. [230] revealed that THR patients tend to compensate for postoperative deficiencies of the operated joint by greater loading of the contralateral ankle joint during stair-climbing. Through gait analyses Foucher and Wimmer [131] observed the peak adduction torque estimated at the contralateral knee to be generally increased in THR patients compared to the knee on the operated side whereas variations were noted to depend on THR positioning. Although these asymmetries persist for gait and stair-climbing, similar patterns in hip joint kinematics were found between operated and non-operated hips for stand-to-sit and sit-to-stand tasks [231]. This means that the symmetry conditions are acceptable for the seating-to-rising maneuver and most likely for knee bending due to comparable motion sequences; but they are to be reconsidered when other scenarios are subject of subsequent studies.

One way to resolve the dependencies of the joint coordinates could be to identify a set of minimal coordinates in whose directions the equations of motion (compare Eq. 3.11 in chapter 3.3.2) could be transformed, such that constraint forces are eliminated [196]. Vaughan et al. [390] handled closed loops arising in human activities as optimization problem using a quadratic cost function of the joint torques and forces/torques at the end points of the extremities. They indicated that their outcomes support the idea of the neuromuscular strategy being based on minimizing joint torques during activities with at least one loop closure. As the latter avoids computationally expensive calculations of explicit loop closure conditions, a similar approach was pursued in this work. Furthermore, the topology starting at the right foot and being closed at the sagittal plane permitted evaluation of the ground reaction force. Thus, one source of errors was erased typical for inverse dynamic analyses [166].

The second redundancy consisted of the distribution problem of muscle forces. In order to find a unique set of muscle forces from an infinite number of possible solutions, the problem has often been dealt with by using optimization techniques following Seireg and Arvikar [346] and Penrod et al. [307], respectively. Although it seems appealing that the nervous system governs motion by controlling muscle forces in an optimal manner, it is an intricate task to find physiological or even neurophysiological evidence of appropriate cost functions. Numerous researchers analyzed and controversially discussed a number of cost functions concerning the prediction of physiological muscle forces including patterns such as synergistic activation and antagonistic co-contraction in the lower extremities [27, 64, 76, 77, 130, 144, 199, 200, 305, 318, 385]. Constraining muscle forces within physiological boundaries remarkably reduces the number of possible solutions [63, 70, 76]. Both synergistic and antagonistic activity comparable to EMG data were found to be estimated when using non-linear cost functions in contrast to linear ones [144, 273, 302]. Other factors such as the definition of weighting coefficients may also promote antagonistic prediction [316]. However, Herzog and Binding [178] showed that co-contraction is only predicted when multi-joint antagonists are present. Independent from the cost function's definition, it was also observed that muscle force prediction reacts with great sensitivity to model-based deviations of kinematic data [301], lever arms and physiological cross section areas [47, 317]. These findings and the aspects mentioned above support the notion that detailed modeling of the musculoskeletal system rather leads to realistic results than the optimization procedure per se. Hence, an approach similar to the one described by Anderson and Pandy [5] was followed in this work, which allowed incorporation of muscle architecture and physiology explicitly in the equations of motion.

As far as the hip joint is concerned, musculoskeletal models were developed to estimate contact forces in addition to muscle forces based on inverse dynamics analysis [78, 144, 158, 303, 328, 347]. Despite afore mentioned idealizations and simplifications, several models have shown good agreements in direct comparison with in vivo measured data. Brand et al. [46]

compared resultant and defined out-of-plane hip joint contact forces against gait data arising from one patient with an instrumented implant. They reported that the modeling methods used enable comparable peak predictions and patterns. Heller et al. [171] used a cycle-to-cycle comparison in order to validate predicted contact forces against in vivo data from four patients for two daily activities. The calculated absolute force values deviated for all patients by 14 % during stair climbing and 12 % during walking revealing good agreement in both patterns and magnitudes. Likewise, the model by Stansfield et al. [358] predicted comparable forces for various activities performed at relatively slow speeds considering two patients with instrumented THRs. Further studies [5, 254, 273, 274] demonstrated reasonable results of their lower-extremity models which were validated against joint contact forces and EMG data derived from the literature.

In the same manner, the outcomes of the HiL simulation were compared to data derived from three instrumented patients [33] for two common maneuvers. Regarding the seating-to-rising maneuver, the outcomes revealed an overall good correlation in magnitude and trend for all force components. Apart from the trend, the reaction force prediction for the knee bending maneuver overestimated the patient derived data. The deviations can be explained by the fact that the patients performed lower hip joint flexion with maximum angles between 45° and 65° [33], in contrast to about 83° of the HiL subject. On closer examination of the patient data, inter-individual differences even show that increasing flexion angles correlate well with augmented contact forces. Furthermore, Nadzadi et al. [284] estimated considerably higher contact forces for maneuvers with larger flexion angles up to 110°. Besides the contact forces, the estimated ground reaction forces reflected well realistic motion data and inertia properties. Given these results it can be stated that the HiL simulation is able to reproduce the dynamic behavior of THRs under physiological conditions.

Supposing that estimated muscle forces are still physiologically reasonable in case of extreme maneuvers [284], there are numerous challenging tasks in orthopedic research where HiL simulations can assist to achieve further insights. From the clinician's point of view, positioning of THR components according to preoperative planning is a vital contribution to a stable artificial hip joint for a given implant system. Inspired by Lewinnek et al.'s proposed zone of safe cup placement [240], clinicians focused on cup inclination and anteversion to be a crucial factor for dislocation [36, 202, 205, 261, 270, 300, 422]. Apart from pure RoM analyses, biomechanical studies [110–113, 283, 284, 304] closely illuminated the risk of dislocation with respect to cup orientation under realistic motion and loading patterns including muscle forces. Unfortunately, these studies were bound to limitations, arising from prescribed load conditions aforementioned, that weaken the reliability of their statements concerning the simulated dislocation processes. Moreover, except of only one study [111], they missed to take the stem antetorsion into their considerations which was shown to affect incidences of dislocation [120, 174, 194]. Widmer and Zurfluh [414] demonstrated that there is a linear

correlation between cup anteversion and stem antetorsion when acquiring a maximized and safe RoM. Changes of antetorsion, however, also impacts the geometric proportions along the kinematic chain of the skeletal system with more far-reaching implications for the patient. Heller et al. [170] revealed that muscle and hip joint loading may substantially change due to modification of the antetorsion. Similar results were reported by varying antetorsion as well as design parameters of the femoral component which also alter the location of the hip joint center with respect to the femoral bone [83, 238, 239]. These effects were overlooked in recent analyses of dislocation risk with varying neck length [112] or stem antetorsion [111]. Hence, the question remains whether the combined orientation still holds for safe component placement when taking dynamic, not prescribed, musculoskeletal loading into account.

Another crucial issue characterized by diverging sentiments among orthopedic surgeons is the contribution of muscular and capsular structures to joint stability. Depending on the surgical approach specific muscular and capsular structures are intraoperatively incised, resected or damaged to gain access to the hip joint. Especially, the posterior approach involves larger loss of soft tissue as it requires resection of the external rotators (Mm. gemelli, Mm. obturatorii, M. piriformis and M. quadratus femoris) as well as incision of the posterior capsule [26, 394]. Hence, it seems not surprising that this approach was reported to entail higher dislocation rates than others [87, 203, 229, 326, 392]. Pellicci et al. [306] argued that these unsatisfactory outcomes are caused by the dead space, left after resected soft tissue and usually found posteriorly in revision procedures. In the same study, they performed restoration of the normal anatomy by reattaching all rotator muscles and the posterior capsule before closure. The enhanced repair of soft tissue succeeded to significantly improve the postoperative results as confirmed subsequently by other clinicians [185, 229, 353, 407].

Although the mechanical aspects of the hip capsule have been illuminated to a certain extent [141, 179, 190, 255, 365, 396], there are only few studies providing insights in how soft tissue structures contribute to resistance against dislocation. Delp et al. [83] stated that extension of the femoral offset, a widespread medium by surgeons to adjust tension on the hip joint, increases the muscles' active moment-generation capacity and passive muscular forces. Specimen-based studies [268, 355] indicated that full repair of muscle and capsule tissue after the posterior approach lead to augmentation of the torque measured along internal/external rotation until final dislocation in contrast to no or minor repairs. Elkins et al. [114] concluded that well-designed repairs are able to restore stability of capsular structures which was proven by similar resisting torques against dislocation as obtained for the intact capsule. Whereas studies based on specimens generally suffer from tissue deterioration and challenges of integrating active muscle forces, several shortcomings within Elkins et al.'s study, concerning their approach and boundary conditions as mentioned above, make it difficult to clarify whether a sufficiently repaired capsule is able to prevent the femoral head from dislocating. With introduction of passive force elements into the present musculoskeletal model, it can

be further analyzed how reattached muscles and reconstructed capsular structures effect hip joint stability after following the posterior approach. Subsequent research may broaden the picture by considering all relevant surgical approaches along with their potential soft tissue damage and their interaction with THR design and positioning.

With regard to joint stability, orthopedic surgeons often use larger head sizes in order to treat hip joints being at risk of instability or suffering from recurrent dislocation. It is well-established that THRs equipped with larger femoral heads and therefore advantageous head-neck ratios generally benefit from an enhanced RoM [3, 24, 52, 65, 103] and higher resting torques after impingement [15, 215] in contrast to their smaller counterparts. Although their properties were reflected in diminishing dislocation rates, complications other than instability have emerged, even leading to implant failure [354]. These include elevated friction torques in the case of lubrication breakdown [37], and wear mechanisms seen at the taper connection [38]. Elkins and co-workers [110, 111] substantiated the trade-offs between maximizing stability and minimizing wear such that almost no benefits were seen in using larger head sizes.

Meanwhile, so-called tripolar THR systems demonstrated to reliably reduce the dislocation rates in high-risk patients [152, 315], offering prospects for an alternative approach without the complications affecting larger heads. Tripolar THRs additionally use an intermediate component which articulates between the acetabular cup and the femoral head [25]. Besides retrospective clinical outcomes and theoretical groundwork on functionality [222], however, little is known about wear, joint stability and dislocation resistance of these type of implants. Fabry et al. [119] revealed an unstable dynamic behavior of tripolar designs with concentrically aligned center of rotation, where the intermediate component is moved only by contacting the stem, and tends to stick on extreme positions. This behavior may cause subsequent complications such as joint instability or wear-associated failure. On the contrary, the same study proved over a number of load cycles that the dynamics of eccentric designs rely on a self-centering effect and relative motion being controlled by the direction of the force vector. Whereas these results were obtained under in vivo load conditions [118], investigations addressing THR dislocation were solely performed under idealized load and movement conditions [119, 151]. In this sense, HiL simulations may help to further elucidate the stability of eccentric tripolar THRs for dislocation-associated maneuvers in comparison to standard THRs with comparable head sizes.

In the context of fundamental research, it remains a challenging question of how the neuromusculoskeletal system actually governs joint motion and loading in response to rapid instability processes. Inverse dynamics used in the implemented musculoskeletal model takes the form of an ideal motion control maintaining the exact angular motion according to the data provided no matter the costs. Applied torques due to impingement or passive soft tissue forces are simply added or subtracted from the net joint torque. This implicates that

in case of instability no response along the free directions, such as acceleration, deceleration or stop of the movement, is possible which one might expect. As this approach may be considered as valid working hypothesis due to lack of data to study THR dislocation without reaction of the nervous system, it may not reflect reality completely. Bergmann et al. [35] recorded force data from instrumented patients experiencing unexpected stumbling that largely exceeded maximum voluntary contraction. As interpreted by the authors, the nervous system tries to regain stability by full muscle activation escalating joint resistance due to friction and stiffened muscle structures against external torques. Regarding the force data retrieved under test conditions in the same study, the triggered reflex mechanism is reflected by a drop of the hip joint contact force followed by a sudden but time-delayed force increase. This may suggest that joint instability involve first poorly controlled motion due to an unexpected alteration in the dynamic equilibrium and second a time-delayed full muscle activation as neurophysiological response. One promising way to transfer this behavior into a musculoskeletal model might be to follow a forward dynamics approach (compare chapter 2.3.3). Within this approach, neural excitation patterns may be determined for instability-associated tasks according to a dynamic optimization procedure whose physiological cost function accounts for the reflex mechanism. The activation dynamics ensures a time delay between neural excitation and muscle activation. Implemented into the HiL environment, this approach would allow for complex analyses of THR dislocation dynamics including the influence of neurophysiological parameters.

Given these prospects for applications in orthopedic research, the HiL approach constitutes a comprehensive testing tool that complements existing simulation and experimental methods. Apart from dislocation scenarios, it may also contribute to investigations addressing other failure mechanisms of THRs. For instance, Damm et al. [80] suspected an association between friction and implant loosening. By calculation of friction related quantities from eight in vivo measurements using ceramic-on-polyethylene bearings in the instrumented implants, they estimated peak friction torques of 0.26 %BWm on average. Two- to three-fold higher friction torques obtained in the scope of this work disclose comparable magnitudes in view of the metal-on-polyethylene bearing being used here under dry conditions. Furthermore, Heller et al. [172] assembled load profiles including hip joint contact forces and muscle loading from a validated musculoskeletal model for further in vitro testing. Beyond both studies mentioned, HiL based analyses deliver complete sets of physiological-like data concerning consistent hip joint contact forces and friction torques, active muscle and passive soft tissue forces, if implemented, and the corresponding relative motion. These data sets may be used as boundary conditions in subsequent FEM studies to investigate effects on implant loosening, wear or primary and secondary implant stability. Moreover, the data sets may provide a solid groundwork for pre-clinical, standardized testing promoting more realistic test conditions in terms of physiological loading.

5.3 Instability of Total Knee Replacements under Physiological Conditions

While considerable improvements have been achieved in implant technology and surgical techniques, complications after total knee arthroplasty remain an insistent challenge to orthopedic surgeons. This is especially the case where patients suffer from constant pain and functional impairment with no signs of infection or loosening. The difficulty in treatment even aggravates for patient and surgeon alike when subtle instability patterns evolve into multiple instability phenomena, or provoke other failure mechanisms such as aseptic loosening, wear and fracture [356]. In this manner, instability prevails as one of the major reasons for TKR revision. Clinical assessments, however, illustrate great uncertainties and inconsistencies in specifying related causes and risk factors. Ligamentous insufficiency, which is generally the cause of an unstable native knee joint, is not necessarily identical to TKR instability. Nevertheless, it seems to provide the basis of the clinical perception that instability is equivalent to kinematic discrepancies of the artificial tibiofemoral joint [11,286,327]. Such effects may be barely distinguishable in daily clinical practice from kinematic implications due to loosened, worn or broken implant components or fractured bones, without elaborate examination. The circumscribed problem is substantiated by the fact that there are almost no profound definitions of underlying failure mechanisms associated to TKR instability apart from patterns and phenomena categorized by clinicians [221, 276, 299, 327, 393, 427]. Therefore, the question is still what the driving mechanisms are along with their influencing factors leading to erratic, adverse or excessive relative motion.

From the orthopedic surgeon's perspective, successful implantation depends on an appropriate balance between the extension and flexion gaps and correct placement of TKR components. Keeping that in mind, a variety of potential chains of effects can be postulated set in relation to six distinct instability phenomena described by clinicians for rather unconstrained TKRs: Symmetric extension instability [299,327] is viewed as a result of an enlarged rectangular extension gap, due to increased bone resection at the distal femoral and/or the proximal tibial side and its inadequate filling. This may lead to larger compliance in all directions and hence erratic relative motion in knee extension. The extension gap is defined by the amount of bone resection at the distal end of the femur and the proximal part of the tibia along with the tension of the collateral ligaments. Its filling depends on the choice of the component sizes, augments used and inlay thickness. In the absence of neuromuscular disorders, additional laxity of the collateral ligaments enhances hyperextension, also known as genu recurvatum [122, 263, 299, 393, 427].

The phenomena most perceived by clinicians is asymmetric (or varus-valgus) extension instability [122, 146, 276, 299, 327, 393, 427]. One potential mechanism is seen in angular errors of bone resection generating an asymmetric extension gap. Subsequent axial malalignment

of the components may provoke lateral or medial opening in extended position where only one condyle is in contact (condylar lift-off). Here, the shape of the distal femoral and the proximal tibial bone cuts as well as the component alignment with respect to the mechanical axis are crucial influencing factors. Another cause for an asymmetric extension gap is given by improper balanced collateral ligaments due to one-sided contracture or excessive release. The consequent laxity in one of the collateral ligaments gives room for erratic movements within the frontal plane in full extension. Matsueda et al. [258] expounded in their specimen-based study the impact of medial or lateral soft tissue release sequences on the corresponding gap angulation in the frontal plane. Furthermore, varus-valgus alignment was shown to determine the load distribution within the two compartments [154, 406]. In specimens with more lax collateral ligaments, Werner et al. [406] even noticed aberrant abduction (adduction) and lateral (medial) loading at full extension for valgus (varus) aligned knees, unacceptable for patients.

Condylar lift-off phenomena are also present in flexion [146, 313]. A profuse rotated femoral component along the femoral shaft, often regarded as malrotation, fills the flexion gap in an asymmetric manner. The asymmetry narrows the space between the condyles in one compartment towards 90°, such that the other opens up. Lateral or medial lift-off phenomena were detected in vivo during fluoroscopic analyses [91, 366]. Insall et al. [187] confirmed a definite correlation to the rotational positioning of the femoral component, stating that the incidence is reduced by an alignment parallel to the epicondylar axis. Further specimen-based testing by Anouchi et al. [8] exposed that an internally rotated femoral component, along with perpendicular tibial resection, augments medial and relieves lateral collateral ligament tension in flexion due to altered dimensions of the posterior femur; with the effect of lateral opening, forced into tibial abduction (valgus) under load. Similar kinematic interrelations were also observed within a MBS study [382].

Some patients suffer from pain and a sense of instability during flexion despite correct TKR alignment and fixation. After careful examinations, these indications were often ascribed to anteroposterior instability [276, 299, 313, 393, 427]. In theory, a couple of chains of effects can be linked with such phenomena depending on the TKR type [122, 298, 342, 348, 403]. In PCR total knee implants, over resection of the posterior femur or a raised tibial slope widens the flexion gap in comparison to the extension gap. The mismatch along with an inadequate filling of the flexion gap may permit larger compliance and hence relative movements, especially in anteroposterior direction during flexion. In addition, the posterior cruciate ligament is known to be the primary restraint to posterior translation in the native knee [53, 143, 145, 149]. Insufficiency of this structure due to excessive release, intraoperative damage or rupture after implantation may therefore be related to anomalous anterior or posterior translations until subluxation.

In fact, there is biomechanical evidence on the impact of tibial slope and posterior cruciate ligament tension using PCR implants. Catani et al. [56] found a correlation in their fluoroscopic study of daily maneuvers between the posterior slope and the maximal position of the lateral contact point in posterior direction. The posterior cruciate ligament was identified as an important structure for restoration of normal anteroposterior knee kinematics [244, 280]. Release of this ligament was noted to enlarge the flexion gap [258]. Furthermore, a larger tibial slope was demonstrated to reduce posterior cruciate tension at higher flexion angles [297,436], such that overloading may be prevented often regarded to induce late postoperative rupture. Zelle et al. [436] detected within their FEM study that an over-tight posterior cruciate ligament can also generate excessive femoral rollback till subluxation. In cases emulating release instead, they noticed anterior translation of the femoral component with respect to the tibia during flexion; a motion pattern contrary to the native knee which was monitored earlier in PCR TKRs within fluoroscopic studies [29, 66, 89, 367, 368, 404] or during mechanical testing [93, 250]. As concluded by Clary et al. [67], such adverse femoral translation is caused by an abrupt reduction from the distal to the posterior radii of the femoral component. The opposite relation apparently yields femoral rollback.

In PS implants, anteroposterior translation is governed by the cam-post mechanism which is designed to limit motion especially in posterior direction. Its functionality and mechanics were verified in various biomechanical investigations [9, 55, 85, 88, 121, 126, 186, 242–244, 257, 280, 295, 310]. But as for PCR implants, an enlarged flexion gap due to excessive bone resection or tibial slope provides anteroposterior and proximodistal compliance such that substantial posterior translation may occur, whereas the dislocation process is only constrained by the cam-post engagement. In this context, the tibial slope was highlighted to affect these cam-post interactions [127,128,312]. A similar impact is contributed to excessive lateral release including the posterior oblique ligament and the posterolateral corner; structures known to prevent augmented posterior translation in the native knee after resection of the posterior cruciate ligament [53, 145, 149, 309, 325, 391]. Depending on the post's height, further distraction may unlock the cam-post mechanism followed by frank dislocation in any direction. The same may apply to more constraint TKR types such as VVC or rotating hinge implants, where the flexion gap is additionally compromised due to further ligamentous and capsular insufficiencies [313, 401, 402]. Such a dislocation phenomena to occur may require deficiencies of the extensor mechanism like patellar subluxation or dislocation, fracture or tendon rupture [348].

A phenomenon controversially discussed by clinicians is midflexion instability [299, 313, 327, 427], with no signs of an unstable knee at full extension and 90° flexion. Over resection of the distal femur or under resection of the proximal tibia elevates the tibiofemoral joint line in extension. If not compensated by implant size or augments, it is assumed that the elevated joint line induces ligament laxity around 45° flexion providing larger compliance in all direc-

tions with unpredictable mediolateral and adduction/abduction movements in PCR or PS implants. A similar effect is attributed to a large medial release which manifests in laxity of the medial collateral ligament during flexion, in addition to the relaxed lateral and posterior structures [221,393]. Compensating excessive resection of the distal femur by a thicker tibial inlay, on the contrary, leaves the joint line elevated, but stretches the flexion gap and tensions the posterior cruciate (in PCR implants) and the collateral ligaments in flexion. This enables restriction of motion towards higher degrees of flexion. Likewise, femoral under or tibial over resection results into a lowered joint line which tightens the ligaments during flexion. The pronounced ligament forces may impede knee motion in midrange with a tendency to knee stiffness.

This problem of ligament laxity or tightening during flexion was subjected to a few biomechanical analyses. The position of the joint line was de facto shown to correlate with forces of the posterior cruciate and collateral ligaments [128], and effect both tibio- and patellofemoral loading [219]. Whiteside et al. [410] investigated the effect of inlay thickness with reference to a normal implanted knee, indicating amplified adduction/abduction rotations for a thinner inlay at all flexion positions tested, in contrast to decreased varus-valgus and internal/external rotations towards higher flexion for a thicker inlay. Furthermore, Martin et al. [256] positioned the femoral component in human knee specimens 5 mm in equivalent anterior and proximal direction with respect to the native joint line. Their testing revealed significantly larger adduction/abduction rotations and anteroposterior translations in midflexion compared to native knees, whereas two specimens could even be dislocated under lowered quadriceps load. By placing the femoral component posterodistally, they observed a reduction of relative motion in all directions tested along with binding phenomena during flexion. In this sense, positioning of the joint line appears to vitally contribute to midflexion stability, set by the femoral and tibial resection depths, implant size and positioning, as well as inlay thickness.

In the native knee, it is well documented that regular tibiofemoral flexion is accompanied by external rotation of the femur relative to the tibial plateau [314], whereas free motion is feasible along internal and external rotational direction, respectively, with higher degrees of flexion [41,42]. After TKR implantation, however, certain phenomena appear to disturb rotational kinematics, all related to rotational instability [32]. The medial parapatellar approach is characterized by incision of all medial restraints of the patella what tends to lateralize the extensor mechanism [336]. As a consequence, the quadriceps muscle applies an external torque on the tibia augmenting tibial external rotation during extension. Another pattern is seen to emerge from an externally malrotated femoral component which implies tightening of the posterolateral corner including the popliteal tendon. The preloaded structures exert an additional torque which amplifies internal rotation of the tibia during flexion.

This effect was proven by Nagamine et al. [285] who noticed increased internal and decreased external rational compliance beyond 45° flexion after placing the femoral component 8° externally with respect to the posterior condyles. Besides excessive motion patterns, kinematics opposite to the native knee were reported earlier in fluoroscopic studies of TKR patients [21, 90, 366]. Werner et al. [406] indicated that a varus-aligned femoral component provokes external and a valgus-aligned component internal rotation at maximum flexion during an emulated gait cycle; findings which connect axial malalignment with adverse rotations. In TKRs with mobile bearing inlays [313, 383], an asymmetric flexion gap due to collateral ligament imbalance enforces condylar engagement in one compartment during flexion. This is believed to generate an additional torque on the inlay inducing excessive rotational motion until its lateral or medial spin-out. Stukenborg-Colsman et al. [370] also mentioned in their specimen-based study that inadvertent relative motion of the mobile bearing occurred when placing the tibial tray in more than 10° malrotation. In general, Whiteside and coworkers [409,410] emphasized the importance of correct collateral ligament tension to restore normal rotational kinematics for TKRs.

It is clear that the chains of effects postulated above may only reflect idealizations of the situation in situ. They may also occur in combination intensifying the severity of the instability patterns, what may result in often noted global instability [122, 146, 356, 393]. These postulations, however, point out two essential aspects. On the one hand, clinical observation and experience indeed allow delineation of possible chain of effects and identification of factors contributing to instability phenomena. But those descriptions often appear ambiguous and not far-reaching enough to distinguish between cause and effect. On the other hand, there is almost no biomechanical evidence for the majority of the outlined instability patterns and their precise kinematic consequences for patients. As displayed for each phenomena, only a few studies deal with the impact of influencing factors, let alone the investigation and quantification of actual processes leading to instability in vivo. One reason for this circumstance is certainly due to the major concern of illuminating the overall performance of TKR implants in comparison to the native knee rather than mere stability effects. Another reason is to be seen in the limitations inherent in present biomechanical approaches.

The crucial issue for investigating instability processes is to generate realistic TKR dynamics with incorporation of ligament and muscle forces. In this respect, fluoroscopic studies [9, 29, 55–57, 85, 88, 121, 218, 257, 269] provided insights on TKR kinematics under in vivo conditions for weight bearing or step up tasks. Although some of them even identified instability patterns such as condylar lift-off or movements opposite to the native knee [21, 66, 89–91, 187, 366–368, 404], ethical reasoning prohibits any variations of influencing factors related to joint failure putting patients at risk. The same applies to all investigations with instrumented TKRs [96–99, 101, 154, 168, 228, 281, 376, 377, 388, 438].

Hence, specimen-based testing has taken on a key role which allows at least TKR assessment under the influence of a physiological ligament apparatus. Several experimental setups [204, 295–297, 370] were established emulating only flexion/extension movements driven by an actuated quadriceps tendon. Robotic systems were utilized for specifying the tibiofemoral motion during passive TKR flexion as reference to the path obtained under loaded conditions and/or varying implant types [242–244, 280]. Within other approaches the specimens were mounted into a test rig resembling a closed kinematic chain, similar to the Oxford knee simulator [435]. Those test rigs were used to study the effect of constant loads applied along internal/external, varus/valgus and/or anterior/posterior directions at flexion angles kept constant by fixation or a quadriceps force counterbalancing the net weight [8, 198, 256, 285, 333, 408–411]. The test protocols mentioned may represent an excellent way to characterize the condition of the ligament apparatus after TKR implantation or the effect of certain design features, but remain too idealized as regards instability scenarios. Further studies based on closed-loop test rigs [8, 50, 102, 251, 256, 319, 320, 369, 429] considered TKR kinematics under quadriceps-driven load situations comparable to knee bending or stair climbing. All these studies, however, suffer from a major shortcoming apart from non-reproducibility and complicated comparability. They generally disregard the passive and active contribution to TKR dynamics of all other muscular structures spanning the knee joint, such as the gastrocnemius, sartorius, gracilis and popliteus muscles as well as the iliotibial tract. The same limitation holds for MBS simulations which reproduced these in vitro test conditions [71, 186, 204, 310, 382].

In order to emulate dynamic activities, Maletsky and Hillberry [252] introduced load profiles in their test rig applied onto actuated axis along with a compliant, position controlled quadriceps actuator. This approach enabled them to indirectly consider active muscle forces by duplicating desired tibiofemoral flexion angle and compressive force, obtained from a musculoskeletal model, by means of an integrated control strategy. Based on the test rig, Werner et al. [406] assessed the influence of varus-valgus malalignment during gait. Other researchers generated valid dynamic FEM models which reproduced the functionality of the test rig to simulate walking and/or deep knee bending of TKR equipped specimens [17,18,67,155]. Fitzpatrick et al. [123] even refined the FEM analyses by incorporating additional actuators along with an enhanced control system to match more complex tibiofemoral load conditions. Using these advancements, several FEM studies [126–128] were conducted for stance-phase gait, squatting or step-down activities with variations of implant design and positioning, whereas the desired load conditions were derived from data of instrumented TKR patients [228].

In general, the approach followed by these researches allows to find consistent TKR kinematics and load profiles for the actuators at the hip and ankle joints. Yet prescribing tibiofemoral loading or external actuator forces adhere to the assumption that these quantities remain invariant for a given TKR implanted into a task-specific musculoskeletal system.

Besides the kinematic impact, however, numerous studies documented that alterations of TKR design [96,101,168,228], alignment [154,173,381], joint line position [219] or soft tissue balancing [97] entail changes in tibiofemoral contact forces and load distribution in vivo. More precisely, this means that any variation in implant type and design, positioning and alignment as well as soft tissue structures affects the musculoskeletal dynamics of the entire system disproving the assumption of invariant tibiofemoral, hip and ankle loads. This is particularly the case for instability scenarios where the actual dynamics of the process and hence joint loading is a priori unknown. In a couple of other FEM and MBS models, respectively, researchers applied a constant ground reaction force to the tibia instead [22,248,433,436,437]. The external load was counterbalanced by a quadriceps force with a constrained femur to mimic physiological conditions during a flexion task. Apart from the apparent lack of active muscle structures, none of these studies provided sufficient validation in terms of tibiofemoral loading. Zelle et al. [436] even chose to omit collateral ligaments, bringing their noted spin-out subluxation of a PCR implant into question.

In this context, HiL simulations have the potential to broaden the present approaches for investigating TKR stability. Clinicians recognized that instability phenomena were often reported by patients during weight-bearing or knee bending, rising from a chair, and stair ascending or descending [298, 403, 428]. By embedding an MBS model with an adequate representation of soft tissue structures into the HiL environment, such activities can be examined in more detail, while varying influencing factors related to the possible chains of effects postulated above. The MBS model ensures to deliver physiological boundary conditions required to simulate TKR dynamics even during extreme maneuvers, making prescribed loading used in other approaches redundant. Whilst the HiL simulation is in progress, the fed back displacements may provoke changes of TKR dynamics due to ligament elongation, as demonstrated in a previous study [177]. Studies based on musculoskeletal models [350, 417], however, revealed that muscles essentially contribute to relative knee motion and stability besides the ligament apparatus. Due to the superimposing effect of active muscle and passive ligament forces on TKR motion, validation of the HiL approach seems to be more complicated than for THR testing. Therefore, the HiL simulation presented within this work focused primarily on the replication of TKR dynamics in vitro.

Given this validation strategy for testing TKRs, certain implications need to be mentioned concerning the current HiL configuration. The embedded MBS model emulates the in vitro test conditions of Kessler et al.'s experimental setup [204]. Hence, it bears similar limitations. The motion simulated is restricted to open-chain flexion or extension of one PCR implant. Only major ligament structures (patellar, posterior cruciate and collateral ligaments) were implemented. Influences on TKR kinematics due to active muscles, the posterior aspects of the ligament apparatus as well as medial/lateral patellar soft tissue restraints were neglected. Any results using this configuration may, therefore, not be comparable to other TKR types or

designs, and activities close to in vivo conditions. Furthermore, the model is based on a MBS approach involving analogous idealizations and simplifications of the real mechanical system [68, 69, 337–339, 420] as specified in detail for the musculoskeletal model aforementioned (see chapter 5.2). These include the discretization into rigid segments, the modeling of inertia properties and the representation of articulations as idealized joints. The patellofemoral motion was prescribed by experimental data such that parameters known to alter patellar dynamics [71,124,129,176,204,219,319,320] may not be surveyed further. Moreover, ligament structures were represented by straight line elements assuming parallel, homogeneous fiber bundles. The elements were modeled as spring-damper combination which may not reflect all viscoelastic properties of real ligaments [237].

Despite these limitations the results of the HiL simulation agreed well with the specimen-based measurements [204]. Only predicted internal/external rotations deviated from the measurements, reproducing well the general trend but remaining outside the envelope of the in vitro values. The deviations may be explained by varying implant positioning used for the HiL simulation and during experimental testing. All other predictions fell within the envelopes of the in vitro data. Given this outcome it can be inferred that the HiL test system is already capable of generating comparable TKR kinematics and loading as seen in vitro. However, it can certainly be disputed whether such limited test conditions allow investigation of realistic instability processes. In that respect, further improvements appear obligatory for the embedded MBS model.

On the one hand, the representation of the ligament apparatus by only the posterior cruciate and the collateral ligaments, each represented as single bundle, does not replicate the anatomic situation completely. It is well appreciated that other structures play an important role in restraining tibiofemoral motion, like the posterior oblique ligament [232, 309, 325], the oblique popliteal ligament [234], and the posterolateral corner [53, 145, 148, 149, 233, 247, 259, 391, 405] including the popliteus complex, the popliteofibular ligament and the fabellofibular ligament. Researchers additionally differentiate ligamentous structures into several fiber bundles. Depending on the study quoted the posterior cruciate ligament, for instance, is subdivided into two up to four bundles [75, 160], the medial collateral ligament into at least two [232]. In this manner, each ligament may be implemented into the MBS model according to anatomic attachment sites with a sufficient amount of bundles modeled as straight line elements. Some elements may even require integration of bone wrapping, in order to account for potential bone-ligament interactions [39].

Besides anatomically correct representation, the forces applied by those elements crucially depend on the choice of the constitutive law. The parallel spring-damper combination used in this work may reproduce the elastic material behavior of ligaments to a valid extent [40, 241], but entails weaknesses in time-dependent effects such as creeping or relaxation. These effects vitally contribute to the material behavior at accelerations beyond quasi-static conditions,

which may also be expected during instability events. One way to resolve this problem is by implementing the viscoelastic constitutive law proposed by Lehner [237] which was validated against specimens tested under various load conditions. The constitutive law even describes the stress-strain behavior until rupture. This denotes a crucial aspect for TKR stability, especially concerning the posterior cruciate ligament [403].

A major challenge in biomechanical modeling, however, remains the identification of appropriate values for all ligament parameters involved. Baldwin et al. [19] assessed ligament stiffnesses, initial strains and attachment points, parameters well-known for their inherent variability in situ, by using a probabilistic approach within their FEM analyses of the native knee. They found a valid representation for these parameters adjusted to experimental test data. Since probabilistic methods do not necessarily determine the global optimum within the parameter space due to the mathematical formulation they are based on, Baldwin et al.'s approach may be enhanced by incorporating a more comprehensive test protocol [8,198,256,285,333,408–411], and varying states of the ligament apparatus as performed during selective characterization of ligament function [53,145,148,149,247,309,325,334,372,391]. This way not only a high level of detail may be achieved within the MBS model, but also adequate validity in terms of ligament functionality.

On the other hand, investigation of instability-associated maneuvers necessitates implementation of active muscular structures. An important element of this task is the physiological representation of the extensor mechanism and the patellofemoral joint within musculoskeletal models [69]. One simplified way is to solely provide the patellar deflection along the trochlear groove by introducing segment-fixed via-points (compare chapter 3.3.3). More commonly, the spatial path of the patella is prescribed or fully constrained, respectively, either as a function of knee flexion [142, 171] or by an inextensible link to the tibia [273, 274]. Although these options comply with an inverse dynamics approach, they have their drawbacks concerning any implication on patellar tracking after TKR implantation, not to mention patellar subluxation or dislocation. Such effects are included when describing patellar motion with six degrees of freedom and imposing contact conditions for the patellofemoral articulation [164, 176, 206, 246, 311].

Notwithstanding this and other modeling tasks, a number of musculoskeletal models have shown to reproduce TKR loading close to in vivo conditions using inverse or forward dynamics. Lu et al. [249] compared axial forces for two patients assuming a planar load case. They estimated well hip extension and flexion exercises in both subjects, but obtained larger deviations for level walking. Taylor et al. [378] assessed tibiofemoral loading during stair climbing and gait using a MBS model previously validated against in vivo hip contact forces [171], revealing reasonable outcomes compared to the literature. Furthermore, Kim et al. [210] and Lin et al. [246] predicted muscle forces during gait on the basis of data from one patient equipped with an instrumented TKR [438]. Both models showed

good agreement between calculated and in vivo measured knee contact forces. Other studies [5, 142, 164, 206, 274, 311, 381, 417] also displayed outcomes comparable to in vivo joint contact forces derived from the literature.

These considerations emphasize the opportunity to gain physiologically realistic boundary conditions for TKR evaluation within the HiL environment. Therefore, the first objective for improving the current HiL configuration should be focused on implementing an appropriate and valid ligament apparatus; the second is to extend the MBS model by active muscle structures. The musculoskeletal model presented earlier within this work provides a sound basis for achieving these goals, following the example of Taylor et al. [378]. Overall validity of the HiL test system can then be assessed for normal activities against complete load data derived from instrumented TKR patients [96, 101, 135, 168, 228]. Supposing still reasonable muscle force estimation TKR dynamics can be replicated for instability-associated maneuvers [298, 403, 428] within the scope of further analyses. These allow for close illumination of all possible chains of effects and factors affecting knee stability such as implant type, design and positioning, as well as release sequences. In order to detect erratic, adverse or excessive motion comparisons can be drawn with the kinematics of a stable TKR, or the native tibiofemoral joint [134, 314] specified as baseline. A promising method may also consist in taking accelerations as basis of valuation [324]. In this manner, HiL simulation may give more profound insights on actual instability processes present in patients and verify potential mechanisms related to TKR instability.

6 Conclusions and Outlook

Instability-associated failure prevails as a fundamental problem after total hip and knee arthroplasty. The only option in treatment often consists of revision surgery. Such an intervention can comprise further drawbacks and risks, particularly in cases where the driving cause is not eliminated intraoperatively. Thus, it is of great importance for surgeons and patients alike, to prevent instability and related consequences from the outset. Prevention, however, requires knowledge and understanding of underlying mechanisms and factors contributing to the failure process. As regards THRs, impingement-based levering out and spontaneous separation were identified as relevant mechanisms leading to a dislocated hip. Implant design and positioning are well known to be crucial impact factors for standard THR types. In contrast to that, there is little evidence in how exactly soft tissue structures engage during dislocation. This also applies to the impact of specific implant parameters which alter the geometric proportions and hence musculoskeletal dynamics. As far as TKRs are concerned, tremendous efforts were spent to gain insights on TKR functionality and performance compared to the native knee. These include investigation of factors influencing TKR kinematics, such as implant type, design and positioning as well as surgical parameters. Apart from a few instability patterns, however, a wide gap is prevalent between biomechanical comprehension and phenomena set in reference to instability by clinicians; let alone the precise definition of underlying mechanisms and influencing factors. It is still unclear how both ligament and muscular structures effect the process leading to erratic, adverse or excessive TKR motion.

Given these circumstances, biomechanical investigations appear inevitable which ideally cope with the demands of in vivo conditions. As measurements in patients are afflicted with ethical objections, researchers generally operate on the basis of three approaches, each with inherent shortcomings. Retrospective studies are primarily limited in illuminating cause and effect on a systematic framework, unlike real testing or simulations. Both mechanical and in vitro test setups do not allow adequate incorporation of active muscle structures. Besides, human specimens make reproducible and comparable evaluations difficult due to their time-dependent decay and individual variability. The problem of reproducibility and comparability appears to be resolved by using simulations based on MBS or FEM models, though complex contact modeling is limited. Within a couple of studies prescribed load situations were applied derived from musculoskeletal models or instrumented patients. Although this

method promises physiological conditions, it neglects the a priori unknown impact of soft tissue interaction during instability processes, and alterations in musculoskeletal dynamics due to parameter variations. Therefore, the purpose of this work was to present a comprehensive approach which is capable of overcoming these trade-offs. The essential idea of this approach lies in the extraction of the anatomic and physiological environment of the joint of interest into a MBS model. The model interacts with the real implant components by means of a physical setup forming a HiL simulation. In this way, the advantages of real testing and model-based simulation are combined, permitting stability assessment under dynamic, reproducible and physiological conditions.

In order to ensure physiologically realistic test conditions, validation of the HiL test system is mandatory. As the main function of the embedded model is to deliver physiological boundary conditions, the validation strategy within this work was to compare predicted joint loading against experimental data. For THR testing, a musculoskeletal model was developed which allows for muscle force estimations whilst the HiL simulation is in progress. The outcomes for two common maneuvers agreed well in trend and magnitude with the hip joint contact force components derived from three patients with instrumented THRs. Hence, it can be inferred that the HiL test system is able to replicate comparable THR dynamics as present in patients. Under the assumption that estimated muscle forces are still physiologically reasonable for extreme maneuvers, several challenges regarding THR stability can be addressed in subsequent studies based on the current HiL configuration. These include the dynamic influence of implant design and positioning, the contribution of muscular and capsular structures, or the performance of eccentric tripolar systems.

Concerning TKR testing, a MBS model was implemented into the HiL environment which emulates in vitro test conditions derived from an experimental setup. The outline of the model enabled direct comparison to the corresponding specimen-based measurements revealing overall good correlation. Given this outcome, it can be concluded that the HiL test system is also capable of reproducing comparable TKR kinematics and loading as present under in vitro conditions. But the configuration at this stage does not meet the requirements for investigating realistic instability processes without further improvements. These involve the implementation of a more complex ligament apparatus into the model, along with active muscle structures.

In the long term, HiL simulations have the potential to play a key role in the advancement of orthopedic research. Apart from ongoing optimization of the test system, the concept of HiL simulations can be easily transferred to other joints of the human body. Unsatisfactory outcomes after total shoulder arthroplasty, for instance, are frequently characterized by stiffness, instability, component malpositioning or malalignment [132, 163]. By implementing a validated musculoskeletal model of the shoulder complex [293], the HiL approach may assist in assessing functional impairment of total shoulder replacements, analogous to THR

and TKR testing. The same may apply to failures after total elbow or ankle arthroplasty, respectively. Moreover, wear testing standards were criticized not to replicate reality due to non-physiological load conditions [118, 289, 290]. In this regard, the HiL approach may represent a convenient way to introduce more physiological conditions into wear simulators. Depending on the model embedded several wear-associated maneuvers can be considered at different levels of intensity, what may be restricted with mere implementation of prescribed in vivo data. Beyond that, each HiL based analysis delivers a complete and consistent data set containing at best the entire musculoskeletal dynamics. These data sets may be used as boundary conditions in further studies to investigate effects on implant loosening, wear or fracture.

In the context of upcoming trends, there are a couple of aspects with regard to TJR instability which can be addressed in line with the HiL approach. Fregly et al. [135] stressed the importance of utilizing subject-specific models which reflect the musculoskeletal properties of unique patients. Based on such models, the risk of instability may be evaluated for each patient individually in the scope of HiL based assessments. Proceeding investigations may also consider a variety of individuals summarized into populations that represent male and female, young and elderly, or active and non-active patients. These would allow for more general conclusions to be drawn with respect to risk factors, in contrast to the "one model fits all" approach. The enormous task may be facilitated by incorporating sophisticated reduction, scaling and calibration methods into the modeling process comprising interindividual differences in bone morphology, soft tissue physiology, or motion control. Besides subject specificity, the high degree of parameter variability remains a huge challenge to be dealt with, including implant type, design and positioning, soft tissue condition, or type and intensity of maneuvers. Given the infinite amount of possible combinations, a few researchers [19,106,125] introduced probabilistic methods into the field of orthopedic research, such as Monte Carlo or advanced mean value approaches, which account for distributional characteristics instead of a manually fixed number. Incorporation of such methods into the HiL environment would not only offer effective treatment of crucial parameters, but also holistic evaluations with respect to their impact on TJR stability.

These prospects provide a vague idea of how the HiL approach can be utilized in the future. Insights based upon such evaluations may help researchers and implant developers to enhance and optimize existing implant designs and surgical techniques. They may be beneficial for the clinical practice alike. Orthopedic surgeons may be advised more effectively with respect to preoperative planning and surgical treatment in the case of primary, revision or tumor surgery.

Bibliography

[1] Y. Abu-Amer, I. Darwech, and J. Clohisy. Aseptic loosening of total joint replacements: mechanisms underlying osteolysis and potential therapies. *Arthritis Research & Therapy*, 9(Suppl. 1):S6 (doi:10.1186/ar2170), 2007.

[2] A. Ahmed and N. Duncan. Correlation of patellar tracking pattern with trochlear and retropatellar surface topographies. *Journal of Biomechanical Engineering*, 122(6):652–660, 2000.

[3] H. Amstutz, R. Lodwig, D. Schurman, and A. Hodgson. Range of motion studies for total hip replacements. A comparative study with a new experimental apparatus. *Clinical Orthopaedics and Related Research*, 111:124–130, 1975.

[4] K. An, K. Kaufman, and E. Chao. Physiological considerations of muscle force through the elbow joint. *Journal of Biomechanics*, 22(11-12):1249–1256, 1989.

[5] F. Anderson and M. Pandy. Static and dynamic optimization solutions for gait are practically equivalent. *Journal of Biomechanics*, 34(2):153–161, 2001.

[6] T. Andriacchi, J. Galante, and R. Fermier. The influence of total knee replacement design on walking and stair-climbing. *Journal of Bone and Joint Surgery - Series A*, 64(9):1328–1335, 1982.

[7] A. Andrianakos, L. Kontelis, D. Karamitsos, S. Aslanidis, A. Georgountzos, G. Kaziolas, K. Pantelidou, E. Vafiadou, and P. Dantis. Prevalence of symptomatic knee, hand, and hip osteoarthritis in Greece. The ESORDIG study. *The Journal of Rheumatology*, 33(12):2507–2513, 2006.

[8] Y. Anouchi, L. Whiteside, A. Kaiser, and M. Milliano. The effects of axial rotational alignment of the femoral component on knee stability and patellar tracking in total knee arthroplasty demonstrated on autopsy specimens. *Clinical Orthopaedics and Related Research*, 287:170–177, 1993.

[9] J.-N. Argenson, G. Scuderi, R. Komistek, W. Scott, M. Kelly, and J.-M. Aubaniac. In vivo kinematic evaluation and design considerations related to high flexion in total knee arthroplasty. *Journal of Biomechanics*, 38(2):277–284, 2005.

[10] M. Arnold, B. Burgermeister, and A. Eichberger. Linearly implicit time integration methods in real-time applications: DAEs and stiff ODEs. *Multibody System Dynamics*, 17(2–3):99–117, 2007.

[11] K. Athwal, N. Hunt, A. Davies, D. Deehan, and A. Amis. Clinical biomechanics of instability related to total knee arthroplasty. *Clinical Biomechanics*, 29(2):119–128, 2014.

[12] Australian Orthopaedic Association National Joint Replacement Registry, Adelaide, Australia. *Annual Report*, 2012.

[13] R. Bader, W. Mittelmeier, and E. Steinhauser. Failure analysis of total knee replacement. Basics and methodological aspects of the damage analysis. *Orthopade*, 35(9):896–903, 2006.

[14] R. Bader, R. Scholz, E. Steinhauser, R. Busch, and W. Mittelmeier. Method for the evaluation of factors influencing the dislocation stability of total hip endoprotheses. *Biomedical Engineering*, 49(5):137–144, 2004.

[15] R. Bader, R. Scholz, E. Steinhauser, S. Zimmermann, R. Busch, and W. Mittelmeier. The influence of head and neck geometry on stability of total hip replacement: A mechanical test study. *Acta Orthopaedica Scandinavica*, 75(4):415–421, 2004.

[16] R. Baker. Letter to the editor: ISB recommendation on definition of joint coordinate systems for the reporting of human joint motion – Part I: Ankle, hip and spin. *Journal of Biomechanics*, 36(2):300–302, 2003.

[17] M. Baldwin, C. Clary, C. Fitzpatrick, J. Deacy, L. Maletsky, and P. Rullkoetter. Dynamic finite element knee simulation for evaluation of knee replacement mechanics. *Journal of Biomechanics*, 45(3):474–483, 2012.

[18] M. Baldwin, C. Clary, L. Maletsky, and P. Rullkoetter. Verification of predicted specimen-specific natural and implanted patellofemoral kinematics during simulated deep knee bend. *Journal of Biomechanics*, 42(14):2341–2348, 2009.

[19] M. Baldwin, P. Laz, J. Stowe, and P. Rullkoetter. Efficient probabilistic representation of tibiofemoral soft tissue constraint. *Computer Methods in Biomechanics and Biomedical Engineering*, 12(6):651–659, 2009.

[20] H. Bang, Y. Chiu, S. Memtsoudis, L. Mandl, A. Della Valle, A. Mushlin, R. Marx, and M. Mazumdar. Total hip and total knee arthroplasties: Trends and disparities revisited. *American Journal of Orthopedics*, 39(9):E95–E102, 2010.

[21] S. Banks, G. Markovich, and W. Hodge. In vivo kinematics of cruciate-retaining and -substituting knee arthroplasties. *Journal of Arthroplasty*, 12(3):297–304, 1997.

[22] M. Barink, M. De Waal Malefijt, P. Celada, P. Vena, A. Van Kampen, and N. Verdonschot. A mechanical comparison of high-flexion and conventional total knee arthroplasty. *Proceedings of the Institution of Mechanical Engineers, Part H: Journal of Engineering in Medicine*, 222(3):297–307, 2008.

[23] R. Barrack. Dislocation after total hip arthroplasty: Implant design and orientation. *Journal of the American Academy of Orthopaedic Surgeons*, 11(2):89–99, 2003.

[24] R. Bartz, P. Noble, N. Kadakia, and H. Tullos. The effect of femoral component head size on posterior dislocation of the artificial hip joint. *Journal of Bone and Joint Surgery - Series A*, 82(9):1300–1307, 2000.

[25] J. Bateman. The classic: Single-assembly total hip prosthesis – Preliminary report. *Clinical Orthopaedics and Related Research*, 251:3–6, 1990.

[26] R. Bauer, F. Kerschbaumer, and S. Poisel. *Orthopädische Operationslehre in drei Bänden, Band 2: Becken und untere Extremität*. Thieme, Stuttgart, 1994.

[27] J. Bean, D. Chaffin, and A. Schultz. Biomechanical model calculation of muscle contraction forces: A double linear programming method. *Journal of Biomechanics*, 21(1):59–66, 1988.

[28] L. Beimers, G. Tuijthof, L. Blankevoort, R. Jonges, M. Maas, and C. van Dijk. In-vivo range of motion of the subtalar joint using computed tomography. *Journal of Biomechanics*, 41(7):1390–1397, 2008.

[29] J. Bellemans, S. Banks, J. Victor, H. Vandenneucker, and A. Moemans. Fluoroscopic analysis of the kinematics of deep flexion in total knee arthroplasty. *Journal of Bone and Joint Surgery - Series B*, 84(1):50–53, 2002.

[30] M. Benedetti, F. Catani, T. Bilotta, M. Marcacci, E. Mariani, and S. Giannini. Muscle activation pattern and gait biomechanics after total knee replacement. *Clinical Biomechanics*, 18(9):871–876, 2003.

[31] R. Berger, L. Crossett, J. Jacobs, and H. Rubash. Malrotation causing patellofemoral complications after total knee arthroplasty. *Clinical Orthopaedics and Related Research*, 356:144–153, 1998.

[32] R. Berger and H. Rubash. Rotational instability and malrotation after total knee arthroplasty. *Orthopedic Clinics of North America*, 32(4):639–647, 2001.

[33] G. Bergmann, G. Deuretzbacher, M. Heller, F. Graichen, A. Rohlmann, J. Strauss, and G. Duda. Hip contact forces and gait patterns from routine activities. *Journal of Biomechanics*, 34(7):859–871, 2001.

[34] G. Bergmann, F. Graichen, and A. Rohlmann. Hip joint loading during walking and running, measured in two patients. *Journal of Biomechanics*, 26(8):969–990, 1993.

[35] G. Bergmann, F. Graichen, and A. Rohlmann. Hip joint contact forces during stumbling. *Langenbeck's Archives of Surgery*, 389(1):53–59, 2004.

[36] R. Biedermann, A. Tonin, M. Krismer, F. Rachbauer, G. Eibl, and B. Stockl. Reducing the risk of dislocation after total hip arthroplasty - The effect of orientation of the acetabular component. *Journal of Bone and Joint Surgery - Series B*, 87(6):762–769, 2005.

[37] N. Bishop, A. Hothan, and M. Morlock. High friction moments in large hard-on-hard hip replacement bearings in conditions of poor lubrication. *Journal of Orthopaedic Research*, 31(5):807–813, 2013.

[38] N. Bishop, F. Witt, R. Pourzal, A. Fischer, M. Rütschi, M. Michel, and M. Morlock. Wear patterns of taper connections in retrieved large diameter metal-on-metal bearings. *Journal of Orthopaedic Research*, 31(7):1116–1122, 2013.

[39] L. Blankevoort and R. Huiskes. Ligament-bone interaction in a three-dimensional model of the knee. *Journal of Biomechanical Engineering*, 113(3):263–269, 1991.

[40] L. Blankevoort and R. Huiskes. Validation of a three-dimensional model of the knee. *Journal of Biomechanics*, 29(7):955–961, 1996.

[41] L. Blankevoort, R. Huiskes, and A. de Lange. The envelope of passive knee joint motion. *Journal of Biomechanics*, 21(9):705–720, 1988.

[42] L. Blankevoort, R. Huiskes, and A. de Lange. Helical axes of passive knee joint motions. *Journal of Biomechanics*, 23(12):1219–1229, 1990.

[43] T. Boge and O. Ma. Using advanced industrial robotics for spacecraft rendezvous and docking simulation. In *International Conference on Robotics and Automation 2011 Communications*, Shanghai, China, 2011.

[44] K. Bozic, S. Kurtz, E. Lau, K. Ong, T. Vail, and D. Berry. The epidemiology of revision total hip arthroplasty in the United States. *Journal of Bone and Joint Surgery - Series A*, 91(1):128–133, 2009.

[45] R. Brand, R. Crowninshield, C. Wittstock, D. Pedersen, C. Clark, and F. van Krieken. A model of lower extremity muscular anatomy. *Journal of Biomechanical Engineering*, 104(4):304–310, 1982.

[46] R. Brand, D. Pedersen, D. Davy, G. Kotzar, K. Heiple, and V. Goldberg. Comparison of hip force calculations and measurements in the same patient. *Journal of Arthroplasty*, 9(1):45–51, 1994.

[47] R. Brand, D. Pedersen, and J. Friederich. The sensitivity of muscle force predictions to changes in physiological cross-sectional area. *Journal of Biomechanics*, 19(8):589–596, 1986.

[48] J.-L. Briard and D. Hungerford. Patellofemoral instability in total knee arthroplasty. *Journal of Arthroplasty*, 4(Suppl.):S87–S97, 1989.

[49] T. Buchanan, D. Lloyd, K. Manal, and T. Besier. Neuromusculoskeletal modeling: Estimation of muscle forces and joint moments and movements from measurements of neural command. *Journal of Applied Biomechanics*, 20(4):367–395, 2004.

[50] A. Bull, O. Kessler, M. Alam, and A. Amis. Changes in knee kinematics reflect the articular geometry after arthroplasty. *Clinical Orthopaedics and Related Research*, 466(10):2491–2499, 2008.

[51] B. Burgermeister, M. Arnold, and B. Esterl. DAE time integration for real-time applications in multi-body dynamics. *Journal of Applied Mathematics and Mechanics*, 86(10):759–771, 2006.

[52] B. Burroughs, B. Hallstrom, G. Golladay, D. Hoeffel, and W. Harris. Range of motion and stability in total hip arthroplasty with 28-, 32-, 38-, and 44-mm femoral head sizes - An in vitro study. *Journal of Arthroplasty*, 20(1):11–19, 2005.

[53] D. Butler, F. Noyes, and E. Grood. Ligamentous restraints to anterior-posterior drawer in the human knee. A biomechanical study. *Journal of Bone and Joint Surgery - Series A*, 62(2):259–270, 1980.

[54] V. Carbone, M. van der Krogt, H. Koopman, and N. Verdonschot. Sensitivity of subject-specific models to errors in musculo-skeletal geometry. *Journal of Biomechanics*, 45(14):2476–2480, 2012.

[55] F. Catani, A. Ensini, C. Belvedere, A. Feliciangeli, M. Benedetti, A. Leardini, and S. Giannini. In vivo kinematics and kinetics of a bi-cruciate substituting total knee arthroplasty: A combined fluoroscopic and gait analysis study. *Journal of Orthopaedic Research*, 27(12):1569–1575, 2009.

[56] F. Catani, S. Fantozzi, A. Ensini, A. Leardini, D. Moschella, and S. Giannini. Influence of tibial component posterior slope on in vivo knee kinematics in fixed-bearing total knee arthroplasty. *Journal of Orthopaedic Research*, 24(4):581–587, 2006.

[57] H. Cates, R. Komistek, M. Mahfouz, M. Schmidt, and M. Anderle. In vivo comparison of knee kinematics for subjects having either a posterior stabilized or cruciate retaining high-flexion total knee arthroplasty. *Journal of Arthroplasty*, 23(7):1057–1067, 2008.

[58] Centers for Disease Control and Prevention, National Center for Health Statistics, Hyattsville, Maryland, United States. *Number of all-listed procedures for discharges from short-stay hospitals, by ICD-9-CM code, sex, age, and geographic region*, 2006.

[59] Centers for Disease Control and Prevention, National Center for Health Statistics, Hyattsville, Maryland, United States. *Number of all-listed procedures for discharges from short-stay hospitals, by ICD-9-CM code, sex, age, and geographic region*, 2007.

[60] Centers for Disease Control and Prevention, National Center for Health Statistics, Hyattsville, Maryland, United States. *Number of all-listed procedures for discharges from short-stay hospitals, by ICD-9-CM code, sex, age, and geographic region*, 2008.

[61] Centers for Disease Control and Prevention, National Center for Health Statistics, Hyattsville, Maryland, United States. *Number of all-listed procedures for discharges from short-stay hospitals, by ICD-9-CM code, sex, age, and geographic region*, 2009.

[62] Centers for Disease Control and Prevention, National Center for Health Statistics, Hyattsville, Maryland, United States. *Number of all-listed procedures for discharges from short-stay hospitals, by ICD-9-CM code, sex, age, and geographic region*, 2010.

[63] J. Challis. Producing physiologically realistic individual muscle force estimations by imposing constraints when using optimization techniques. *Medical Engineering & Physics*, 19(3):253–261, 1997.

[64] J. Challis and D. Kerwin. An analytical examination of muscle force estimations using optimization techniques. *Proceedings of the Institution of Mechanical Engineers H: Journal of Engineering in Medicine*, 207(3):139–148, 1993.

[65] D. Chandler, R. Glousman, D. Hull, P. McGuire, I. Kim, I. Clarke, and A. Sarmiento. Prosthetic hip range of motion and impingement. The effects of head and neck geometry. *Clinical Orthopaedics and Related Research*, 166:284–291, 1982.

[66] J. Chouteau, J. Lerat, R. Testa, B. Moyen, M. Fessy, and S. Banks. Kinematics of a cementless mobile bearing posterior cruciate ligament-retaining total knee arthroplasty. *Knee*, 16(3):223–227, 2009.

[67] C. Clary, C. Fitzpatrick, L. Maletsky, and P. Rullkoetter. The influence of total knee arthroplasty geometry on mid-flexion stability: An experimental and finite element study. *Journal of Biomechanics*, 46(7):1351–1357, 2013.

[68] D. Cleather and A. Bull. The development of lower limb musculoskeletal models with clinical relevance is dependent upon the fidelity of the mathematical description of the lower limb. Part I: Equations of motion. *Proceedings of the Institution of Mechanical Engineers H: Journal of Engineering in Medicine*, 226(2):120–132, 2012.

[69] D. Cleather and A. Bull. The development of lower limb musculoskeletal models with clinical relevance is dependent upon the fidelity of the mathematical description of the lower limb. Part II: Patient-specific geometry. *Proceedings of the Institution of Mechanical Engineers H: Journal of Engineering in Medicine*, 226(2):133–145, 2012.

[70] J. Collins. The redundant nature of locomotor optimization laws. *Journal of Biomechanics*, 28(3):251–267, 1995.

[71] C. Colwell Jr., P. Chen, and D. D'Lima. Extensor malalignment arising from femoral component malrotation in knee arthroplasty: Effect of rotating-bearing. *Clinical Biomechanics*, 26(1):52–57, 2011.

[72] T. Conlan, W. Garth Jr., and J. Lemons. Evaluation of the medial soft-tissue restraints of the extensor mechanism of the knee. *Journal of Bone and Joint Surgery - Series A*, 75(5):682–693, 1993.

[73] Council of the European Union, Brussel, Belgium. *Council Directive 93/42/EEC of 14 June 1993 concerning medical devices*, 1993.

[74] M. Coventry. Late dislocations in patients with Charnley total hip arthroplasty. *Journal of Bone and Joint Surgery - Series A*, 67(6):832–841, 1985.

[75] D. Covey, A. Sapega, and G. Sherman. Testing for isometry during reconstruction of the posterior cruciate ligament: Anatomic and biomechanical considerations. *American Journal of Sports Medicine*, 24(6):740–746, 1996.

[76] R. Crowninshield. Use of optimization techniques to predict muscle forces. *Journal of Biomechanical Engineering*, 100(2):88–92, 1978.

[77] R. Crowninshield and R. Brand. A physiologically based criterion of muscle force prediction in locomotion. *Journal of Biomechanics*, 14(11):793–801, 1981.

[78] R. Crowninshield, R. Johnston, J. Andrews, and R. Brand. A biomechanical investigation of the human hip. *Journal of Biomechanics*, 11(1–2):75–85, 1978.

[79] D. Dalury, D. Pomeroy, R. Gorab, and M. Adams. Why are total knee arthroplasties being revised? *Journal of Arthroplasty*, 28(Suppl. 1):120–121, 2013.

[80] P. Damm, J. Dymke, R. Ackermann, A. Bender, F. Graichen, A. Halder, A. Beier, and G. Bergmann. Friction in total hip joint prosthesis measured in vivo during walking. *PLoS One*, 8(11):e78373, 2013.

[81] D. Davy, G. Kotzar, R. Brown, K. Heiple, V. Goldberg, K. J. Heiple, J. Berilla, and A. Burstein. Telemetric force measurements across the hip after total arthroplasty. *Journal of Bone and Joint Surgery - Series A*, 70(1):45–50, 1988.

[82] P. de Leva. Adjustments to Zatsiorsky-Seluyanov's segment inertia parameters. *Journal of Biomechanics*, 29(9):1223–1230, 1996.

[83] S. Delp, A. Komattu, and R. Wixson. Superior displacement of the hip in total joint replacement: Effects of prosthetic neck length, neck-stem angle, and anteversion angle on the moment-generating capacity of the muscles. *Journal of Orthopaedic Research*, 12(6):860–870, 1994.

[84] S. Delp and W. Maloney. Effects of hip center location on the moment-generating capacity of the muscle. *Journal of Biomechanics*, 26(4–5):485–499, 1993.

[85] H. Delport, S. Banks, J. De Schepper, and J. Bellemans. A kinematic comparison of fixed- and mobile-bearing knee replacements. *Journal of Bone and Joint Surgery - Series B*, 88(8):1016–1021, 2006.

[86] H. Delport, L. Labey, R. De Corte, B. Innocenti, J. Vander Sloten, and J. Bellemans. Collateral ligament strains during knee joint laxity evaluation before and after TKA. *Clinical Biomechanics*, 28(7):777–782, 2013.

[87] H. Demos, C. Rorabeck, R. Bourne, S. MacDonald, and R. McCalden. Instability in primary total hip arthroplasty with the direct lateral approach. *Clinical Orthopaedics and Related Research*, 393:168–180, 2001.

[88] D. Dennis, R. Komistek, C. Colwell Jr., C. Ranawat, R. Scott, T. Thornhill, and M. Lapp. In vivo anteroposterior femorotibial translation of total knee arthroplasty: A multicenter analysis. *Clinical Orthopaedics and Related Research*, 356:47–57, 1998.

[89] D. Dennis, R. Komistek, W. Hoff, and S. Gabriel. In vivo knee kinematics derived using an inverse perspective technique. *Clinical Orthopaedics and Related Research*, 331:107–117, 1996.

[90] D. Dennis, R. Komistek, M. Mahfouz, S. Walker, and A. Tucker. A multicenter analysis of axial femorotibial rotation after total knee arthroplasty. *Clinical Orthopaedics and Related Research*, 428:180–189, 2004.

[91] D. Dennis, R. Komistek, S. Walker, E. Cheal, and J. Stiehl. Femoral condylar lift-off in vivo in total knee arthroplasty. *Journal of Bone and Joint Surgery - Series B*, 83(1):33–39, 2001.

[92] S. Desio, R. Burks, and K. Bachus. Soft tissue restraints to lateral patellar translation in the human knee. *American Journal of Sports Medicine*, 26(1):59–65, 1998.

[93] J. DesJardins, P. Walker, H. Haider, and J. Perry. The use of a force-controlled dynamic knee simulator to quantify the mechanical performance of total knee replacement designs during functional activity. *Journal of Biomechanics*, 33(10):1231–1242, 2000.

[94] P. Dieppe and L. Lohmander. Pathogenesis and management of pain in osteoarthritis. *Lancet*, 365:965–973, 2005.

[95] A. DiGioia, B. Jaramaz, M. Blackwell, D. Simon, F. Morgan, J. Moody, C. Nikou, B. Colgan, C. Aston, R. Labarca, E. Kischell, and T. Kanade. Image guided navigation system to measure intraoperatively acetabular implant alignment. *Clinical Orthopaedics and Related Research*, 355:8–22, 1998.

[96] D. D'Lima, S. Patil, N. Steklov, S. Chien, and C. Colwell Jr. In vivo knee moments and shear after total knee arthroplasty. *Journal of Biomechanics*, 40(Suppl. 1):S11–S17, 2007.

[97] D. D'Lima, S. Patil, N. Steklov, and C. Colwell Jr. Dynamic intraoperative ligament balancing for total knee arthroplasty. *Clinical Orthopaedics and Related Research*, 463:208–212, 2007.

[98] D. D'Lima, S. Patil, N. Steklov, J. Slamin, and C. Colwell Jr. In vivo knee forces after total knee arthroplasty. *Clinical orthopaedics and Related Research*, 440:45–49, 2005.

[99] D. D'Lima, S. Patil, N. Steklov, J. Slamin, and C. Colwell Jr. Tibial forces measured in vivo after total knee arthroplasty. *Journal of Arthroplasty*, 21(2):255–262, 2006.

[100] D. D'Lima, N. Steklov, B. Fregly, S. Banks, and C. Colwell Jr. In vivo contact stresses during activities of daily living after knee arthroplasty. *Journal of Orthopaedic Research*, 26(12):1549–1555, 2008.

[101] D. D'Lima, N. Steklov, S. Patil, and C. Colwell Jr. In vivo knee forces during recreation and exercise after knee arthroplasty. *Clinical Orthopaedics and Related Research*, 466(11):2605–2611, 2008.

[102] D. D'Lima, M. Trice, A. Urquhart, and C. Colwell Jr. Comparison between the kinematics of fixed and rotating bearing knee prostheses. *Clinical Orthopaedics and Related Research*, 380:151–157, 2000.

[103] D. D'Lima, A. Urquhart, K. Buehler, R. Walker, and C. Colwell Jr. The effect of the orientation of the acetabular and femoral components on the range of motion of the hip at different head-neck ratios. *Journal of Bone and Joint Surgery - Series A*, 82(3):315–321, 2000.

[104] L. Dorr and Z. Wan. Causes of and treatment protocol for instability of total hip replacement. *Clinical Orthopaedics and Related Research*, 355:144–151, 1998.

[105] L. Dorr, A. Wolf, R. Chandler, and J. Conaty. Classification and treatment of dislocations of total hip arthroplasty. *Clinical Orthopaedics and Related Research*, 173:151–158, 1983.

[106] S. Easley, S. Pal, P. Tomaszewski, A. Petrella, P. Rullkoetter, and P. Laz. Finite element-based probabilistic analysis tool for orthopaedic applications. *Computer Methods and Programs in Biomedicine*, 85(1):32–40, 2007.

[107] A. Eichberger. *Generating multibody real-time models for hardware-in-the-loop applications*. INTEC GmbH, Wessling, Germany, 2002.

[108] A. Eichberger and G. Hofmann. TMPT: multi-body package SIMPACK. *Vehicle System Dynamics*, 45(Suppl. 1):207–216, 2007.

[109] S. Eisenhuth, K. Saleh, Q. Cui, C. Clark, and T. Brown. Patellofemoral instability after total knee arthroplasty. *Clinical Orthopaedics and Related Research*, 446:149–160, 2006.

[110] J. Elkins, J. Callaghan, and T. Brown. Stability and trunnion wear potential in large-diameter metal-on-metal total hips: A finite element analysis. *Clinical Orthopaedics and Related Research*, 472(2):529–542, 2014.

[111] J. Elkins, J. Callaghan, and T. Brown. The 'landing zone' for wear and stability in total hip arthroplasty is smaller than we thought: A computational analysis. *Clinical Orthopaedics and Related Research*, 473(2):441–452, 2015.

[112] J. Elkins, M. Daniel, D. Pedersen, B. Singh, H. Yack, J. Callaghan, and T. Brown. Morbid obesity may increase dislocation in total hip patients: A biomechanical analysis hip. *Clinical Orthopaedics and Related Research*, 471(3):971–980, 2013.

[113] J. Elkins, K. Kruger, D. Pedersen, J. Callaghan, and T. Brown. Edge-loading severity as a function of cup lip radius in metal-on-metal total hips-a finite element analysis. *Journal of Orthopaedic Research*, 30(2):169–177, 2012.

[114] J. Elkins, N. Stroud, M. Rudert, Y. Tochigi, D. Pedersen, B. Ellis, J. Callaghan, J. Weiss, and T. Brown. The capsule's contribution to total hip construct stability – A finite element analysis. *Journal of Orthopaedic Research*, 29(11):1642–1648, 2011.

[115] T. English and M. Kilvington. In vivo records of hip loads using a femoral implant with telemetric output (A preliminary report). *Journal of Biomedical Engineering*, 1(2):111–115, 1979.

[116] A. Erdemir, S. McLean, W. Herzog, and A. van den Bogert. Model-based estimation of muscle forces exerted during movements. *Clinical Biomechanics*, 22(2):131–154, 2007.

[117] J. Essinger, P. Leyvraz, J. Heegard, and D. Robertson. A mathematical model for the evaluation of the behaviour during flexion of condylar-type knee prostheses. *Journal of Biomechanics*, 22(11–12):1229–1241, 1989.

[118] C. Fabry, S. Herrmann, M. Kaehler, E. Klinkenberg, C. Woernle, and R. Bader. Generation of physiological parameter sets for hip joint motions and loads during daily life activities for application in wear simulators of the artificial hip joint. *Medical Engineering & Physics*, 35(1):131–139, 2013.

[119] C. Fabry, M. Kaehler, S. Herrmann, C. Woernle, and R. Bader. Dynamic behavior of tripolar hip endoprostheses under physiological conditions and their effect on stability. *Medical Engineering & Physics*, 36(1):65–71, 2014.

[120] C. Fackler and R. Poss. Dislocation in total hip arthroplasties. *Clinical Orthopaedics and Related Research*, 151:169–178, 1980.

[121] S. Fantozzi, F. Catani, A. Ensini, A. Leardini, and S. Giannini. Femoral rollback of cruciate-retaining and posterior-stabilized total knee replacements: In vivo fluoroscopic analysis during activities of daily living. *Journal of Orthopaedic Research*, 24(12):2222–2229, 2006.

[122] T. Fehring and A. Valadie. Knee instability after total knee arthroplasty. *Clinical Orthopaedics and Related Research*, 299:157–162, 1994.

[123] C. Fitzpatrick, M. Baldwin, C. Clary, L. Maletsky, and P. Rullkoetter. Evaluating knee replacement mechanics during ADL with PID-controlled dynamic finite element analysis. *Computer Methods in Biomechanics and Biomedical Engineering*, 17(4):360–369, 2014.

[124] C. Fitzpatrick, M. Baldwin, C. Clary, A. Wright, P. Laz, and P. Rullkoetter. Identifying alignment parameters affecting implanted patellofemoral mechanics. *Journal of Orthopaedic Research*, 30(7):1167–1175, 2012.

[125] C. Fitzpatrick, M. Baldwin, P. Rullkoetter, and P. Laz. Combined probabilistic and principal component analysis approach for multivariate sensitivity evaluation and application to implanted patellofemoral mechanics. *Journal of Biomechanics*, 44(1):13–21, 2011.

[126] C. Fitzpatrick, C. Clary, A. Cyr, L. Maletsky, and P. Rullkoetter. Mechanics of post-cam engagement during simulated dynamic activity. *Journal of Orthopaedic Research*, 31(9):1438–1446, 2013.

[127] C. Fitzpatrick, C. Clary, P. Laz, and P. Rullkoetter. Relative contributions of design, alignment, and loading variability in knee replacement mechanics. *Journal of Orthopaedic Research*, 30(12):2015–2024, 2012.

[128] C. Fitzpatrick, C. Clary, and P. Rullkoetter. The role of patient, surgical, and implant design variation in total knee replacement performance. *Journal of Biomechanics*, 45(12):2092–2102, 2012.

[129] S. Fornalski, M. McGarry, C. Bui, W. Kim, and T. Lee. Biomechanical effects of joint line elevation in total knee arthroplasty. *Clinical Biomechanics*, 27(8):824–829, 2012.

[130] E. Forster, U. Simon, P. Augat, and L. Claes. Extension of a state-of-the-art optimization criterion to predict co-contraction. *Journal of Biomechanics*, 37(4):577–581, 2004.

[131] K. Foucher and M. Wimmer. Does hip implant positioning affect the peak external adduction moments of the healthy knees of subjects with total hip replacements? *Journal of Orthopaedic Research*, 31(8):1187–1194, 2013.

[132] A. Franta, T. Lenters, D. Mounce, B. Neradilek, and F. Matsen III. The complex characteristics of 282 unsatisfactory shoulder arthroplasties. *Journal of Shoulder and Elbow Surgery*, 16(5):555–562, 2007.

[133] F. Fraysse, R. Dumas, L. Cheze, and X. Wang. Comparison of global and joint-to-joint methods for estimating the hip joint load and the muscle forces during walking. *Journal of Biomechanics*, 42(14):2357–2362, 2009.

[134] M. Freeman and V. Pinskerova. The movement of the normal tibio-femoral joint. *Journal of Biomechanics*, 38(2):197–208, 2005.

[135] B. Fregly, T. Besier, D. Lloyd, S. Delp, S. Banks, M. Pandy, and D. D'Lima. Grand challenge competition to predict in vivo knee loads. *Journal of Orthopaedic Research*, 30(4):503–513, 2012.

[136] M. Frey, R. Burgkart, F. Regenfelder, and R. Riener. Optimised robot-based system for the exploration of elastic joint properties. *Medical & Biological Engineering & Computing*, 42:674–678, 2004.

[137] J. Friederich and R. Brand. Muscle fiber architecture in the human lower limb. *Journal of Biomechanics*, 23(1):91–95, 1990.

[138] H. Fujie, K. Mabuchi, S. Woo, G. Livesay, S. Arai, and Y. Tsukamoto. The use of robotics technology to study human joint kinematics: A new methodology. *Journal of Biomechanical Engineering*, 115(3):211–217, 1993.

[139] Y. Fung. Elasticity of soft tissues in simple elongation. *American Journal of Physiology*, 213(6):1532–1544, 1967.

[140] F. Fuss. Principles and mechanisms of automatic rotation during terminal extension in the human knee joint. *Journal of Anatomy*, 180:297–304, 1992.

[141] F. Fuss and A. Bacher. New aspects of the morphology and function of the human hip joint ligaments. *American Journal of Anatomy*, 192(1):1–13, 1991.

[142] P. Gerus, M. Sartori, T. Besier, B. Fregly, S. Delp, S. Banks, M. Pandy, D. D'Lima, and D. Lloyd. Subject-specific knee joint geometry improves predictions of medial tibiofemoral contact forces. *Journal of Biomechanics*, 46(16):2778–2786, 2013.

[143] F. Girgis, J. Marshall, and A. Al Monajem. The cruciate ligaments of the knee joint. Anatomical, functional and experimental analysis. *Clinical Orthopaedics and Related Research*, 106:216–231, 1975.

[144] U. Glitsch and W. Baumann. The three-dimensional determination of internal loads in the lower extremity. *Journal of Biomechanics*, 30(11–12):1123–1131, 1997.

[145] D. Gollehon, P. Torzilli, and R. Warren. The role of the posterolateral and cruciate ligaments in the stability of the human knee. A biomechanical study. *Journal of Bone and Joint Surgery - Series A*, 69(2):233–242, 1987.

[146] H. Graichen, M. Strauch, T. Katzhammer, L. Zichner, and R. Voneisenhart-Rothe. Ligament instability in total knee arthroplasty – Causal analysis. *Orthopade*, 36(7):650–656, 2007.

[147] H. Gray. *Anatomy of the Human Body*. Lea & Febiger, Philadelphia, 1918.

[148] E. Grood, F. Noyes, D. Butler, and W. Suntay. Ligamentous and capsular restraints preventing straight medial and lateral laxity in intact human cadaver knees. *Journal of Bone and Joint Surgery - Series A*, 63(8):1257–1269, 1981.

[149] E. Grood, S. Stowers, and F. Noyes. Limits of movement in the human knee. Effect of sectioning the posterior cruciate ligament and posterolateral structures. *Journal of Bone and Joint Surgery - Series A*, 70(1):88–97, 1988.

[150] M. Günther, S. Grimmer, T. Siebert, and R. Blickhan. All leg joints contribute to quiet human stance: A mechanical analysis. *Journal of Biomechanics*, 42(16):2739–2746, 2009.

[151] O. Guyen, Q. Chen, J. Bejui-Hugues, D. Berry, and K. An. Unconstrained tripolar hip implants – Effect on hip stability. *Clinical Orthopaedics and Related Research*, 455:202–208, 2007.

[152] O. Guyen, V. Pibarot, G. Vaz, C. Chevillotte, J. Carret, and J. Bejui-Hugues. Unconstrained tripolar implants for primary total hip arthroplasty in patients at risk for dislocation. *Journal of Arthroplasty*, 22(6):849–858, 2007.

[153] H. Haider and P. Walker. Measurements of constraint of total knee replacement. *Journal of Biomechanics*, 38(2):341–348, 2005.

[154] A. Halder, I. Kutzner, F. Graichen, B. Heinlein, A. Beier, and G. Bergmann. Influence of limb alignment on mediolateral loading in total knee replacement: In vivo measurements in five patients. *Journal of Bone and Joint Surgery - Series A*, 94(11):1023–1029, 2012.

[155] J. Halloran, C. Clary, L. Maletsky, M. Taylor, A. Petrella, and P. Rullkoetter. Verification of predicted knee replacement kinematics during simulated gait in the Kansas knee simulator. *Journal of Biomechanical Engineering*, 132(8), 2010.

[156] B. Hanson, M. Levesley, K. Watterson, and P. Walker. Hardware-in-the-loop-simulation of the cardiovascular system, with assist device testing application. *Medical Engineering & Physics*, 29(3):367–374, 2007.

[157] G. Hanson, J. Suggs, A. Freiberg, S. Durbhakula, and G. Li. Investigation of in vivo 6DOF total knee arthoplasty kinematics using a dual orthogonal fluoroscopic system. *Journal of Orthopaedic Research*, 24(5):974–981, 2006.

[158] D. Hardt. Determining muscle forces in the leg during normal human walking – An application and evaluation of optimization methods. *Journal of Biomechanical Engineering*, 100(2):72–78, 1978.

[159] S. Hariri, S. Chun, J. Cowan, C. Bragdon, H. Malchau, and H. Rubash. Range of motion in a modular femoral stem system with a variety of neck options. *Journal of Arthroplasty*, 28(9):1625–1633, 2013.

[160] C. Harner, G. H. Baek, T. Vogrin, G. Carlin, S. Kashiwaguchi, and S.-Y. Woo. Quantitative analysis of human cruciate ligament insertions. *Arthroscopy*, 15(7):741–749, 1999.

[161] W. Harris. The problem is osteolysis. *Clinical Orthopaedics and Related Research*, 311:46–53, 1995.

[162] W. Harris. Wear and periprosthetic osteolysis: The problem. *Clinical Orthopaedics and Related Research*, 393:66–70, 2001.

[163] S. Hasan, J. Leith, B. Campbell, R. Kapil, K. Smith, and F. Matsen III. Characteristics of unsatisfactory shoulder arthroplasties. *Journal of Shoulder and Elbow Surgery*, 11(5):431–441, 2002.

[164] M. Hast and S. Piazza. Dual-joint modeling for estimation of total knee replacement contact forces during locomotion. *Journal of Biomechanical Engineering*, 135(2):021004, 2013.

[165] H. Hatze. The inverse dynamics problem of neuromuscular control. *Biological Cybernetics*, 82(2):133–141, 2000.

[166] H. Hatze. The fundamental problem of myoskeletal inverse dynamics and its implications. *Journal of Biomechanics*, 35(1):109–115, 2002.

[167] M. Hefzy, W. Jackson, S. Saddemi, and Y.-F. Hsieh. Effects of tibial rotations on patellar tracking and patello-femoral contact areas. *Journal of Biomedical Engineering*, 14(4):329–343, 1992.

[168] B. Heinlein, I. Kutzner, F. Graichen, A. Bender, A. Rohlmann, A. Halder, A. Beier, and G. Bergmann. Complete data of total knee replacement loading for level walking and stair climbing measured in vivo with a follow-up of 6-10 months. *Clinical Biomechanics*, 24(4):315–326, 2009.

[169] L. Heller and J. Langman. The menisco-femoral ligaments of the human knee. *Journal of Bone and Joint Surgery - Series B*, 46(2):307–313, 1964.

[170] M. Heller, G. Bergmann, G. Deuretzbacher, L. Claes, N. Haas, and G. Duda. Influence of femoral anteversion on proximal femoral loading: Measurement and simulation in four patients. *Clinical Biomechanics*, 16(8):644–649, 2001.

[171] M. Heller, G. Bergmann, G. Deuretzbacher, L. Durselen, M. Pohl, L. Claes, N. Haas, and G. Duda. Musculo-skeletal loading conditions at the hip during walking and stair climbing. *Journal of Biomechanics*, 34(7):883–893, 2001.

[172] M. Heller, G. Bergmann, J. Kassi, L. Claes, N. Haas, and G. Duda. Determination of muscle loading at the hip joint for use in pre-clinical testing. *Journal of Biomechanics*, 38(5):1155–1163, 2005.

[173] M. Heller, W. Taylor, C. Perka, and G. Duda. The influence of alignment on the musculo-skeletal loading conditions at the knee. *Langenbeck's Archives of Surgery*, 388(5):291–297, 2003.

[174] K. Herrlin, G. Selvik, H. Pettersson, P. Kesek, R. Onnerfält, and A. Ohlin. Position, orientation and component interaction in dislocation of the total hip prosthesis. *Acta Radiologica*, 29(4):441–444, 1988.

[175] S. Herrmann, M. Kaehler, R. Souffrant, R. Rachholz, J. Zierath, D. Kluess, W. Mittelmeier, C. Woernle, and R. Bader. HiL simulation in biomechanics: A new approach for testing total joint replacements. *Computer Methods and Programs in Biomedicine*, 105(2):109–119, 2012.

[176] S. Herrmann, R. Lenz, A. Geier, S. Lehner, R. Souffrant, C. Woernle, T. Tischer, and R. Bader. Musculoskeletal modeling of the patellofemoral joint. Dynamic analysis of patellar tracking. *Orthopade*, 41(4):252–259, 2012.

[177] S. Herrmann, C. Woernle, M. Kaehler, R. Rachholz, R. Souffrant, J. Zierath, D. Kluess, and R. Bader. HiL simulation for testing joint stability after total knee arthroplasty. *Multibody System Dynamics*, 28(1–2):55–67, 2012.

[178] W. Herzog and P. Binding. Cocontraction of pairs of antagonistic muscles - Analytical solution for planar static nonlinear optimization approaches. *Mathematical Biosciences*, 118(1):83–95, 1993.

[179] J. Hewitt, F. Guilak, R. Glisson, and T. Vail. Regional material properties of the human hip joint capsule ligaments. *Journal of Orthopaedic Research*, 19(3):359–364, 2001.

[180] M. Higa, H. Tanino, M. Abo, S. Kakunai, and S. Banks. Effect of acetabular component anteversion on dislocation mechanisms in total hip arthroplasty. *Journal of Biomechanics*, 44(9):1810–1813, 2011.

[181] A. Hill. The heat of shortening and the dynamic constants of muscle. *Proceedings of the Royal Society B*, 126:136–195, 1938.

[182] T. Hisatome and H. Doi. Theoretically optimum position of the prosthesis in total hip arthroplasty to fulfill the severe range of motion criteria due to neck impingement. *Journal of Orthopaedic Science*, 16(2):229–237, 2011.

[183] W. Hoff, R. Komistek, D. Dennis, S. Gabriel, and S. Walker. Three-dimensional determination of femoral-tibial contact positions under in vivo conditions using fluoroscopy. *Clinical Biomechanics*, 13(7):455–472, 1998.

[184] C. Hubley-Kozey, G. Hatfield, J. Wilson, and M. Dunbar. Alterations in neuromuscular patterns between pre and one-year post-total knee arthroplasty. *Clinical Biomechanics*, 25(10):995–1002, 2010.

[185] M. Hummel, A. Malkani, M. Yakkanti, and D. Baker. Decreased dislocation after revision total hip arthroplasty using larger femoral head size and posterior capsular repair. *Journal of Arthroplasty*, 24(6 Suppl. 1):73–76, 2009.

[186] B. Innocenti, S. Pianigiani, L. Labey, J. Victor, and J. Bellemans. Contact forces in several TKA designs during squatting: A numerical sensitivity analysis. *Journal of Biomechanics*, 44(8):1573–1581, 2011.

[187] J. Insall, G. Scuderi, R. Komistek, K. Math, D. Dennis, and D. Anderson. Correlation between condylar lift-off and femoral component alignment. *Clinical Orthopaedics and Related Research*, 403:143–152, 2002.

[188] R. Isermann. *Mechatronic Systems*. Springer, Berlin, 2005.

[189] R. Isermann, J. Schaffnit, and S. Sinsel. Hardware-in-the-loop simulation for the design and testing of engine-control systems. *Control Engineering Practice*, 7(5):643–653, 1999.

[190] H. Ito, Y. Song, D. Lindsey, M. Safran, and N. Giori. The proximal hip joint capsule and the zona orbicularis contribute to hip joint stability in distraction. *Journal of Orthopaedic Research*, 27(8):989–995, 2009.

[191] B. Jaramaz, A. DiGioia, M. Blackwell, and C. Nikou. Computer assisted measurement of cup placement in total hip replacement. *Clinical Orthopaedics and Related Research*, 354:70–81, 1998.

[192] A. Jinha, R. Ait-Haddou, and W. Herzog. Predictions of co-contraction depend critically on degrees-of-freedom in the musculoskeletal model. *Journal of Biomechanics*, 39(6):1145–1152, 2006.

[193] R. Johnston and G. Smidt. Hip motion measurements for selected activities of daily living. *Clinical Orthopaedics and Related Research*, 72:205–215, 1970.

[194] B. Jolles, P. Zangger, and P. Leyvraz. Factors predisposing to dislocation after primary total hip arthroplasty: A multivariate analysis. *Journal of Arthroplasty*, 17(3):282–288, 2002.

[195] J. Julin, J. E., T. Puolakka, Y. Konttinen, and T. Moilanen. Younger age increases the risk of early prosthesis failure following primary total knee replacement for osteoarthritis. A follow-up study of 32,019 total knee replacements in the Finnish Arthroplasty Register. *Acta Orthopaedica*, 81(4):413–419, 2010.

[196] M. Kaehler, R. Rachholz, S. Herrmann, J. Zierath, R. Souffrant, D. Kluess, R. Bader, and C. Woernle. Model based dynamic analysis of total hip endoprostheses by means of hardware-in-the-loop simulation. In *Second Joint International Conference on Multibody System Dynamics*, Stuttgart, Germany, 2012.

[197] M. Kaehler, C. Woernle, and R. Bader. Hardware-in-the-loop-simulaton of constraint elements in mechanical systems. In A. Kecskeméthy and A. Müller, editors, *Computational Kinematics*, pages 159–166. Springer, Berlin, 2009.

[198] T. Kanamiya, L. Whiteside, T. Nakamura, W. Mihalko, J. Steiger, and M. Naito. Effect of selective lateral ligament release on stability in knee arthroplasty. *Clinical Orthopaedics and Related Research*, 404:24–31, 2002.

[199] K. Kaufman, K. An, W. Litchy, and E. Chao. Physiological prediction of muscle forces – I. Theoretical formulation. *Neuroscience*, 40(3):781–792, 1991.

[200] K. Kaufman, K. An, W. Litchy, and E. Chao. Physiological prediction of muscle forces – II. Application to isokinetic exercise. *Neuroscience*, 40(3):793–804, 1991.

[201] K. Kaufman, N. Kovacevic, S. Irby, and C. Colwell. Instrumented implant for measuring tibiofemoral forces. *Journal of Biomechanics*, 29(5):667–671, 1996.

[202] J. Kennedy, W. Rogers, K. Soffe, R. Sullivan, D. Griffen, and L. Sheehan. Effect of acetabular component orientation on recurrent dislocation, pelvic osteolysis, polyethylene wear, and component migration. *Journal of Arthroplasty*, 13(5):530–534, 1998.

[203] F. Kerschbaumer, G. Kerschbaumer, and F. Deghani. Is a dorsal access associated with an elevated luxation rate following total hip replacement? *Orthopade*, 36(10):928–934, 2007.

[204] O. Kessler, S. Patil, C. Colwell Jr., and D. D'Lima. The effect of femoral component malrotation on patellar biomechanics. *Journal of Biomechanics*, 41(16):3332–3339, 2008.

[205] M. Khan, P. Brakenbury, and I. Reynolds. Dislocation following total hip replacement. *Journal of Bone and Joint Surgery - Series B*, 63(2):214–218, 1981.

[206] M. Kia, A. Stylianou, and T. Guess. Evaluation of a musculoskeletal model with prosthetic knee through six experimental gait trials. *Medical Engineering & Physics*, 36(3):335–344, 2014.

[207] K. Kiguchi, T. Horie, A. Yamashita, M. Ueno, T. Kobayashi, M. Mawatari, and T. Hotokebuchi. A study of the effect of the femoral head diameter on prosthetic hip joint dislocation using a hip-joint motion simulator. In *31st Annual International Conference of the IEEE EMBS*, pages 6058–6061, Minneapolis, Minnesota, United States, 2009.

[208] K. Kiguchi, K. Tamura, Y. Hayashi, M. Ueno, T. Kobayashi, and M. Mawatari. Influence of origins and insertions of muscles on artificial hip joint dislocation. In *Proceedings*

of the IEEE-EMBS International Conference on Biomedical and Health Informatics, pages 555–558, Hong Kong and Shenzhen, China, 2012.

[209] K. Kiguchi, A. Yamashita, M. Sasaki, M. Ueno, T. Kobayashi, M. Mawatari, and T. Hotokebuchi. Control of an artificial-hip-joint simulator to evaluate dislocation. In *International Conference on Control, Automation and Systems*, pages 1942–1945, Seoul, Korea, 2008.

[210] H. Kim, J. Fernandez, M. Akbarshahi, J. Walter, B. Fregly, and M. Pandy. Evaluation of predicted knee-joint muscle forces during gait using an instrumented knee implant. *Journal of Orthopaedic Research*, 27(10):1326–1331, 2009.

[211] S.-S. Kim and W. Jeong. Real-time multibody vehicle model with bush compliance effect using quasi-static analysis for HILS. *Multibody System Dynamics*, 22(4):367–382, 2009.

[212] Y.-H. Kim, Y. Choi, and J. Kim. Influence of patient-, design-, and surgery-related factors on rate of dislocation after primary cementless total hip arthroplasty. *Journal of Arthroplasty*, 24(8):1258–1263, 2009.

[213] M. Klein Horsman, H. Koopman, F. van der Helm, L. Prose, and H. Veeger. Morphological muscle and joint parameters for musculoskeletal modelling of the lower extremity. *Clinical Biomechanics*, 22(2):239–247, 2007.

[214] C. Kliewe, R. Souffrant, D. Kluess, C. Woernle, K. Brökel, and R. Bader. Analytical computational model for the determination of the influence of design and surgical factors on the range of motion of total hip replacements. *Biomedical Engineering*, 55(1):47–55, 2010.

[215] D. Kluess, H. Martin, W. Mittelmeier, K. Schmitz, and R. Bader. Influence of femoral head size on impingement, dislocation and stress distribution in total hip replacement. *Medical Engineering & Physics*, 29(4):465–471, 2007.

[216] D. Kluess, R. Souffrant, W. Mittelmeier, A. Wree, K. Schmitz, and R. Bader. A convenient approach for finite-element-analyses of orthopaedic implants in bone contact: Modeling and experimental validation. *Computer Methods and Programs in Biomedicine*, 95(1):23–30, 2009.

[217] B. Ko and Y. Yoon. Optimal orientation of implanted components in total hip arthroplasty with polyethylene on metal articulation. *Clinical Biomechanics*, 23(8):996–1003, 2008.

[218] R. Komistek, M. Mahfouz, K. Bertin, A. Rosenberg, and W. Kennedy. In vivo determination of total knee arthroplasty kinematics. A multicenter analysis of an asymmetrical posterior cruciate retaining total knee arthroplasty. *Journal of Arthroplasty*, 23(1):41–50, 2008.

[219] C. König, A. Sharenkov, G. Matziolis, W. Taylor, C. Perka, G. Duda, and M. Heller. Joint line elevation in revision TKA leads to increased patellofemoral contact forces. *Journal of Orthopaedic Research*, 28(1):1–5, 2010.

[220] G. Kotzar, D. Davy, V. Goldberg, K. Heiple, J. Berilla, K. J. Heiple, R. Brown, and A. Burstein. Telemeterized in vivo hip joint force data: A report on two patients after total hip surgery. *Journal of Orthopaedic Research*, 9(5):621–633, 1991.

[221] K. Krackow. Instability in total knee arthroplasty: Loose as a goose. *Journal of Arthroplasty*, 18(3 Suppl. 1):45–47, 2003.

[222] S. Krein and E. Chao. Biomechanics of bipolar hip endoprostheses. *Journal of Orthopaedic Research*, 2(4):356–368, 1984.

[223] R. Krenn and B. Schäfer. Limitations of hardware-in-the-loop simulations of space robotics dynamics using industrial robots. In *Proceedings of the 5th International Symposium on Artificial Intelligence, Robotics and Automation in Space*, Noordwijk, The Netherlands, 1999.

[224] R. Krushell, D. Burke, and W. Harris. Elevated-rim acetabular components. Effect on range of motion and stability in total hip arthroplasty. *Journal of Arthroplasty*, 6(Suppl.):S53–S58, 1991.

[225] R. Krushell, D. Burke, and W. Harris. Range of motion in contemporary total hip arthroplasty. The impact of modular head-neck components. *Journal of Arthroplasty*, 6(2):97–101, 1991.

[226] F. Kummer, S. Shah, S. Iyer, and P. DiCesare. The effect of acetabular cup orientations on limiting hip rotation. *Journal of Arthroplasty*, 14(4):509–513, 1999.

[227] S. Kurtz, K. Ong, E. Lau, F. Mowat, and M. Halpern. Projections of primary and revision hip and knee arthroplasty in the United States from 2005 to 2030. *Journal of Bone and Joint Surgery - Series A*, 89(4):780–785, 2007.

[228] I. Kutzner, B. Heinlein, F. Graichen, A. Bender, A. Rohlmann, A. Halder, A. Beier, and G. Bergmann. Loading of the knee joint during activities of daily living measured in vivo in five subjects. *Journal of Biomechanics*, 43(11):2164–2173, 2010.

[229] M. Kwon, M. Kuskowski, K. Mulhall, W. Macaulay, T. Brown, and K. Saleh. Does surgical approach affect total hip arthroplasty dislocation rates? *Clinical Orthopaedics and Related Research*, 447:34–38, 2006.

[230] M. Lamontagne, M. Beaulieu, and P. Beaulé. Comparison of joint mechanics of both lower limbs of THA patients with healthy participants during stair ascent and descent. *Journal of Orthopaedic Research*, 29(3):305–311, 2011.

[231] M. Lamontagne, M. Beaulieu, D. Varin, and P. Beaulé. Lower-limb joint mechanics after total hip arthroplasty during sitting and standing tasks. *Journal of Orthopaedic Research*, 30(10):1611–1617, 2012.

[232] R. LaPrade, A. Engebretsen, T. Ly, S. Johansen, F. Wentorf, and L. Engebretsen. The anatomy of the medial part of the knee. *Journal of Bone and Joint Surgery - Series A*, 89(9):2000–2010, 2007.

[233] R. LaPrade, T. Ly, F. Wentorf, and L. Engebretsen. The posterolateral attachments of the knee. A qualitative and quantitative morphologic analysis of the fibular collateral ligament, popliteus tendon, popliteofibular ligament, and lateral gastrocnemius tendon. *American Journal of Sports Medicine*, 31(6):854–860, 2003.

[234] R. LaPrade, P. Morgan, F. Wentorf, S. Johansen, and L. Engebretsen. The anatomy of the posterior aspect of the knee: An anatomic study. *Journal of Bone and Joint Surgery - Series A*, 89(4):758–764, 2007.

[235] Y. Lee, J. Yoo, K. Koo, K. Yoon, and H. Kim. Metal neck and liner impingement in ceramic bearing total hip arthroplasty. *Journal of Orthopaedic Research*, 29(2):218–222, 2011.

[236] T. Lehmann, K. Schittkowski, and T. Spickenreuther. *MIQL: A Fortran Code for Convex Mixed-Integer Quadratic Programming – User's Guide*. Department of Computer Science, University of Bayreuth, 2009.

[237] S. Lehner. *Entwicklung und Validierung biomechanischer Computermodelle und deren Einsatz in der Sportwissenschaft*. PhD thesis, University of Koblenz-Landau, 2008.

[238] G. Lenaerts, W. Bartels, F. Gelaude, M. Mulier, A. Spaepen, G. Van der Perre, and I. Jonkers. Subject-specific hip geometry and hip joint centre location affects calculated contact forces at the hip during gait. *Journal of Biomechanics*, 42(9):1246–1251, 2009.

[239] G. Lenaerts, F. De Groote, B. Demeulenaere, M. Mulier, G. Van der Perre, A. Spaepen, and I. Jonkers. Subject-specific hip geometry affects predicted hip joint contact forces during gait. *Journal of Biomechanics*, 41(6):1243–1252, 2008.

[240] G. Lewinnek, J. Lewis, R. Tarr, C. Compere, and J. Zimmerman. Dislocations after total hip-replacement arthroplasties. *Journal of Bone and Joint Surgery - Series A*, 60(2):217–220, 1978.

[241] G. Li, J. Gil, A. Kanamori, and S.-Y. Woo. A validated three-dimensional computational model of a human knee joint. *Journal of Biomechanical Engineering*, 121(6):657–662, 1999.

[242] G. Li, E. Most, E. Otterberg, K. Sabbag, S. Zayontz, T. Johnson, and H. Rubash. Biomechanics of posterior-substituting total knee arthroplasty: An in vitro study. *Clinical Orthopaedics and Related Research*, 404:214–225, 2002.

[243] G. Li, R. Papannagari, E. Most, S. Park, T. Johnson, L. Tanamal, and H. Rubash. Anterior tibial post impingement in a posterior stabilized total knee arthroplasty. *Journal of Orthopaedic Research*, 23(3):536–541, 2005.

[244] G. Li, S. Zayontz, E. Most, E. Otterberg, K. Sabbag, and H. Rubash. Cruciate-retaining and cruciate-substituting total knee arthroplasty: An in vitro comparison of the kinematics under muscle loads. *Journal of Arthroplasty*, 16(8 Suppl. 1):150–156, 2001.

[245] R. Lieber and J. Fridén. Functional and clinical significance of skeletal muscle architecture. *Muscle & Nerve*, 23(11):1647–1666, 2000.

[246] Y. Lin, J. Walter, S. Banks, M. Pandy, and B. Fregly. Simultaneous prediction of muscle and contact forces in the knee during gait. *Journal of Biomechanics*, 43(5):945–952, 2010.

[247] J. Lipke, C. Janecki, C. Nelson, P. McLeod, C. Thompson, J. Thompson, and D. Haynes. The role of incompetence of the anterior cruciate and lateral ligaments in anterolateral and anteromedial instability. A biomechanical study of cadaver knees. *Journal of Bone and Joint Surgery - Series A*, 63(6):954–960, 1981.

[248] Y.-L. Liu, K.-J. Lin, C.-H. Huang, W.-C. Chen, C.-H. Chen, T.-W. Chang, Y.-S. Lai, and C.-K. Cheng. Anatomic-like polyethylene insert could improve knee kinematics after total knee arthroplasty – A computational assessment. *Clinical Biomechanics*, 26(6):612–619, 2011.

[249] T.-W. Lu, J. O'Connor, S. Taylor, and P. Walker. Validation of a lower limb model with in vivo femoral forces telemetered from two subjects. *Journal of Biomechanics*, 31(1):63–69, 1998.

[250] E. Luger, S. Sathasivam, and P. Walker. Inherent differences in the laxity and stability between the intact knee and total knee replacements. *Knee*, 4(1):7–14, 1997.

[251] O. Mahoney, P. Noble, D. Rhoads, J. Alexander, and H. Tullos. Posterior cruciate function following total knee arthroplasty: A biomechanical study. *Journal of Arthroplasty*, 9(6):569–578, 1994.

[252] L. Maletsky and B. Hillberry. Simulating dynamic activities using a five-axis knee simulator. *Journal of Biomechanical Engineering*, 127(1):123–133, 2005.

[253] D. Mandeville, L. Osternig, and L.-S. Chou. The effect of total knee replacement on dynamic support of the body during walking and stair ascent. *Clinical Biomechanics*, 22(7):787–794, 2007.

[254] S. Martelli, F. Taddei, A. Cappello, S. van Sint Jan, A. Leardini, and M. Viceconti. Effect of sub-optimal neuromotor control on the hip joint load during level walking. *Journal of Biomechanics*, 44(9):1716–1721, 2011.

[255] H. Martin, A. Savage, B. Braly, I. Palmer, D. Beall, and B. Kelly. The function of the hip capsular ligaments: A quantitative report. *Arthroscopy: The Journal of Arthroscopic and Related Surgery*, 24(2):188–195, 2008.

[256] J. Martin and L. Whiteside. The influence of joint line position on knee stability after condylar knee arthroplasty. *Clinical Orthopaedics and Related Research*, 259:146–156, 1990.

[257] S. Maruyama, S. Yoshiya, N. Matsui, R. Kuroda, and M. Kurosaka. Functional comparison of posterior cruciate-retaining versus posterior stabilized total knee arthroplasty. *Journal of Arthroplasty*, 19(3):349–353, 2004.

[258] M. Matsueda, T. Gengerke, M. Murphy, W. Lew, and R. Gustilo. Soft tissue release in total knee arthroplasty: Cadaver study using knees without deformities. *Clinical Orthopaedics and Related Research*, 366:264–273, 1999.

[259] M. Maynard, X. Deng, T. Wickiewicz, and R. Warren. The popliteofibular ligament: Rediscovery of a key element in posterolateral stability. *American Journal of Sports Medicine*, 24(3):311–316, 1996.

[260] J. McAuley and G. Engh. Constraint in total knee arthroplasty: When and what? *Journal of Arthroplasty*, 18(3 Suppl. 1):51–54, 2003.

[261] D. McCollum and W. Gray. Dislocation after total hip-arthroplasty – Causes and prevention. *Clinical Orthopaedics and Related Research*, 261:159–170, 1990.

[262] K. McGinnis, L. Snyder-Mackler, P. Flowers, and J. Zeni. Dynamic joint stiffness and co-contraction in subjects after total knee arthroplasty. *Clinical Biomechanics*, 28(2):205–210, 2013.

[263] J. Meding, E. Keating, M. Ritter, P. Faris, and M. Berend. Genu recurvatum in total knee replacement. *Clinical Orthopaedics and Related Research*, 416:64–67, 2003.

[264] A. Merican and A. Amis. Anatomy of the lateral retinaculum of the knee. *Journal of Bone and Joint Surgery - Series B*, 90(4):527–534, 2008.

[265] A. Merican, S. Sanghavi, F. Iranpour, and A. Amis. The structural properties of the lateral retinaculum and capsular complex of the knee. *Journal of Biomechanics*, 42(14):2323–2329, 2009.

[266] S. Metz-Schimmerl, G. Bhatia, and M. Vannier. Visualization and quantitative analysis of talocrural joint kinematics. *Computerized Medical Imaging and Graphics*, 18(6):443–448, 1994.

[267] J. Michael, K. Schlüter-Brust, and P. Eysel. Epidemiologie, Ätiologie, Diagnostik und Therapie der Gonarthrose. *Deutsches Ärzteblatt*, 107:152–161, 2010.

[268] W. Mihalko and L. Whiteside. Hip mechanics after posterior structure repair in total hip arthroplasty. *Clinical Orthopaedics and Related Research*, 420:194–198, 2004.

[269] Y. Mikashima, T. Tomatsu, M. Horikoshi, T. Nakatani, S. Saito, S. Momohara, and S. Banks. In vivo deep-flexion kinematics in patients with posterior-cruciate retaining and anterior-cruciate substituting total knee arthroplasty. *Clinical Biomechanics*, 25(1):83–87, 2010.

[270] Y. Minoda, T. Kadowaki, and M. Kim. Acetabular component orientation in 834 total hip arthroplasties using a manual technique. *Clinical Orthopaedics and Related Research*, 445:186–191, 2006.

[271] R. Mizner and L. Snyder-Mackler. Altered loading during walking and sit-to-stand is affected by quadriceps weakness after total knee arthroplasty. *Journal of Orthopaedic Research*, 23(5):1083–1090, 2005.

[272] L. Modenese, A. Gopalakrishnan, and A. Phillips. Application of a falsification strategy to a musculoskeletal model of the lower limb and accuracy of the predicted hip contact force vector. *Journal of Biomechanics*, 46(6):1193–1200, 2013.

[273] L. Modenese, A. Phillips, and A. Bull. An open source lower limb model: Hip joint validation. *Journal of Biomechanics*, 44(12):2185–2193, 2011.

[274] F. Moissenet, L. Chèze, and R. Dumas. A 3D lower limb musculoskeletal model for simultaneous estimation of musculo-tendon, joint contact, ligament and bone forces during gait. *Journal of Biomechanics*, 47(1):50–58, 2014.

[275] M. Moran, S. Bhimji, J. Racanelli, and S. Piazza. Computational assessment of constraint in total knee replacement. *Journal of Biomechanics*, 41(9):2013–2020, 2008.

[276] J. Moreland. Mechanisms of failure in total knee arthroplasty. *Clinical Orthopaedics and Related Research*, 226:49–64, 1988.

[277] H. Morgan, V. Battista, and S. Leopold. Constraint in primary total knee arthroplasty. *The Journal of the American Academy of Orthopaedic Surgeons*, 13(8):515–524, 2005.

[278] B. Morrey. Instability after total hip arthroplasty. *Orthopedic Clinics of North America*, 23(2):237–248, 1992.

[279] B. Morrey. Difficult complications after hip joint replacement. *Clinical Orthopaedics and Related Research*, 344:179–187, 1997.

[280] E. Most, S. Zayontz, G. Li, E. Otterberg, K. Sabbag, and H. Rubash. Femoral rollback after cruciate-retaining and stabilizing total knee arthroplasty. *Clinical Orthopaedics and Related Research*, 410:101–113, 2003.

[281] A. Mündermann, C. Dyrby, D. D'Lima, C. Colwell Jr., and T. Andriacchi. In vivo knee loading characteristics during activities of daily living as measured by an instrumented total knee replacement. *Journal of Orthopaedic Research*, 26(9):1167–1172, 2008.

[282] D. Murray. The definition and measurement of acetabular orientation. *Journal of Bone and Joint Surgery - Series B*, 75(2):228–232, 1993.

[283] M. Nadzadi, D. Pedersen, J. Callaghan, and T. Brown. Effects of acetabular component orientation on dislocation propensity for small-head-size total hip arthroplasty. *Clinical Biomechanics*, 17(1):32–40, 2002.

[284] M. Nadzadi, D. Pedersen, H. Yack, J. Callaghan, and T. Brown. Kinematics, kinetics, and finite element analysis of commonplace maneuvers at risk for total hip dislocation. *Journal of Biomechanics*, 36(4):577–591, 2003.

[285] R. Nagamine, S. White, D. McCarthy, and L. Whiteside. Effect of rotational malposition of the femoral component on knee stability kinematics after total knee arthroplasty. *Journal of Arthroplasty*, 10(3):265–270, 1995.

[286] H. Nägerl, D. Kubein-Meesenburg, H. Cotta, and J. Fanghanel. Biomechanische Prinzipien in Diarthrosen und Synarthrosen. Teil III: Mechanik des Tibiofemoralgelenkes und Rolle der Kreuzbänder. *Zeitschrift fur Orthopädie und Ihre Grenzgebiete*, 131(5):385–396, 1993.

[287] National Joint Registry for England, Wales and Northern Ireland, Hertfordshire, England. *5th Annual Report*, 2008.

[288] National Joint Registry for England, Wales and Northern Ireland, Hertfordshire, England. *10th Annual Report*, 2013.

[289] V. Ngai, T. Schwenke, and M. Wimmer. In-vivo kinematics of knee prostheses patients during level walking compared with the ISO force-controlled simulator standard. *Proceedings of the Institution of Mechanical Engineers, Part H: Journal of Engineering in Medicine*, 223(7):889–896, 2009.

[290] V. Ngai and M. Wimmer. Kinematic evaluation of cruciate-retaining total knee replacement patients during level walking: A comparison with the displacement-controlled ISO standard. *Journal of Biomechanics*, 42(14):2363–2368, 2009.

[291] R. Nicholas, J. Orr, R. Mollan, J. Calderwood, J. Nixon, and P. Watson. Dislocation of total hip replacements. A comparative study of standard, long posterior wall and augmented acetabular components. *Journal of Bone and Joint Surgery - Series B*, 72(3):418–422, 1990.

[292] R. Nicholls, A. Schirm, B. Jeffcote, and M. Kuster. Tibiofemoral force following total knee arthroplasty: Comparison of four prosthesis designs in vitro. *Journal of Orthopaedic Research*, 25(11):1506–1512, 2007.

[293] A. Nikooyan, H. Veeger, P. Westerhoff, F. Graichen, G. Bergmann, and F. van der Helm. Validation of the Delft Shoulder and Elbow Model using in-vivo glenohumeral joint contact forces. *Journal of Biomechanics*, 43(15):3007–3014, 2010.

[294] E. Nomura, Y. Horiuchi, and M. Kihara. Medial patellofemoral ligament restraint in lateral patellar translation and reconstruction. *Knee*, 7(2):121–127, 2000.

[295] S. Ostermeier, M. Bohnsack, C. Hurschler, and C. Stukenborg-Colsman. A rotating inlay decreases contact pressure on inlay post after posterior cruciate substituting total knee arthroplasty. *Clinical Biomechanics*, 24(5):446–450, 2009.

[296] S. Ostermeier, C. Hurschler, and C. Stukenborg-Colsman. Quadriceps function after TKA – An in vitro study in a knee kinematic simulator. *Clinical Biomechanics*, 19(3):270–276, 2004.

[297] S. Ostermeier, C. Schlomach, C. Hurschler, H. Windhagen, and C. Stukenborg-Colsman. Dynamic in vitro measurement of posterior cruciate ligament load and tibiofemoral stress after TKA in dependence on tibiofemoral slope. *Clinical Biomechanics*, 21(5):525–532, 2006.

[298] M. Pagnano, A. Hanssen, D. Lewallen, and M. Stuart. Flexion instability after primary posterior cruciate retaining total knee arthroplasty. *Clinical Orthopaedics and Related Research*, 356:39–46, 1998.

[299] S. Parratte and M. Pagnano. Instability after total knee arthroplasty. *Journal of Bone and Joint Surgery - Series A*, 90(1):184–194, 2008.

[300] S. Paterno, P. Lachiewicz, and S. Kelley. The influence of patient-related factors and the position of the acetabular component on the rate of dislocation after total hip replacement. *Journal of Bone and Joint Surgery - Series A*, 79(8):1202–1210, 1997.

[301] A. Patriarco, R. Mann, S. Simon, and J. Mansour. An evaluation of the approaches of optimization models in the prediction of muscle forces during human gait. *Journal of Biomechanics*, 14(8):513–525, 1981.

[302] D. Pedersen, R. Brand, C. Cheng, and J. Arora. Direct comparison of muscle force predictions using linear and nonlinear programming. *Journal of Biomechanical Engineering*, 109(3):192–199, 1987.

[303] D. Pedersen, R. Brand, and D. Davy. Pelvic muscle and acetabular contact forces during gait. *Journal of Biomechanics*, 30(9):959–965, 1997.

[304] D. Pedersen, J. Callaghan, and T. Brown. Activity-dependence of the "safe zone" for impingement versus dislocation avoidance. *Medical Engineering & Physics*, 27(4):323–328, 2005.

[305] A. Pedotti, V. Krishnan, and L. Stark. Optimization of muscle-force sequencing in human locomotion. *Mathematical Biosciences*, 38(1-2):57–76, 1978.

[306] P. Pellicci, M. Bostrom, and R. Poss. Posterior approach to total hip replacement using enhanced posterior soft tissue repair. *Clinical Orthopaedics and Related Research*, 355:224–228, 1998.

[307] D. Penrod, D. Davy, and D. Singh. An optimization approach to tendon force analysis. *Journal of Biomechanics*, 7(2):123–129, 1974.

[308] C. Perka, F. Haschke, and S. Tohtz. Dislocation after total hip arthroplasty. *Zeitschrift für Orthopädie und Unfallchirurgie*, 150(2):e89–e103, 2012.

[309] W. Petersen, S. Loerch, S. Schanz, M. Raschke, and T. Zantop. The role of the posterior oblique ligament in controlling posterior tibial translation in the posterior

cruciate ligament-deficient knee. *American Journal of Sports Medicine*, 36(3):495–501, 2008.

[310] S. Pianigiani, Y. Chevalier, L. Labey, V. Pascale, and B. Innocenti. Tibio-femoral kinematics in different total knee arthroplasty designs during a loaded squat: A numerical sensitivity study. *Journal of Biomechanics*, 45(13):2315–2323, 2012.

[311] S. Piazza and S. Delp. Three-dimensional dynamic simulation of total knee replacement motion during a step-up task. *Journal of Biomechanical Engineering*, 123(6):599–606, 2001.

[312] S. Piazza, S. Delp, S. Stulberg, and S. Stern. Posterior tilting of the tibial component decreases femoral rollback in posterior-substituting knee replacement: A computer simulation study. *Journal of Orthopaedic Research*, 16(2):264–270, 1998.

[313] M. Pietsch and S. Hofmann. From tibiofemoral instability to dislocation in total knee arthroplasty. *Orthopade*, 36(10):917–927, 2007.

[314] V. Pinskerova, P. Johal, S. Nakagawa, A. Sosna, A. Williams, W. Gedroyc, and M. Freeman. Does the femur roll-back with flexion? *Journal of Bone and Joint Surgery - Series B*, 86(6):925–931, 2004.

[315] J. Prudhon, A. Ferreira, and R. Verdier. Dual mobility cup: Dislocation rate and survivorship at ten years of follow-up. *International Orthopaedics*, 37(12):2345–2350, 2013.

[316] R. Raikova. About weight factors in the non-linear objective functions used for solving indeterminate problems in biomechanics. *Journal of Biomechanics*, 32(7):689–694, 1999.

[317] R. Raikova and B. Prilutsky. Sensitivity of predicted muscle forces to parameters of the optimization-based human leg model revealed by analytical and numerical analyses. *Journal of Biomechanics*, 34(10):1243–1255, 2001.

[318] J. Rasmussen, M. Damsgaard, and M. Voigt. Muscle recruitment by the min/max criterion – A comparative numerical study. *Journal of Biomechanics*, 34(3):409–415, 2001.

[319] D. Rhoads, P. Noble, J. Reuben, O. Mahoney, and H. Tullos. The effect of femoral component position on patellar tracking after total knee arthroplasty. *Clinical Orthopaedics and Related Research*, 260:43–51, 1990.

[320] D. Rhoads, P. Noble, J. Reuben, and H. Tullos. The effect of femoral component position on the kinematics of total knee arthroplasty. *Clinical Orthopaedics and Related Research*, 286:122–129, 1993.

[321] J. Ritchie and D. Wilkie. The dynamics of muscular contraction. *The Journal of Physiology*, 143(1):104–113, 1958.

[322] G. Robbins, B. Masri, D. Garbuz, and C. Duncan. Preoperative planning to prevent instability in total knee arthroplasty. *Orthopedic Clinics of North America*, 32(4):611–626, 2001.

[323] G. Robbins, B. Masri, D. Garbuz, N. Greidanus, and C. Duncan. Treatment of hip instability. *Orthopedic Clinics of North America*, 32(4):593–610, 2001.

[324] D. Roberts, H. Khan, J. Kim, J. Slover, and P. Walker. Acceleration-based joint stability parameters for total knee arthroplasty that correspond with patient-reported instability. *Proceedings of the Institution of Mechanical Engineers, Part H: Journal of Engineering in Medicine*, 227(10):1104–1113, 2013.

[325] J. Robinson, A. Bull, R. Thomas, and A. Amis. The role of the medial collateral ligament and posteromedial capsule in controlling knee laxity. *American Journal of Sports Medicine*, 34(11):1815–1823, 2006.

[326] R. Robinson, H. Robinson, and E. Salvati. Comparison of the transtrochanteric and posterior approaches for total hip replacement. *Clinical Orthopaedics and Related Research*, 147:143–147, 1980.

[327] E. Rodriguez-Merchan. Instability following total knee arthroplasty. *HSS Journal*, 7(3):273–278, 2011.

[328] H. Röhrle, R. Scholten, C. Sigolotto, W. Sollbach, and H. Kellner. Joint forces in the human pelvis leg skeleton during walking. *Journal of Biomechanics*, 17(6):409–424, 1984.

[329] T. Rudy, G. Livesay, S. Woo, and F. Fu. A combined robotic/universal force sensor approach to determine in situ forces of knee ligaments. *Journal of Biomechancis*, 29(10):1357–1360, 1996.

[330] W. Rulka. SIMPACK – A computer program for simulation of large-motion multibody systems. In W. Schiehlen, editor, *Multibody Systems Handbook*, pages 265–284. Springer, Berlin, 1990.

[331] W. Rulka and E. Pankiewicz. MBS approach to generate equations of motions for HiL-simulations in vehicle dynamics. *Multibody System Dynamics*, 14(3–4):367–386, 2005.

[332] N. Rydell. Forces acting on the femoral head-prosthesis. A study on strain gauge supplied prostheses in living persons. *Acta Orthopaedica Scandinavica*, 37(Suppl. 88):1–132, 1966.

[333] K. Saeki, W. Mihalko, V. Patel, J. Conway, M. Naito, H. Thrum, H. Vandenneuker, and L. Whiteside. Stability after medial collateral ligament release in total knee arthroplasty. *Clinical Orthopaedics and Related Research*, 392:184–189, 2001.

[334] M. Sakane, G. Livesay, R. Fox, T. Rudy, T. Runco, and S.-Y. Woo. Relative contribution of the ACL, MCL, and bony contact to the anterior stability of the knee. *Knee Surgery, Sports Traumatology, Arthroscopy*, 7(3):93–97, 1999.

[335] J. Sanchez-Sotelo and D. Berry. Epidemiology of instability after total hip replacement. *Orthopedic Clinics of North America*, 32(4):543–552, 2001.

[336] M. Scheibel, M. Thomas, and G. von Salis-Soglio. Surgical approaches for primary endoprosthesis of the knee joint. *Orthopade*, 31(9):934–946, 2002.

[337] W. Schiehlen. Multibody system dynamics: Roots and perspectives. *Multibody System Dynamics*, 1(2):149–188, 1997.

[338] W. Schiehlen. Computational dynamics: Theory and applications of multibody systems. *European Journal of Mechanics, A/Solids*, 25(4):566–594, 2006.

[339] W. Schiehlen and P. Eberhard. *Technische Dynamik: Modelle für Regelung und Simulation*. Vieweg & Teubner, Stuttgart, 2004.

[340] W. Schroer, K. Berend, A. Lombardi, C. Barnes, M. Bolognesi, M. Berend, M. Ritter, and R. Nunley. Why are total knees failing today? Etiology of total knee revision in 2010 and 2011. *Journal of Arthroplasty*, 28(Suppl. 1):116–119, 2013.

[341] M. Schuenke, E. Schulte, and U. Schumacher. *Thieme Atlas of Anatomy: General Anatomy and Musculoskeletal System*. Thieme, New York, 2005.

[342] J. Schwab, G. Haidukewych, A. Hanssen, D. Jacofsky, and M. Pagnano. Flexion instability without dislocation after posterior stabilized total knees. *Clinical Orthopaedics and Related Research*, 440:96–100, 2005.

[343] C. Scifert, T. Brown, and J. Lipman. Finite element analysis of a novel design approach to resisting total hip dislocation. *Clinical Biomechanics*, 14(10):697–703, 1999.

[344] C. Scifert, T. Brown, D. Pedersen, and J. Callaghan. A finite element analysis of factors influencing total hip dislocation. *Clinical Orthopaedics and Related Research*, 355:152–162, 1998.

[345] C. Scifert, P. Noble, T. Brown, R. Bartz, N. Kadakia, N. Sugano, R. Johnston, D. Pedersen, and J. Callaghan. Experimental and computational simulation of total hip arthroplasty dislocation. *Orthopedic Clinics of North America*, 32(4):553–567, 2001.

[346] A. Seireg and R. Arvikar. Mathematical-model for evaluation of forces in lower extremities of musculoskeletal system. *Journal of Biomechanics*, 6(3):313–326, 1973.

[347] A. Seireg and R. Arvikar. The prediction of muscular load sharing and joint forces in the lower extremities during walking. *Journal of Biomechanics*, 8(2):89–102, 1975.

[348] P. Sharkey, W. Hozack, R. Booth Jr., R. Balderston, and R. Rothman. Posterior dislocation of total knee arthroplasty. *Clinical Orthopaedics and Related Research*, 278:128–133, 1992.

[349] A. Sharma, F. Leszko, R. Komistek, G. Scuderi, H. Cates Jr., and F. Liu. In vivo patellofemoral forces in high flexion total knee arthroplasty. *Journal of Biomechanics*, 41(3):642–648, 2008.

[350] K. Shelburne, M. Torry, and M. Pandy. Contributions of muscles, ligaments, and the ground-reaction force to tibiofemoral joint loading during normal gait. *Journal of Orthopaedic Research*, 24(10):1983–1990, 2006.

[351] W. Shon, T. Baldini, M. Peterson, T. Wright, and E. Salvati. Impingement in total hip arthroplasty. A study of retrieved acetabular components. *Journal of Arthroplasty*, 20(4):427–435, 2005.

[352] B. Siciliano, L. Sciavicco, L. Villani, and G. Oriolo. *Robotics: Modelling, Planning and Control*. Springer, Berlin, 2008.

[353] R. Sierra, J. Raposo, R. Trousdale, and M. Cabanela. Dislocation of primary THA done through a posterolateral approach in the elderly. *Clinical Orthopaedics and Related Research*, 441:262–267, 2005.

[354] G. Singh, H. Meyer, M. Ruetschi, K. Chamaon, B. Feuerstein, and C. Lohmann. Large-diameter metal-on-metal total hip arthroplasties: A page in orthopedic history? *Journal of Biomedical Materials Research Part A*, 101(11):3320–3326, 2013.

[355] W. Sioen, J. Simon, L. Labey, and R. Van Audekercke. Posterior transosseous capsulotendinous repair in total hip arthroplasty: A cadaver study. *Journal of Bone and Joint Surgery - Series A*, 84(10):1793–1798, 2002.

[356] S. Song, R. Detch, W. Maloney, S. Goodman, and J. Huddleston. Causes of instability after total knee arthroplasty. *Journal of Arthroplasty*, 29(2):360–364, 2014.

[357] V. Spitzer, M. Ackerman, A. Scherzinger, and D. Whitlock. The visible human male: A technical report. *Journal of the American Medical Informatics Association*, 3(2):118–130, 1996.

[358] B. Stansfield, A. Nicol, J. Paul, I. Kelly, F. Graichen, and G. Bergmann. Direct comparison of calculated hip joint contact forces with those measured using instrumented implants. An evaluation of a three-dimensional mathematical model of the lower limb. *Journal of Biomechanics*, 36(7):929–936, 2003.

[359] Statistisches Bundesamt, Wiesbaden, Germany. *Fallpauschalenbezogene Krankenhausstatistik (DRG-Statistik) – Operationen und Prozeduren der vollstationären Patientinnen und Patienten der Krankenhäuser 2007*, 2009.

[360] Statistisches Bundesamt, Wiesbaden, Germany. *Fallpauschalenbezogene Krankenhausstatistik (DRG-Statistik) – Operationen und Prozeduren der vollstationären Patientinnen und Patienten der Krankenhäuser 2008*, 2009.

[361] Statistisches Bundesamt, Wiesbaden, Germany. *Fallpauschalenbezogene Krankenhausstatistik (DRG-Statistik) – Operationen und Prozeduren der vollstationären Patientinnen und Patienten der Krankenhäuser 2009*, 2010.

[362] Statistisches Bundesamt, Wiesbaden, Germany. *Fallpauschalenbezogene Krankenhausstatistik (DRG-Statistik) – Operationen und Prozeduren der vollstationären Patientinnen und Patienten der Krankenhäuser 2010*, 2011.

[363] Statistisches Bundesamt, Wiesbaden, Germany. *Fallpauschalenbezogene Krankenhausstatistik (DRG-Statistik) – Operationen und Prozeduren der vollstationären Patientinnen und Patienten der Krankenhäuser 2011*, 2012.

[364] Statistisches Bundesamt, Wiesbaden, Germany. *Fallpauschalenbezogene Krankenhausstatistik (DRG-Statistik) – Operationen und Prozeduren der vollstationären Patientinnen und Patienten der Krankenhäuser 2012*, 2013.

[365] K. Stewart, R. Edmonds-Wilson, R. Brand, and T. Brown. Spatial distribution of hip capsule structural and material properties. *Journal of Biomechanics*, 35(11):1491–1498, 2002.

[366] J. Stiehl, D. Dennis, R. Komistek, and H. Crane. In vivo determination of condylar lift-off and screw-home in a mobile-bearing total knee arthroplasty. *Journal of Arthroplasty*, 14(3):293–299, 1999.

[367] J. Stiehl, D. Dennis, R. Komistek, and P. Keblish. In vivo kinematic analysis of a mobile bearing total knee prosthesis. *Clinical Orthopaedics and Related Research*, 345:60–66, 1997.

[368] J. Stiehl, R. Komistek, D. Dennis, R. Paxson, and W. Hoff. Fluroscopic analysis of kinematics after posterior-cruciate-retaining knee arthroplasty. *Journal of Bone and Joint Surgery - Series B*, 77(6):884–889, 1995.

[369] J. Stoddard, D. Deehan, A. Bull, A. McCaskie, and A. Amis. The kinematics and stability of single-radius versus multi-radius femoral components related to mid-range instability after TKA. *Journal of Orthopaedic Research*, 31(1):53–58, 2013.

[370] C. Stukenborg-Colsman, S. Ostermeier, K. Wenger, and C. Wirth. Relative motion of a mobile bearing inlay after total knee arthroplast – Dynamic in vitro study. *Clinical Biomechanics*, 17(1):49–55, 2002.

[371] F.-C. Su, K. Lai, and W. Hong. Rising from chair after total knee arthroplasty. *Clinical Biomechanics*, 13(3):176–181, 1998.

[372] D. Sullivan, M. Levey, and S. Sheskier. Medial restraints to anterior-posterior motion of the knee. *Journal of Bone and Joint Surgery - Series A*, 66(6):930–936, 1984.

[373] Swedish Hip Arthroplasty Register, Goteborg, Sweden. *Annual Report 2010*, 2011.

[374] Swedish Hip Arthroplasty Register, Goteborg, Sweden. *Annual Report 2011*, 2012.

[375] Swedish Knee Arthroplasty Register, Lund, Sweden. *Annual Report 2012*, 2012.

[376] S. Taylor and P. Walker. Forces and moments telemetered from two distal femoral replacements during various activities. *Journal of Biomechanics*, 34(7):839–848, 2001.

[377] S. Taylor, P. Walker, J. Perry, S. Cannon, and R. Woledge. The forces in the distal femur and the knee during walking and other activities measured by telemetry. *Journal of Arthroplasty*, 13(4):428–435, 1998.

[378] W. Taylor, M. Heller, G. Bergmann, and G. Duda. Tibio-femoral loading during human gait and stair climbing. *Journal of Orthopaedic Research*, 22(3):625–632, 2004.

[379] W. Taylor, E. Roland, H. Ploeg, D. Hertig, R. Klabunde, M. Warner, M. Hobatho, L. Rakotomanana, and S. Clift. Determination of orthotropic bone elastic constants using FEA and modal analysis. *Journal of Biomechanics*, 35(6):767–773, 2002.

[380] G. Terry, J. Hughston, and L. Norwood. The anatomy of the iliopatellar band and iliotibial tract. *American Journal of Sports Medicine*, 14(1):39–45, 1986.

[381] D. Thelen, K. Choi, and A. Schmitz. Co-simulation of neuromuscular dynamics and knee mechanics during human walking. *Journal of Biomechanical Engineering*, 136(2):021033, 2014.

[382] J. Thompson, M. Hast, J. Granger, S. Piazza, and R. Siston. Biomechanical effects of total knee arthroplasty component malrotation: A computational simulation. *Journal of Orthopaedic Research*, 29(7):969–975, 2011.

[383] N. Thompson, D. Wilson, G. Cran, D. Beverland, and J. Stiehl. Dislocation of the rotating platform after low contact stress total knee arthroplasty. *Clinical Orthopaedics and Related Research*, 425:207–211, 2004.

[384] A. Trepczynski, I. Kutzner, E. Kornaropoulos, W. Taylor, G. Duda, G. Bergmann, and M. Heller. Patellofemoral joint contact forces during activities with high knee flexion. *Journal of Orthopaedic Research*, 30(3):408–415, 2012.

[385] D. Tsirakos, V. Baltzopoulos, and R. Bartlett. Inverse optimization: Functional and physiological considerations related to the force-sharing problem. *Critical Reviews in Biomedical Engineering*, 25(4-5):371–407, 1997.

[386] F. van der Helm and R. Veenbaas. Modelling the mechanical effect of muscles with large attachment sites: Application to the shoulder mechanism. *Journal of Biomechanics*, 24(12):1151–1163, 1991.

[387] A. van Kampen and R. Husikes. The three-dimensional tracking pattern of the human patella. *Journal of Orthopaedic Research*, 8(3):372–382, 1990.

[388] K. Varadarajan, A. Moynihan, D. D'Lima, C. Colwell Jr., and G. Li. In vivo contact kinematics and contact forces of the knee after total knee arthroplasty during dynamic weight-bearing activities. *Journal of Biomechanics*, 41(10):2159–2168, 2008.

[389] C. Vaughan, J. Hay, and J. Andrews. Closed loop problems in biomechanics. Part I – A classification system. *Journal of Biomechanics*, 15(3):197–200, 1982.

[390] C. Vaughan, J. Hay, and J. Andrews. Closed loop problems in biomechanics. Part II – An optimization approach. *Journal of Biomechanics*, 15(3):201–220, 1982.

[391] D. Veltri, X.-H. Deng, P. Torzilli, M. Maynard, and R. Warren. The role of the popliteofibular ligament in stability of the human knee: A biomechanical study. *American Journal of Sports Medicine*, 24(1):19–27, 1996.

[392] A. Vicar and C. Coleman. A comparison of the anterolateral, transtrochanteric, and posterior surgical approaches in primary total hip arthroplasty. *Clinical Orthopaedics and Related Research*, 188:152–159, 1984.

[393] K. Vince, A. Abdeen, and T. Sugimori. The unstable total knee arthroplasty. Causes and cures. *Journal of Arthroplasty*, 21(4 Suppl. 1):44–49, 2006.

[394] D. von Torklus and T. Nicola. *Atlas orthopädisch-chirurgischer Operationsschnitte und Zugangswege*. Urban & Schwarzenberg, München, 1985.

[395] M. Vrahas, R. Brand, T. Brown, and J. Andrews. Contribution of passive tissues to the intersegmental moments at the hip. *Journal of Biomechanics*, 23(4):357–362, 1990.

[396] F. Wagner, J. Negrão, J. Campos, S. Ward, P. Haghighi, D. Trudell, and D. Resnick. Capsular ligaments of the hip: Anatomic, histologic, and positional study in cadaveric specimens with MR arthrography. *Radiology*, 263(1):189–198, 2012.

[397] P. Walker, G. Blunn, D. Broome, J. Perry, A. Watkins, S. Sathasivam, M. Dewar, and J. Paul. A knee simulating machine for performance evaluation of total knee replacements. *Journal of Biomechanics*, 30(1):83–89, 1997.

[398] P. Walker, M. Lowry, and A. Kumar. The effect of geometric variations in posterior-stabilized knee designs on motion characteristics measured in a knee loading machine knee. *Clinical Orthopaedics and Related Research*, 472(1):238–247, 2014.

[399] S. Ward, C. Eng, L. Smallwood, and R. Lieber. Are current measurements of lower extremity muscle architecture accurate? *Clinical Orthopaedics and Related Research*, 467(4):1074–1082, 2009.

[400] S. Ward and R. Lieber. Density and hydration of fresh and fixed human skeletal muscle. *Journal of Biomechanics*, 38(11):2317–2320, 2005.

[401] W. Ward, D. Haight, P. Ritchie, S. Gordon, and J. Eckardt. Dislocation of rotating hinge total knee prostheses. A biomechanical analysis. *Journal of Bone and Joint Surgery - Series A*, 85(3):448–453, 2003.

[402] W. Ward, D. Haight, P. Ritchie, S. Gordon, and J. Eckardt. Dislocation of rotating hinge knee prostheses: A report of four cases. *Journal of Bone and Joint Surgery - Series A*, 87(5):1108–1112, 2005.

[403] G. Waslewski, B. Marson, and J. Benjamin. Early, incapacitating instability of posterior cruciate ligament-retaining total knee arthroplasty. *Journal of Arthroplasty*, 13(7):763–767, 1998.

[404] T. Watanabe, T. Yamazaki, K. Sugamoto, T. Tomita, H. Hashimoto, D. Maeda, S. Tamura, T. Ochi, and H. Yoshikawa. In vivo kinematics of mobile-bearing knee arthroplasty in deep knee bending motion. *Journal of Orthopaedic Research*, 22(5):1044–1049, 2004.

[405] Y. Watanabe, H. Moriya, K. Takahashi, M. Yamagata, M. Sonoda, Y. Shimada, and T. Tamaki. Functional anatomy of the posterolateral structures of the knee. *Journal of Arthroscopic and Related Surgery*, 9(1):57–62, 1993.

[406] F. Werner, D. Ayers, L. Maletsky, and P. Rullkoetter. The effect of valgus/varus malalignment on load distribution in total knee replacements. *Journal of Biomechanics*, 38(2):349–355, 2005.

[407] R. White, T. Forness, J. Allman, and D. Junick. Effect of posterior capsular repair on early dislocation in primary total hip replacement. *Clinical Orthopaedics and Related Research*, 393:163–167, 2001.

[408] L. Whiteside and D. Amador. The effect of posterior tibial slope on knee stability after Ortholoc total knee arthroplasty. *Journal of Arthroplasty*, 3(Suppl.):S51–S57, 1988.

[409] L. Whiteside and D. Amador. Rotational stability of a posterior stabilized total knee arthroplasty. *Clinical Orthopaedics and Related Research*, 242:241–246, 1989.

[410] L. Whiteside, M. Kasselt, and D. Haynes. Varus-valgus and rotational stability in rotationally unconstrained total knee arthroplasty. *Clinical Orthopaedics and Related Research*, 219:147–157, 1987.

[411] L. Whiteside, K. Saeki, and W. Mihalko. Functional medial ligament balancing in total knee arthroplasty. *Clinical Orthopaedics and Related Research*, 380:45–57, 2000.

[412] T. Wickiewicz, R. Roy, P. Powell, and V. Edgerton. Muscle architecture of the human lower limb. *Clinical Orthopaedics and Related Research*, 179:275–283, 1983.

[413] K. Widmer and M. Majewski. The impact of the CCD-angle on range of motion and cup positioning in total hip arthroplasty. *Clinical Biomechanics*, 20(7):723–728, 2005.

[414] K. Widmer and B. Zurfluh. Compliant positioning of total hip components for optimal range of motion. *Journal of Orthopaedic Research*, 22(4):815–821, 2004.

[415] D. Wilkie. The mechanical properties of muscle. *British Medical Bulletin*, 12(3):177–182, 1956.

[416] R. Willing and I. Kim. Design optimization of a total knee replacement for improved constraint and flexion kinematics. *Journal of Biomechanics*, 44(6):1014–1020, 2011.

[417] C. Winby, D. Lloyd, T. Besier, and T. Kirk. Muscle and external load contribution to knee joint contact loads during normal gait. *Journal of Biomechanics*, 42(14):2294–2300, 2009.

[418] D. Winter. *Biomechanics and motor control of human movement*. John Wiley & Sons, New York, 1990.

[419] J. Winters and L. Stark. Muscle models: What is gained and what is lost by varying model complexity. *Biological Cybernetics*, 55(6):403–420, 1987.

[420] C. Woernle. *Mehrkörpersysteme: Eine Einführung in die Kinematik und Dynamik von Systemen starrer Körper*. Springer, Heidelberg, 2011.

[421] A. Wolf, A. DiGioia, A. Mor, and B. Jaramaz. A kinematic model for calculating cup alignment error during total hip arthroplasty. *Journal of Biomechanics*, 38(11):2257–2265, 2005.

[422] S. Woolson and Z. Rahimtoola. Risk factors for dislocation during the first 3 months after primary total hip replacement. *Journal of Arthroplasty*, 14(6):662–668, 1999.

[423] G. Wu and P. Cavanagh. ISB recommendations for standardization in the reporting of kinematic data. *Journal of Biomechanics*, 28(10):1257–1260, 1995.

[424] G. Wu, S. Siegler, P. Allard, C. Kirtley, A. Leardini, D. Rosenbaum, M. Whittle, D. D'Lima, L. Cristofolini, H. Witte, O. Schmid, and H. Stokes. ISB recommendation on definitions of joint coordinate system of various joints for the reporting of human joint motion – Part I: Ankle, hip, and spine. *Journal of Biomechanics*, 35(4):543–548, 2002.

[425] G. Wu, F. van der Helm, H. Veeger, M. Makhsous, P. Van Roy, C. Anglin, J. Nagels, A. Karduna, K. McQuade, X. Wang, F. Werner, and B. Buchholz. ISB recommendation on definitions of joint coordinate systems of various joints for the reporting of human joint motion – Part II: Shoulder, elbow, wrist and hand. *Journal of Biomechanics*, 38(5):981–992, 2005.

[426] Y. Yamamoto, W.-H. Hsu, J. Fisk, A. Van Scyoc, K. Miura, and S.-Y. Woo. Effect of the iliotibial band on knee biomechanics during a simulated pivot shift test. *Journal of Orthopaedic Research*, 24(5):967–973, 2006.

[427] H. Yercan, T. Ait Si Selmi, T. Sugun, and P. Neyret. Tibiofemoral instability in primary total knee replacement: A review, Part 1: Basic principles and classification. *Knee*, 12(4):257–266, 2005.

[428] H. Yercan, T. Selmi, T. Sugun, and P. Neyret. Tibiofemoral instability in primary total knee replacement: A review, Part 2: Diagnosis, patient evaluation, and treatment. *Knee*, 12(5):336–340, 2005.

[429] G. Yildirim, P. Walker, and J. Boyer. Total knees designed for normal kinematics evaluated in an up-and-down crouching machine. *Journal of Orthopaedic Research*, 27(8):1022–1027, 2009.

[430] Y. Yoon, A. Hodgson, J. Tonetti, B. Masri, and C. Duncan. Resolving inconsistencies in defining the target orientation for the acetabular cup angles in total hip arthroplasty. *Clinical Biomechanics*, 23(3):253–259, 2008.

[431] F. Yoshimine. The influence of the oscillation angle and the neck anteversion of the prosthesis on the cup safe-zone that fulfills the criteria for range of motion in total hip replacements. The required oscillation angle for an acceptable cup safe-zone. *Journal of Biomechanics*, 38(1):125–132, 2005.

[432] F. Yoshimine. The safe-zones for combined cup and neck anteversions that fulfill the essential range of motion and their optimum combination in total hip replacements. *Journal of Biomechanics*, 39(7):1315–1323, 2006.

[433] C.-H. Yu, P. Walker, and M. Dewar. The effect of design variables of condylar total knees on the joint forces in step climbing based on a computer model. *Journal of Biomechanics*, 34(8):1011–1021, 2001.

[434] F. Zajac. Muscle and tendon – Properties, models, scaling, and application to biomechanics and motor control. *Critical Reviews in Biomedical Engineering*, 17(4):359–411, 1989.

[435] A. Zavatsky. A kinematic-freedom analysis of a flexed-knee-stance testing rig. *Journal of Biomechanics*, 30(3):277–280, 1997.

[436] J. Zelle, P. Heesterbeek, M. De Waal Malefijt, and N. Verdonschot. Numerical analysis of variations in posterior cruciate ligament properties and balancing techniques on total knee arthroplasty loading. *Medical Engineering & Physics*, 32(7):700–707, 2010.

[437] J. Zelle, A. Van der Zanden, M. De Waal Malefijt, and N. Verdonschot. Biomechanical analysis of posterior cruciate ligament retaining high-flexion total knee arthroplasty. *Clinical Biomechanics*, 24(10):842–849, 2009.

[438] D. Zhao, S. Banks, D. D'Lima, C. Colwell Jr., and B. Fregly. In vivo medial and lateral tibial loads during dynamic and high flexion activities. *Journal of Orthopaedic Research*, 25(5):593–602, 2007.

[439] J. Zierath and C. Woernle. Modeling smooth contacts in elastic multibody systems. In *Multibody Dynamics 2009, ECCOMAS Thematic Conference*, Warsaw, Poland, 2009.